공학박사 학위논문

Synthesis and Dynamic Properties of Ultra-Small-Branched Star Poly(ε-caprolactone)s and Their Application to Alternative Plasticizers

초단가지 성형구조 폴리(입실론-카프로락톤)의 합성과 동역학적 특성 분석 및 이들의 대체가소제 응용

2017년 8월

서울대학교 대학원

재료공학부

최 우 혁

Synthesis and Dynamic Properties of Ultra-Small-Branched Star Poly(ε-caprolactone)s and Their Application to Alternative Plasticizers

초단가지 성형구조 폴리(입실론-카프로락톤)의 합성과 동역학적 특성 분석 및 이들의 대체가소제 응용

지도교수 곽승엽

이 논문을 공학박사 학위논문으로 제출함
2017년 4월

서울대학교 대학원
재료공학부
최 우 혁

최우혁의 공학박사 학위논문을 인준함
2017년 6월

위 원 장 장 지 영 (인)
부위원장 곽 승 엽 (인)
위 원 안 철 희 (인)
위 원 정 재 우 (인)
위 원 황 성 연 (인)

ABSTRACT

In this study, we develop ultra-small-branched star poly(ε-caprolactone)s (USB-SPCLs) as nontoxic alternative plasticizers for flexible poly(vinyl chloride) (PVC) and investigate the interplay of dynamic properties with plasticization.

We successfully synthesize the three- and six-branched SPCLs with extremely small branched segments using a facile pseudo-one-pot process in a pilot scale and investigate the effect of ultra-small branches on their crystallization behaviors. The number of branched segments and the individual branched segment lengths for USB-SPCLs are precisely controlled via manipulating monomer-to-core ratio, adjusting monomer-to-polymer conversion, end-capping the terminal hydroxyl groups, and vacuum purification, which results in USB-SPCLs having the branched segments below five degree of polymerization with a high yield exceeding 93%. The molecular weights obtained from ^{1}H NMR spectroscopy are consistent with that obtained from MALDI-TOF-MS and the molecular weight distributions are narrow with $M_w/M_n \leq 1.2$, indicating that USB-SPCLs have mono-dispersed branches. USB-SPCLs have low melting temperatures and broad double-melting peaks attributed to their extremely small branches, and the crystallization behaviors for USB-SPCLs depend on the end group concentration. On the other hand,

the glass transitions for USB-SPCLs depend on the total molecular weights, regardless of the number and length of branched segments.

The extremely small branched effects on molecular dynamics are investigated using USB-SPCLs. USB-SPCLs interestingly show total-molecular-weight-dependent glass transitions regardless of the molecular architecture parameters, such as the number and length of branches, whereas typical star polymers with polymeric large branches show the end-group-concentration-dependent glass transitions. The viscoelasticity of USB-SPCLs does not depend exponentially on the individual branched molecular weight, as observed in typical star polymers, and instead follows the Mark–Houwink power law and the Bueche-modified Rouse model for unentangled linear polymers. The flow activation energy and the longest Rouse relaxation time of USB-SPCLs show that the individual branches of USB-SPCL are dynamically equivalent and that a whole USB-SPCL molecule moves with a simple uni-motion. These results suggest that a whole USB-SPCL molecule presumably acts as a dynamically-equivalent single coarse-grain unit because of the extremely small branches on the scale of 20–40 atoms.

USB-SPCL is used as a nontoxic plasticizer for the production of phthalate-free flexible PVC. USB-SPCL is a transparent liquid at room temperature and exhibits unentangled Newtonian behavior due to its extremely short branched segments. USB-SPCL is biologically safe without producing an

acute toxicity response. Torque analysis measurements reveals that USB-SPCL offers a faster fusion rate and a higher miscibility with PVC compared to a typical plasticizer, DEHP. The solid-state ^{1}H NMR spectrum reveals that PVC and USB-SPCL are miscible with an average domain size of less than 8 nm. The flexibility and transparency of the PVC/USB-SPCL mixture are comparable to the corresponding properties of the PVC/DEHP mixture, and the stretchability and fracture toughness of PVC/USB-SPCL are superior to the corresponding properties of the PVC/DEHP system. Most of all, PVC/USB-SPCL shows excellent migration resistance with a weight loss of less than 0.6% in a liquid phase, whereas DEHP migrated out of PVC/DEHP into a liquid phase with a weight loss of about 10%.

The dynamic effects of unentangled star-shaped polymers with extremely small branches on the plasticization of miscible polymer blends are investigated using USB-SPCLs, PVC, and their blends. Photon correlation dynamics of USB-SPCLs supports our previous suggestion that a whole USB-SPCL molecule acts as a single coarse-grain unit with dynamically-equivalent branches because of the extremely small branches, resulting in the total-molecular-weight-dependent Rouse dynamic behaviors of USB-SPCLs, regardless of the molecular architectures. The dynamic light scattering intensity autocorrelation curves of miscible PVC/USB-SPCL blends reveal that strong intermolecular interactions between PVC and USB-SPCL

molecules determine the dynamic homogeneous behaviors of the blends despite their significantly different mobilities. The molecular motions of the blends depend on the total-molecular-weight-dependent Rouse dynamic behaviors of USB-SPCLs. These dynamic results clearly show the plasticization of the entangled neat linear PVC matrix by distinctive and rapid molecular mobility of USB-SPCLs.

Free-volume-dependent dynamic behaviors of the pyrene-labeled and -doped PVC blends with different amount of USB-SPCL are analyzed using temperature-dependent FS techniques, to investigate the correlation between the dynamic behaviors of individual polymer chains and the controlled free-volume changes. The individual PVC component in the PVC/USB-SPCL blends interestingly exhibited broad thermal glass transition range from the glass transition of the whole blend system to the glass transition of original PVC, differ from a typical glass transition dynamics of miscible polymer blend with single glass transition temperature, indicating the heterogeneous glass transition dynamic behaviors of the miscible PVC/USB-SPCL blend system. These results suggest that the motion of individual PVC component in PVC/USB-SPCL blends depends on both the enlarged free volume by fast-moved USB-SPCL molecules and the dynamic constraint by entangled PVC chains while general glass transition dynamics is sufficiently described by free-volume of the whole blend system.

Keywords: Ultra-small branches, Poly(ε-caprolactone), Star-shaped polymer, Plasticizer, Poly(vinyl chloride), Molecular dynamics, Dynamic mechanical spectrometry, Photon correlation spectroscopy, Fluorescence spectroscopy

Student Number: 2008-20691

CONTENTS

LIST OF TABLES

LIST OF FIGURES

in a given frequency range at various temperatures.

Figure III-4. The viscoelastic curves of dynamic moduli $G'(\omega)$ (filled symbol) and $G''(\omega)$ (open symbol) as a function of ω at different temperatures for (a) USB-SPCL3-3, (b) USB-SPCL3-5, (c) USB-SPCL6-3, and (d) USB-SPCL6-5.

Figure III-5. Viscoelastic master curves plotting the dynamic moduli $G'(\omega)$ (filled symbol) and $G''(\omega)$ (open symbol) as a function of $\alpha_T\omega$ at 60 ℃, for (a) USB-SPCL3-3, (b) USB-SPCL3-5, (c) USB-SPCL6-3, and (d) USB-SPCL6-5.

Figure III-6. The η^* values as a function of ω at different temperatures for (a) USB-SPCL3-3, (b) USB-SPCL3-5, (c) USB-SPCL6-3, and (d) USB-SPCL6-5.

Figure III-7. Logarithmic plot of the viscosity of star polymers with functionalities of three or more versus span molecular weight, M_s. M_s is the molecular weight of the longest linear span in the molecule and is equal to twice the arm molecular weight of a star. The lower line applies to linear polymers. The difference among the viscosities of star polymers with different arm number is hardly noticeable.

Figure III-8. (a) Logarithmic plots of η_0 versus M_b for USB-SPCLs at various temperatures. (b) Logarithmic plots of η_0 versus total M_w for USB-SPCLs at various temperatures. (c) Logarithmic plots of A_G and J_e^o versus total M_w for USB-SPCLs at the reference temperature T_r = 60 ℃.

Figure III-9. (a) Arrhenius plot of $\ln \eta_0$ versus the inverse temperature for

CHAPTER I

INTRODUCTION

I-1. Ultra-Small-Branched Poly(*ε*-caprolactone)

I-1-1. Poly(*ε*-caprolactone)

Poly(*ε*-caprolactone)s (PCLs), which have been studied extensively over the past 20 years, are one of the most attractive biocompatible and biodegradable polyesters.[1−8] PCL's low glass transition temperature, low melting temperature, and high miscibility with commercial polymers compared to other polyesters provide significant advantages to the use of PCLs in absorbable sutures, surgical fibers, artificial organs, controlled drug delivery applications, tissue regeneration approaches, food packages, and PVC plasticizers.[2−11] PCLs are produced via the ring-opening polymerization (ROP) of the cyclic ester monomer, *ε*-caprolactone (CL) (see Figure I-1).[12,13] The mechanism by which CL undergoes ROP in the presence of an alcohol initiator and a catalyst is well known. The alcohol initiator combines with the catalyst to form a complex that rapidly reaches equilibrium, and the complex initiates and propagates the polymerization of the CL monomer via a

classical coordination−insertion mechanism. This ROP mechanism enables PCLs to polymerize to form a variety of well-controlled architectures, with variations in the number and length of branched segments, depending on the number of hydroxyl groups in the initiator and the molar ratio between the CL monomer and the initiator hydroxyl groups.[3,9] Additionally, the molecular weight distribution (MWD) of PCLs product is narrow. Thus, the ROP of the CL monomer is regarded to as a sort of living polymerization.[14]

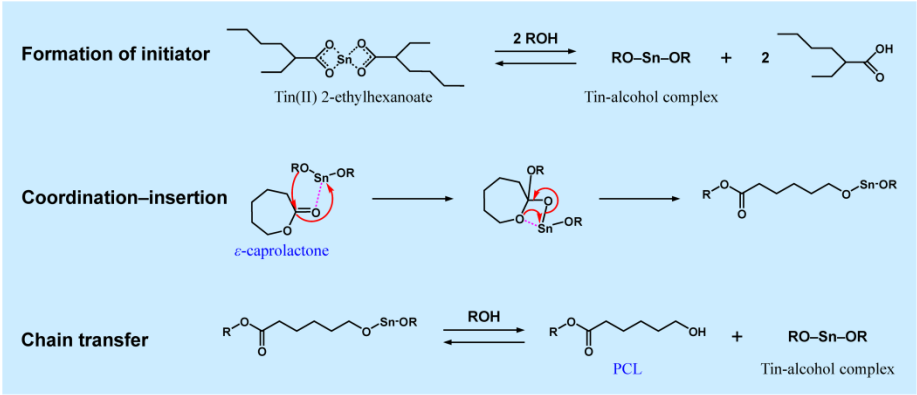

Figure I-1. Ring-opening polymerization mechanism of ε-caprolactone.

I-1-2. Star-shaped poly(ε-caprolactone)

Star-shaped poly(ε-caprolactone)s (SPCLs) are the simplest branched polymers consisting of several PCL branches that emanate from a central core.[15−18] The branches of SPCLs provide a smaller hydrodynamic radius and a greater number of end groups than are obtained from linear PCLs (LPCLs), and SPCLs exhibit useful properties that are not available to conventional LPCLs, such as a low melting point,[15] a low crystallinity,[16] a rapid molecular motion,[16] a low melt viscosity,[18] a low glass transition temperature,[19] a low degree of entanglement in the solid state,[20] and a high solubility in various solvents.[21] In particular, SPCLs provide fundamental insight into structure−property relationships of various and complicated branched polymers, such as H-shaped, comb-shaped, or pom-pom-shaped polymers, due to their simple branched structure and living polymerizable property.

I-1-3. Extremely small branches in SPCL

Most studies of SPCLs have been carried out with large branched segments, and few studies have examined SPCLs with extremely small branches having an average length of fewer than five CL repeating units, *i.e.*, a degree of polymerization (DP) ≤ 5. This is attributed to the backbiting

transesterification side reactions that occur during the CL polymerization (see Figure I-2).[22–26] Such inter- and intramolecular transesterification side reactions of SPCLs proceed via nucleophilic attack of the terminal hydroxyl groups on the ester carbonyl groups in their branched segments, resulting in the collapse of desired SPCL structure and the formation of undesirable cyclic PCLs, and hence a low yield was observed.[22–26] These side reactions tend to proceed readily among SPCLs with small branched segment lengths due to the high end group concentrations and occur rapidly as the monomer-to-polymer conversion approaches completion.[9,22] For this reason, the precise synthesis of SPCLs with extremely small branches is not as easy as we think it will be, although they have highly attractive advantages, including high biocompatibility, facile control over degradation, low softening and melting points, low crystallinity, and good miscibility with other materials compared to conventional SPCLs.[1,27]

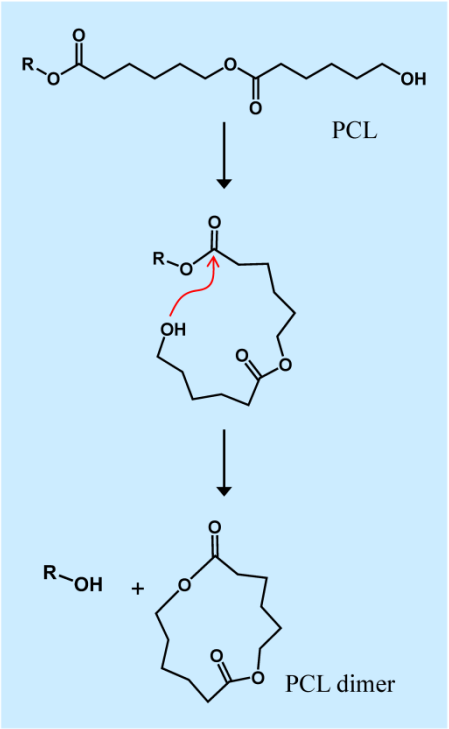

Figure I-2. Backbiting inter- and intramolecular transesterification side reactions of PCL.

I-2. Alternative Plasticizer

I-2-1. Phthalate plasticizer for poly(vinyl chloride)

Poly(vinyl chloride) (PVC) is one of the most prolifically produced thermoplastic material due to its low cost, low combustibility, low flammability, good flame retardation and resistance properties, low heat release profile, good electrical insulation properties, and good chemical resistance (Figure I-3).[28–30] In particular, flexible PVC is widely used in contact with the human body, for example, in medical devices, electronic devices, construction materials, infant care products, toys, and food packaging.[31–33] Flexible PVC contains large amounts of low molecular weight liquid plasticizers that tailor its physical properties to such applications.[34–36] The most common liquid plasticizers are phthalates, which account for more than 80% of the entire plasticizer industry. Di(2-ethylhexyl) phthalate (DEHP) comprises at least 60% of the phthalate plasticizers because it is low in price and performs well.[37,38] The phthalate plasticizers, including DEHP, have been known to display a degree of toxicity since the 1940s.[39,40] In particular, many studies have found that a significant fraction of phthalate plasticizers migrates from the PVC matrix into other media in contact with the matrix (see Figure I-4).[41] The migrated phthalate plasticizers can then act as endocrine disruptors and poison the liver,

heart, kidneys, lungs, testicles, and other organs.[40,42] In addition to serious health hazards, phthalate migration out of the PVC matrix leads to a loss of flexibility relative to the original flexible PVC product.[1] Recent studies report that phthalate plasticizers have already accumulated in the soil, marine ecosystems, indoor air systems, foods, and the human body.[40,43,44] The European Union, the United States, Canada, and other countries have passed laws to regulate the use of phthalate plasticizers in medical devices, childcare articles, and toys.[37,45] Accordingly, the development of a non-toxic, phthalate-free alternative plasticizer is urgently needed for human health and enormous PVC applications.

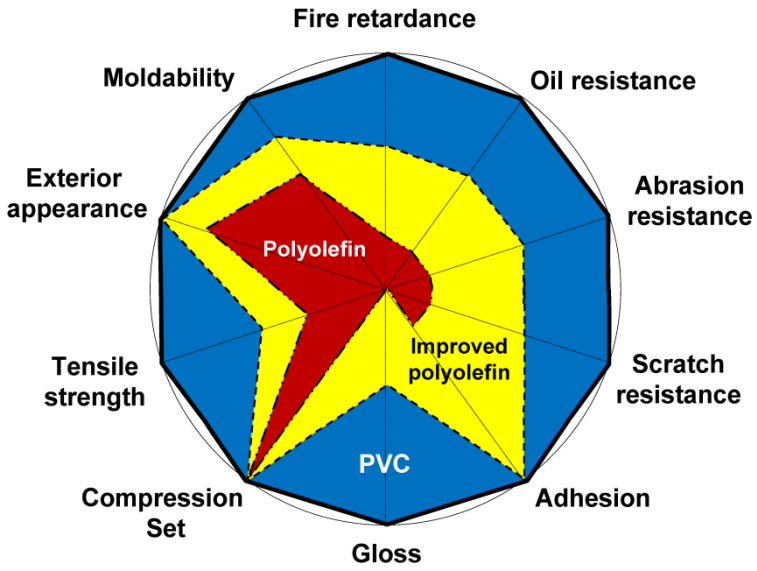

Figure I-3. Comparison of physical properties of PVC with polyolefin.

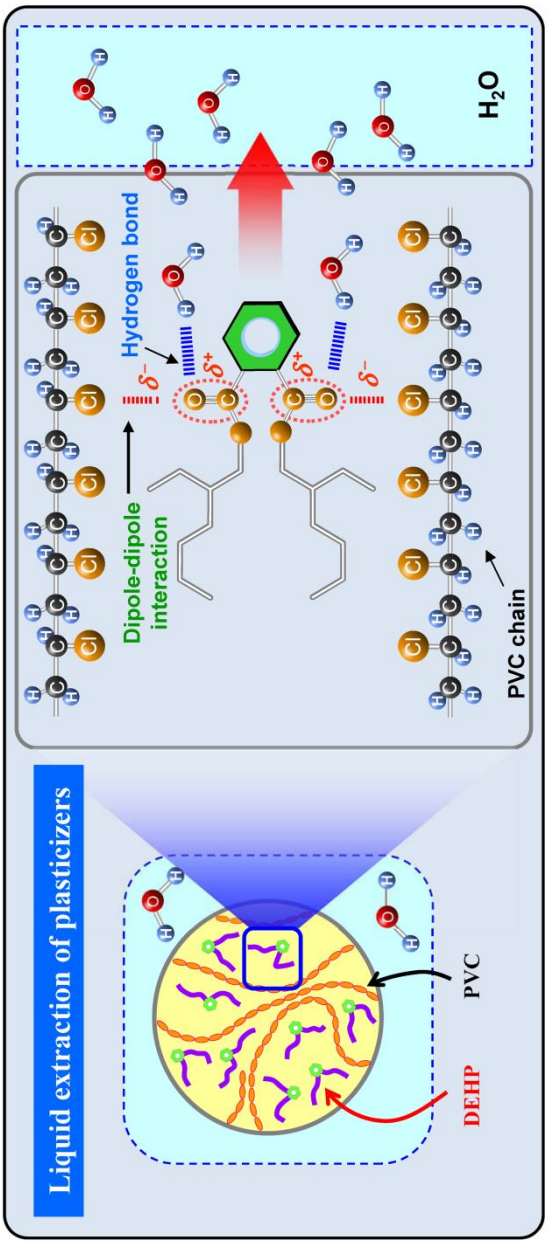

Figure I-4. Mechanism of plasticizer migration to a liquid medium.

I-2-2. PCL plasticizer

PCL is an attractive alternative to phthalate plasticizers because it is non-toxic, biocompatible, and miscible with other polymers, including PVC.[3,46] The low glass transition temperature of PCL provides good flexibility to the PVC chains.[10,47] We reported previously that hyperbranched poly(ε-caprolactone) (HPCL) plasticizers are highly resistant to migration and offer a high plasticizing efficiency.[47] Despite their good properties, the production of HPCL plasticizers has been hampered by the need for complicated synthetic procedures, such as the synthesis of macromonomers through protection–polymerization–deprotection steps and condensation reactions between macromonomers. Shi et al. reported the development of a 'green' plasticizer using a commercially available SPCL.[10] Unfortunately, this 'green' plasticizer underwent significant migration out of the PVC blend, reaching migration levels near those found in DEHP, indicating that the molecular architecture of the commercial SPCL was not as well-controlled as thought due to the back-biting transesterification side reactions from the terminal hydroxyl groups of the SPCL segments. Nevertheless, SPCL bearing short branched segments remains an attractive alternative PVC plasticizer due to its high biocompatibility, low melting point, high free volume, and good miscibility with PVC (Figure I-5).[1,15,16,20,27,48] Furthermore, the degree of entanglement and the relaxation time for SPCL are

smaller than for a linear analogue with the same molecular weight.[49] Thus, it is positively necessary to solve the chronic problems that arise during the synthesis of SPCL, such as back-biting transesterification side reactions, in order to use an SPCL with short branched segments as an alternative plasticizer.

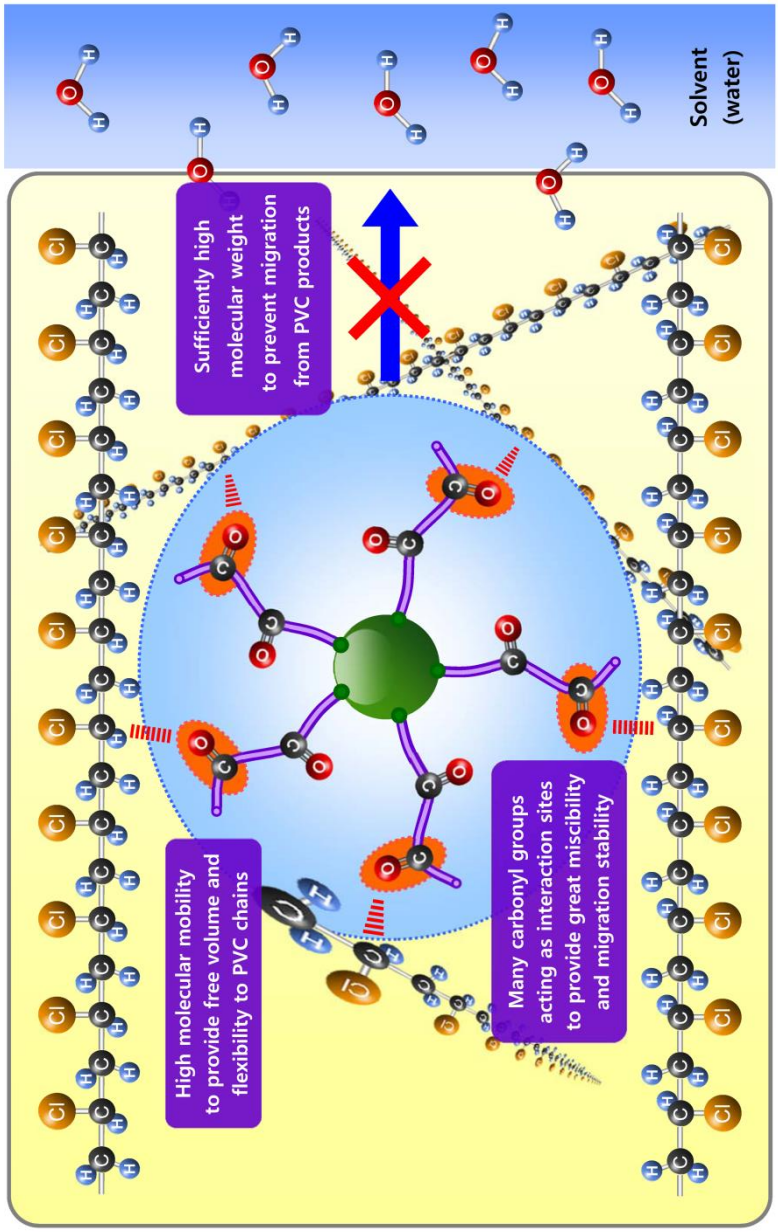

Figure I-5. Plasticizer performance for SPCL in PVC matrix.

I-3. Polymer Dynamics

Polymer dynamics is one of the key factors which determine the mechanical and physical properties of bulk polymers, and thus many researchers have focused their attention on the polymer dynamic behaviors to achieve desired material performance (such as strength, modulus, dimensional stability, permeability to gases and water, and so on).[50−53] Since polymer consist of a large number of atoms and has a very large number of degrees of freedom, polymer dynamics cover a very broad range of motional rates.[54,55] Commonly, the molecular motions in polymer are divided into three classes according to the scale of motional events; (1) the very localized vibrational and torsional motions of individual atoms and groups of an isolated side chain, (2) the less localized segmental motions of short segments of the chain backbone consisting of a small number of monomer units, and (3) the large-scale cooperative diffusional motion involving large sections of the chain, or even the whole macromolecule.[56] Various measurement techniques have been used to prove different modes of polymer dynamics. As shown in Figure I-6, starting from the high-frequency region, the commonly used measurement techniques are Rayleigh−Brillouin Scattering, NMR spin−lattice relaxation times, dielectric relaxation, dynamic depolarized Rayleigh scattering, quasi-elastic neutron scattering, dynamic mechanical spectrum, and so on.[54] Some relaxation phenomena associated with molecular motions are

listed in Table I-1, in terms of the constraint varied and the response observed.[55] It is of both academic and practical importance to relate the different modes of polymer dynamics as probed by these various techniques.

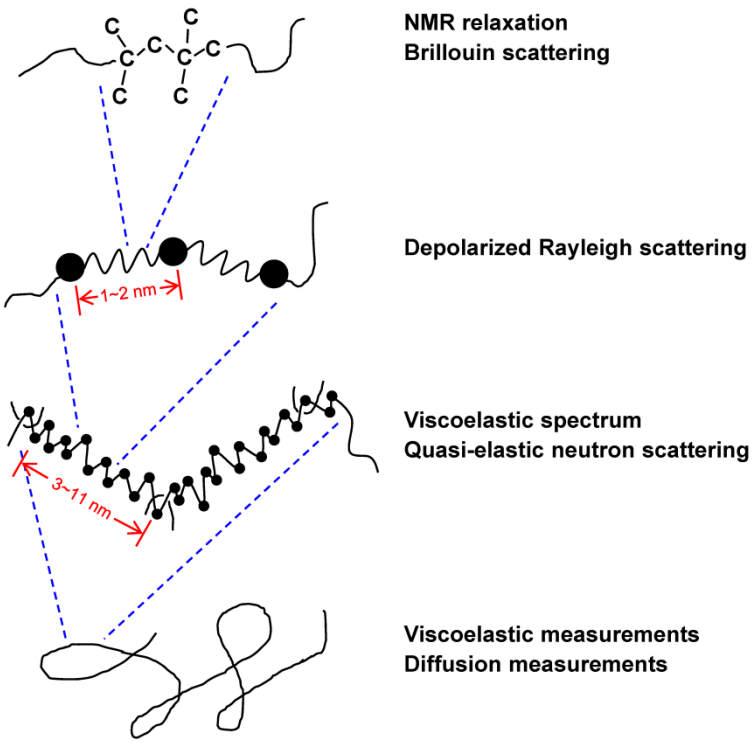

Figure I-6. Polymer dynamics at different length scales (microstructure, Rouse segment, entanglement strand, and whole chain) and some of the usual techniques for probing them.

Table I-1. Some relaxation phenomena associated with molecular motions.

Phenomenon	Constraint varied	Property observed	Motion involved
Dynamic mechanical relaxation	Stress, strain	Strain, stress, modulus	Translation and rotation of molecules and chain segments
Viscoelastic relaxation	Shear stress, shear rate	Dynamic viscosity, shear modulus	Translation and rotation of molecules and chain segments
Ultrasonic relaxation	Pressure, temperature	Acoustic absorption, velocity	Any molecular change for which either $\Delta V^0 \neq 0$ or $\Delta H^0 \neq 0$
Dielectric relaxation	Electric field	Electric polarization, capacitance, loss	Limited translation of charges, rotation of dipoles
Fluorescence depolarization	Polarized electromagnetic field	Polarized fluorescence	Rotation of electronic transition dipole moment
Nuclear magnetic and electron spin relaxation	Magnetic field	Nuclear and electron spin magnetic polarization	Rotation of particle spin transition moment

I-4. Research Objective

The main objective of this study was to develop SPCL with extremely small branches as nontoxic PVC plasticizers and investigate the interplay of dynamic properties with plasticization. In this study, we successfully synthesized ultra-small-branched SPCL (USB-SPCL) using a pilot-scale pseudo-one-pot process via manipulating monomer-to-core ratio, adjusting monomer-to-polymer conversion, end-capping the terminal hydroxyl groups, and vacuum purification. The effects of extremely small branches on the thermal and dynamic properties of USB-SPCL were investigated, and these properties were used in fabricating flexible PVC plasticized by USB-SPCL. In the flexible PVC, the processing properties, plasticizing efficiency, and migration resistance of USB-SPCL as nontoxic plasticizer were compared to a typical toxic plasticizer, di-(2-ethylhexyl) phthalate (DEHP), using conventional flexible PVC manufacturing processes. Furthermore, we investigated how the dynamic behaviors of USB-SPCL affect the plasticization of miscible PVC/USB-SPCL blend using photon correlation spectroscopy (PCS) and how the dynamic behaviors of individual PVC matrix plasticized by USB-SPCL correlate with the plasticization phenomena induced by thermal free-volume changes using fluorescence spectroscopy (FS).

Chapter II: we demonstrated the facile synthesis of USB-SPCLs with precisely controlled architectures using a pilot-scale pseudo-one-pot process via manipulating monomer-to-core ratio, adjusting monomer-to-polymer conversion, end-capping the terminal hydroxyl groups, and vacuum purification.[57] This synthetic protocol did not permit backbiting transesterification side reactions, thereby enabling us to easily control the molecular architectures of SPCLs, even with extremely small branched segments, and to obtain high-purity USB-SPCLs with a high yield. Additionally, this synthetic procedure was green and straightforward, in that organic solvents and additional processes (*e.g.*, precipitation, filtering, washing, and drying steps) were not needed. We further described that USB-SPCLs exhibit the reduced crystallization and the total molecular weight-dependent glass transition attributed to their extremely small branches.

Chapter III: we investigated the effects of extremely small branches on the dynamic behavior of a star polymer using well-defined USB-SPCLs as a model system.[58] The glass transition, viscoelasticity, flow activation energy, and longest Rouse relaxation time of USB-SPCLs interestingly depended on total molecular weight regardless of molecular architecture parameters, such as the number and length of branched segments. Moreover, these dynamic phenomena of USB-SPCLs followed the Mark–Houwink power law and the Bueche-modified Rouse model for unentangled linear polymers rather than

traditional star polymer models that depend exponentially on the individual branched molecular weight. This suggests that a whole USB-SPCL molecule acts as a dynamically-equivalent single coarse-grain unit with one Rouse-segmental motion.

Chapter IV: we developed unentangled SPCLs with extremely small branches capable of providing excellent flexibility to PVC and improving the migration resistance from PVC.[59] At room temperature, USB-SPCLs were transparent viscous liquids and exhibited Newtonian behaviors. USB-SPCLs were biologically safe without producing an acute toxicity response, and they displayed good processability and high miscibility with PVC. The flexible PVCs prepared using USB-SPCLs exhibited good flexibility and transparency properties that were comparable to those obtained from DEHP. Most of all, the migration of USB-SPCLs from the flexible PVCs was negligible, whereas considerable quantities of DEHP migrated out of the flexible PVCs.

Chapter V: the pseudo-bulk dynamics of PVC, USB-SPCLs, and their miscible blends was analyzed using PCS in concentrated solution system at around room temperature, in order to investigate the dynamic effects of USB-SPCLs on the plasticization of miscible PVC/USB-SPCL blends.[60] Photon correlation dynamics of USB-SPCLs depended on their total molecular weights regardless of the molecular architectures, in good agreement with their melt dynamic behaviors. Dynamic homogeneous behaviors of

PVC/USB-SPCL blends were observed and depended on the total-molecular-weight-dependent Rouse dynamics of USB-SPCLs despite their significant mobility difference, resulting from strong intermolecular interactions between PVC and USB-SPCL molecules. These dynamic results showed that the molecular motion of USB-SPCLs is highly reduced by constraint of the entangled linear PVC matrix and, instead, PVC chain motion increases up to the same mobility level of the constrained USB-SPCLs in the PVC matrix. This clearly indicated that the entangled linear PVC matrix was plasticized by distinctive and rapid molecular mobility of USB-SPCLs, resulting in the excellent flexibility of miscible PVC/USB-SPCL blends.

Chapter VI: free-volume-dependent dynamic behaviors of individual PVC component in miscible PVC/USB-SPCL blends were investigated using temperature-dependent FS techniques. The miscible PVC/USB-SPCL blend system exhibited heterogeneous dynamic behaviors with interestingly broad thermal glass transition of individual PVC component, differ from a typical glass transition dynamics of miscible polymer blend. This suggests that the motion of individual PVC component depended on both the enlarged free volume by fast-moved USB-SPCL molecules and the dynamic constraint by entangled PVC chains.

References and Notes

1. Fukuzaki, H.; Yoshida, M.; Asano, M.; Kumakura, M. *Polymer* **1990**, *31*, 2006−2014.

2. Xu, J.; Shi, W. *Polymer* **2006**, *47*, 5161−5173.

3. Noroozi, N.; Thomson, J. A.; Noroozi, N.; Schafer, L. L.; Hatzikiriakos, S. G. *Rheol. Acta.* **2012**, *51*, 179−192.

4. Egevardt, C.; Giese, S. O. K.; Santos, A. D. da C.; Barison, A.; de Sá, E. L.; Filho, A. Z.; da Silva, T. A.; Zawadzki, S. F.; Soares, J. F.; Nunes, G. G. *J. Polym. Sci., Part A: Polym. Chem.* **2014**, *52*, 2509−2517.

5. Hu, X.; Hu, G.; Crawford, K.; Gorman, C. B. *J. Polym. Sci., Part A: Polym. Chem.* **2013**, *51*, 4643−4649.

6. Yamada, S.; Takasu, A.; Kawamura, K. *J. Polym. Sci., Part A: Polym. Chem.* **2013**, *51*, 3732−3739.

7. Gao, C.; Wang, Y.; Gou, P.; Cai, X.; Li, X.; Zhu, W.; Shen, Z. *J. Polym. Sci., Part A: Polym. Chem.* **2013**, *51*, 2824−2833.

8. Liu, J.−X.; Yuan, C.; Su, Z.; Xu, T.−T.; Wei, L.−H.; Ma, Z. *J. Polym. Sci., Part A: Polym. Chem.* **2013**, *51*, 1969−1975.

9. Martin, E.; Dubois, P.; Jérôme, R. *Macromolecules* **2000**, *33*, 1530−1535.

10. Shi, G.; Cooper, D. G.; Maric, M. *Polym. Degrad. Stabil.* **2011**, *96*, 1639−1647.

11. Xie, W.; Gan, Z. *Polym. Degrad. Stabil.* **2009**, *94*, 1040−1046.

12. Kricheldorf, H. R.; Kreiser-Saunders, I.; Stricker, A. *Macromolecules* **2000**, *33*, 702−709.

13. Storey, R. F.; Sherman, J. W. *Macromolecules* **2002**, *35*, 1504−1512.

14. Persenaire, O.; Alexandre, M.; Degée, P.; Dubois, P. *Biomacromolecules* **2001**, *2*, 288−294.

15. Sanda, F.; Sanada, H.; Shibasaki, Y.; Endo, T. *Macromolecules* **2002**, *35*, 680−683.

16. Choi, J.; Kim, I.−K.; Kwak, S.−Y. *Polymer* **2005**, *46*, 9725−9735.

17. van Ruymbeke, E.; Muliawan, E. B.; Vlassopoulos, D.; Gao, H.; Matyjaszewski, K. *Eur. Polym. J.* **2011**, *47*, 746−751.

18. Fetters, L. J.; Kiss, A. D.; Pearson, D. S. *Macromolecules* **1993**, *26*, 647−654.

19. Alam, M. Z.; Ogata, T.; Nonaka, T.; Kurihara, S. *Polym. Int.* **2009**, *58*, 1308−1313.

20. Fréchet, J. M. J. *Science* **1994**, *263*, 1710−1715.

21. Wu, L.; Wang, L.; Wang, X.; Xu, K. *Acta Biomater.* **2010**, *6*, 1079−1089.

22. Kricheldorf, H. R.; Berl, M.; Scharnagl, N. *Macromolecules* **1988**, *21*, 286−293.

23. de Jong, S. J.; Arias, E. R.; Rijkers, D. T. S.; van Nostrum, C. F.; Kettenes-van den Bosch, J. J.; Hennink, W. E. *Polymer* **2001**, *42*, 2795−2802.

24. Dubois, P.; Ropson, N.; Jérôme, R.; Teyssié, P. *Macromolecules* **1996**, *29*, 1965−1975.

25. Kowalski, A.; Duda, A.; Penczek, S. *Macromolecules* **2000**, *33*, 689−695.

26. Kowalski, A.; Duda, A.; Penczek, S. *Macromolecules* **2000**, *33*, 7359−7370.

27. Lin, S.−Y.; Chen, K.−S.; Teng, H.−H.; Li, M.−J. *J. Microencapsul.* **2000**, *17*, 577−586.

28. Navarro, R.; Perrino, M. P.; Tardajos, M. G.; Reinecke, H. *Macromolecules* **2010**, *43*, 2377−2381.

29. Sadat–Shojai, M.; Bakhshandeh, G.−R. *Polym. Degrad. Stab.* **2011**, *96*, 404−415.

30. Makino, T.; Kakou, S. *J. Jpn. Soc. Polym. Process.* **1998**, *10*, 1.

31. Fenollar, O.; Garcia–Sanoguera, D.; Sanchez–Nacher, L.; Lopez, J.; Balart, R. *J. Mater. Sci.* **2010**, *45*, 4406−4413.

32. Gamage, P. K.; Farid, A. S. *J. Appl. Polym. Sci.* **2011**, *121*, 823−838.

33. Daniels, P. H. *J. Vinyl Addit. Technol.* **2009**, *15*, 219−223.

34. Sears, J. K.; Darby, J. R. *The Technology of Plasticizers*; John Wiley & Sons: New York, 1982.

35. Rahman, M.; Brazel, C. S.*Prog. Polym. Sci.* **2004**, *29*, 1223−1248.

36. Mazzeo, P.; Pasquale, D. D.; Ruggieri, F.; Fanelli, M.; D′Archivio, A. A.; Garlucci, G. *Chromatogr.* **2007**, *21*, 1166−1171.

37. Coltro, L.; Pitta, J. B.; Madaleno, E. *Polym. Test.* **2013**, *32*, 272−278.

38. Yin, B.; Hakkarainen, M. *J. Appl. Polym. Sci.* **2011**, *119*, 2400−2407.

39. Tickner, J. A.; Schettler, T.; Guidotti, T.; McCally, M.; Rossi, M. *Am. J. Ind. Med.* **2001**, *39*, 100−111.

40. Heudorf, U.; Mersch–Sundermann, V.; Angerer, J. *Int. J. Hyg. Environ. Health.* **2007**, *210*, 623−634.

41. Yu, B. Y. *Migration Resistance of Phthalate Plasticizer by Incorporation of Organic Nanoparticles Possessing High Degree of Intermolecular Interactions*; MS Thesis, Seoul National Univeristy, Republic of Korea, 2007.

42. Janjua, N. R.; Mortensen, G. K.; Andersson, A.–M.; Kongshoj, B.; Skakkebak, N. E.; Wulf, H. C. *Environ. Sci. Technol.* **2007**, *41*, 5564−5570.

43. Hakkarainen, M. *Adv. Polym. Sci.* **2008**, *211*, 159−185.

44. Simmchen, J.; Ventura, R.; Segura, J. *Transfus. Med. Rev.* **2012**, *26*, 27−37.

45. Yu, B. Y.; Chung, J. W.; Kwak, S.−Y. *Environ. Sci. Technol.* **2008**, *42*, 7522−7527.

46. Nair, L. S.; Laurencin, C. T. *Prog. Polym. Sci.* **2007**, *32*, 762−798.

47. Choi, J.; Kwak, S.−Y. *Environ. Sci. Technol.* **2007**, *41*, 3763−3768.

48. Hanwha Chemical Co, Ltd. *Development of Eco-friendly Alternative Plasticizer Based on Nanobrush Structure*: Final research report; The Ministry of Knowledge Economy of the Republic of Korea, 2011.

49. Ferry, J. D. *Viscoelastic Properties of Polymers*, 3rd ed; Wiley: New York, 1980.

50. Zhang, Q.; Liu, W.; Dai, P. *Polymer* **1998**, *39*, 3787−3792.

51. Priya, L.; Jog, P. *J. Polym. Sci., Part B: Polym. Phys.* **2002**, *40*, 1682−1689.

52. Holt, A. P.; Griffin, P. J.; Bocharova, V.; Agapov, A. L.; Imel, A. E.; Dadmun, M. D.; Sangoro, J. R.; Sokolov, A. P. *Macromolecules* **2014**, *47*, 1837−1843.

53. Lee, J.; Grein-Iankovski, A.; Narayanan, S.; Leheny, R. L. *Macromolecules* **2017**, *50*, 406−415.

54. Lin Y-H: *Polymer Viscoelasticity: Basics, Molecular Theories, Experiments and Simulations*, 2nd ed.; World Scientific: New Jersey, 2011.

55. Bailey, R. T.; North, A. M.; Pethrick, R. A. *Molecular Motion in High Polymers*; Clarendon: Oxford, 1981.

56. Choi, J.; Kwak, S.–Y. *Polymer* **2004**, *45*, 7173−7183.

57. Phublished in: Choi, W.; Chung, J. W.; Kwak, S.–Y. *ACS Appl. Mater. Interfaces* **2014**, *6*, 11118−11128.

58. Phublished in: Choi, W.; Chung, J. W.; Kwak, S.–Y. *J. Polym. Sci., Part A: Polym. Chem.* **2015**, *53*, 1134−1142.

59. Phublished in: Choi, W.; Chung, J. W.; Kwak, S.–Y. *Polymer* **2015**, *79*, 91−98.

60. Phublished in: Choi, W.; Chung, J. W.; Kwak, S.–Y. *Polymer* **2016**, *103*, 19−26.

CHAPTER II

SYNTHESIS OF ULTRA-SMALL-BRANCHED STAR POLY(ε-CAPROLACTONE)S AND THEIR HIGH END GROUP CONCENTRATION EFFECTS ON CRYSTALLIZATION

II-1. Introduction

Extremely small branches, which have fewer than five CL repeating units (degree of polymerization (DP) $\leq$ 5), have been rarely investigated in star-shaped poly(ε-caprolactone)s (SPCLs) while SPCL with large branches have been exhaustively studied. Recently, Shibata et al. reported the synthesis of tetra-armed SPCL with extremely small branches to use as semi-interpenetrating polymer networks.[1–3] Tetra-armed SPCL appeared to be successfully synthesized, but it had a low yield (76%). Bilgin et al. reported the synthesis and characterization of octa-armed SPCL with extremely small branches.[4] They showed that octa-armed SPCL had very low yield (56%) and higher molecular weight compared to the targeted molecular weight. These results are attributed to the synthesis carrying out without consideration

of the chronic backbiting problem associated with PCLs. In those studies, the desired SPCL structure may collapse, and/or the undesireable cyclic PCLs may form.

Herein, we demonstrated the facile synthesis of ultra-small-branched SPCLs (USB-SPCLs) with precisely controlled architectures using a pilot-scale pseudo-one-pot process via manipulating monomer-to-core ratio, adjusting monomer-to-polymer conversion, end-capping the terminal hydroxyl groups, and vacuum purification.[5] This synthetic protocol did not permit backbiting transesterification side reactions, thereby enabling us to easily control the molecular architectures of SPCLs, even with extremely small branched segments, and to obtain high-purity USB-SPCLs with a high yield. Additionally, this synthetic procedure was green and straightforward, in that organic solvents and additional processes (*e.g.*, precipitation, filtering, washing, and drying steps) were not needed. We further described that USB-SPCLs exhibit the reduced crystallization and the total molecular weight-dependent glass transition attributed to their extremely small branches. This study paves the way for the development of various and complicated PCLs with extremely small branched segments and for an understanding of the structure−property relationships affected by their extremely small branches.

II-2. Experimental Section

II-2-1. Materials

ε-Caprolactone (CL) and trimethylolpropane (TMP) were purchased from Alfa Aesar Co., Ltd., USA and Tokyo Chemical Industry Co., Ltd., Japan., respectively. Dipentaerythritol (DPTOL), tin(II) 2-ethylhexanoate ($Sn(Oct)_2$), and acetic anhydride (Ac_2O) were purchased from Sigma-Aldrich Ltd., Korea. TMP and DPTOL were dried under vacuum at room temperature for 24 h prior to use, and other chemicals were used without further purification.

II-2-2. Synthesis of USB-SPCLs

The synthesis of USB-SPCLs was accomplished by the ring-opening polymerization (ROP) of the CL monomer through a facile pseudo-one-pot bulk process without organic solvents. The calculated quantity of core material was added to a 1 L pilot-scale reactor in the presence of 570.70 g (5.00 mol) of the CL branching material, and the mixture was stirred vigorously with heating to form a homogeneous mixture over 1 h. After then, the mixture was heated in an oil bath at 110 ℃, and a catalytic amount of $Sn(Oct)_2$ was added. After polymerization for about 3 h, an excess

quantity of the Ac_2O end-capping agent was added, and the reaction was allowed to proceed at 110 ℃ for 30 min to terminate the polymerization reaction by capping the terminal hydroxyl groups of the as-polymerized USB-SPCLs. The residual unreacted CL monomers and excess Ac_2O were removed under vacuum at 110 ℃ over 24 h, yielding end-capped USB-SPCLs with small acetate end groups (> 93% of yield). The number of branched segments in USB-SPCLs was controlled using initiating core moieties having either 3 (TMP) or 6 (DPTOL) hydroxyl functionalities. The length of the individual branched segments of USB-SPCLs, *i.e.*, the degree of polymerization (DP) of the individual branched segments, was varied by manipulating the molar ratio between the CL monomer and the hydroxyl functionalities of the core moiety ([CL]/[core-OH]). The number of branched segments (*m*) and the DP of the individual branched segments (*n*) of USB-SPCLs were varied to prepare four USB-SPCLs, denoted USB-SPCL*m*-*n*: USB-SPCL3-3, USB-SPCL3-5, USB-SPCL6-3, and USB-SPCL6-5. As a counterpart to USB-SPCLs, the conventional LPCL and SPCL were synthesized from ethanol and TMP core, respectively, using procedure used for the production of USB-SPCL. These conventional LPCL and SPCL had individual branched segment lengths of DP = 10 and were denoted LPCL1-10 and SPCL3-10, respectively. LPCL1-10 had a total molecular weight similar to that of USB-SPCL3-3, and SPCL3-10 had longer branched segment lengths but the same number of branched segments as USB-SPCL3-3. All reactions

were performed under a nitrogen atmosphere with the exception of the vacuum purification.

II-2-3. Characterization

Fourier-transform infrared (FT-IR) spectroscopy was employed to characterize the functional groups present in USB-SPCLs using a Perkin-Elmer GX IR spectrophotometer with a spectral resolution of 4 cm^{-1}. The FT-IR spectrum was collected over the range 4000−400 cm^{-1} using potassium bromide (KBr) powder as the sample matrix and reference material. The chemical structures of USB-SPCLs were analyzed by ^{1}H nuclear magnetic resonance (NMR) spectroscopy using a Bruker Avance spectrometer 600 using chloroform-*d* ($CDCl_3$) as the solvent. The molecular weights of USB-SPCLs were measured by matrix-assisted laser desorption/ionization time-of-flight mass spectrometry (MALDI-TOF-MS) using an Applied Biosystems Voyager-DE STR spectrometer and a matrix comprising di-hydrobenzoic acid (DHB) dissolved in tetrahydrofuran (THF). The melting, crystallization, and glass transition behaviors of USB-SPCLs were measured by differential scanning calorimetry (DSC) using a Netzsch DSC 200 F3. Samples were heated to 140 ℃ at a heating rate of 20 ℃ min^{-1} and were cooled to −110 ℃

at a cooling rate of −5 ℃ min^{-1}. The samples were then reheated to 140 ℃ at a heating rate of 20 ℃ min^{-1} under a nitrogen atmosphere.

II-3. Results and Discussion

II-3-1. Synthesis of USB-SPCLs

We synthesized end-capped three- or six-branched SPCLs with individual branched segment lengths of DP ≤ 5, that is, ultra-small-branched SPCLs (USB-SPCLs). As shown in Figure II-1(a), the FT-IR spectra of USB-SPCLs revealed that the ester C=O stretch absorbance peak at 1730 cm^{-1} shifted to 1735 cm^{-1} after the ROP of the CL monomer from the core materials. Furthermore, the outstanding O-H stretch (3650−3200 cm^{-1}) observed in both core materials disappeared completely, and a weak overtone band resulting from the ester groups in USB-SPCLs appeared at 3700−3300 cm^{-1}. These results indicated that the ROP successfully proceeded without leaving any CL monomers, that the PCL branched segments were successfully grown from a core moiety, and that the terminal hydroxyl groups of USB-SPCLs were completely capped with small acetate groups. A more precise architectural analysis of USB-SPCLs was performed using ^{1}H NMR spectroscopy. As shown in Figure II-1(b), the ^{1}H NMR spectra of USB-SPCLs showed peaks typically observed in conventional PCLs, including the core moiety peaks (0.89 ppm for TMP or 3.39 ppm for DPTOL) and the end-capped acetate peak (2.04 ppm). On thecontrary, the CL monomer peaks (4.22, 2.63, 1.86, and 1.76 ppm) were completely absent, and the methylene

proton peak adjacent to the terminal hydroxyl groups (3.64 ppm) and the hydroxyl proton peak (3.41 ppm) observed in the as-polymerized uncapped USB-SPCLs were also disappeared. These indicated that the synthesis of end-capped USB-SPCLs was successfully accomplished without leftover CL monomers, in good agreement with the FT-IR analysis. The ratios of the integrals of specific ^{1}H NMR peaks obtained from USB-SPCLs identified the number of branched segments, N_{number}, and the average lengths of the individual branched segments, N_{length}, of USB-SPCLs (see Figure II-2). The N_{number} values of USB-SPCLs were calculated from the ratio between the integrals of peak corresponding to the methyl protons (g, 0.89 ppm, $-CH_2C\underline{H}_3$ in TMP) or methylene protons (g′, 3.39 ppm, $-OC\underline{H}_2C-$ in DPTOL) in the core moiety and the peak corresponding to the methyl protons of the end-capped acetate groups (e, 2.04 ppm, $-COC\underline{H}_3$). As listed in Table II-1, the N_{number} values corresponded to the number of hydroxyl groups in the core materials, indicating that the TMP- and DPTOL-cored SPCLs included three- and six-branched segments, respectively. The N_{length} values of USB-SPCLs were calculated by counting the number of CL repeating units, *i.e.*, the degree of polymerization (DP), in one branched segment of USB-SPCLs based on the ratio of the peak integrals corresponding to the methyl protons of the end-capped acetate groups (e, 2.04 ppm, $-COC\underline{H}_3$) and the repeating methylene protons adjacent to the carbonyl groups in the branched segments (a, 2.31

ppm, −COC$\underline{H_2}$CH$_2$−). As listed in Table II-1, USB-SPCLs were obtained with the desired individual branched segment lengths of three (DP = 3) or five (DP = 5) CL repeating units, depending on the molar ratio of the CL to the hydroxyl groups on the core material ([CL]/[core-OH]). These results indicated that the molecular architecture of USB-SPCLs was precisely controlled with below 5 nm branched segment lengths in a fully extended conformation.

The number-average molecular weights of USB-SPCLs were determined using N_{number} and N_{length} obtained from the ^{1}H NMR spectra, as follows:

$$M_{n,NMR} = MW_{core} + \left(MW_{CL} \times N_{length} \times N_{number}\right) + \left(MW_{end-cap} \times N_{number}\right) - \left(MW_H \times N_{number}\right) \quad (1)$$

where MW_{core}, MW_{CL}, MW_H, and $MW_{end\text{-}cap}$ are the molar masses of the core material (TMP or DPTOL), CL monomer, hydrogen, and end- capping moiety (−COCH$_3$), respectively. As shown in Table II-1, the calculated $M_{n,NMR}$ values of USB-SPCLs were close to the actual number- average molecular weights of USB-SPCLs, determined by MALDI-TOF-MS, $M_{n,MALDI}$. The MALDI-TOF mass spectra of USB-SPCLs in Figure II-1(c) displayed that each mass peak corresponded to the molar mass of '$MW_{core} + (n \times MW_{CL}) + MW_{end-moiety} + MW_{Na^+}$ ', where n is positive integer values, $MW_{end-moiety}$ is the molar mass of '$(MW_{end-cap} - MW_H) \times 3$ (for TMP)

or 5 (for DPTOL)', and MW_{Na^+} is the molar mass of the sodium cation. The mass difference between each adjacent peak was 114 m/z (mass-to-charge ratio), which corresponded to the molar mass of a CL repeating unit in branched segments. Moreover, an increase in the total molecular weights of USB-SPCLs shifted the entire MALDI-TOF mass spectrum toward higher molecular weights without significantly altering the shape of the spectrum. These results provided the evidence that USB-SPCLs with well-defined architecture were synthesized without the formation of the undesirable structure, especially cyclic PCLs via the backbiting transesterification side reaction. (MWDs) of USB-SPCLs were narrow ($M_w/M_n \leq 1.2$) and independent of N_{length} for a given N_{number} (see Table II-1), in contrast with previous reports on the MWD of SPCLs with longer N_{length}.[6] Furthermore, the MWD values of USB-SPCLs decreased as N_{number} increased for a given N_{length}. These results suggested that the MWDs of USB-SPCLs were affected not by N_{length}, but rather by N_{number}.

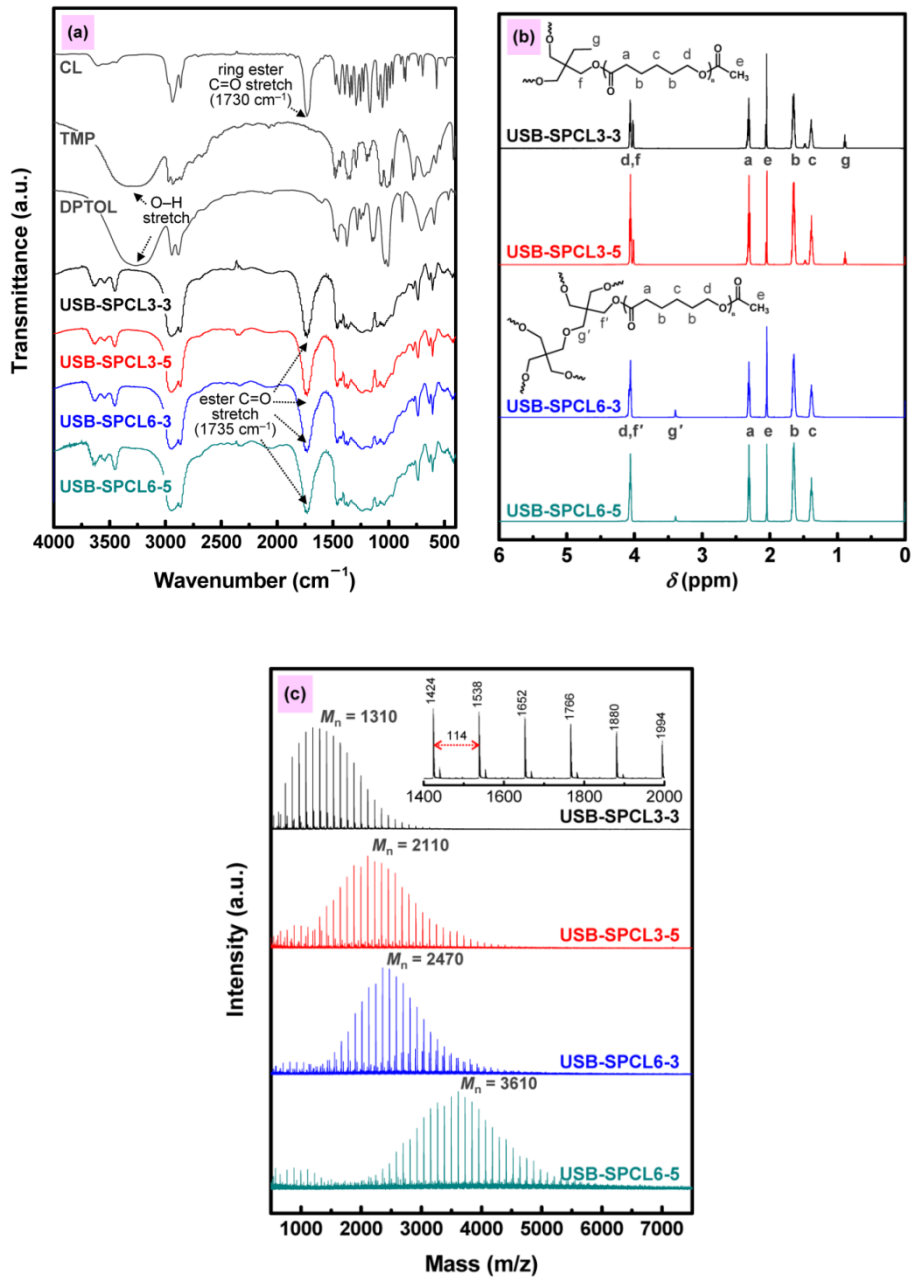

Figure II-1. (a) ^{1}H NMR spectra of USB-SPCLs. (b) FT-IR spectra of USB-SPCLs. (c) MALDI-TOF mass spectra of USB-SPCLs.

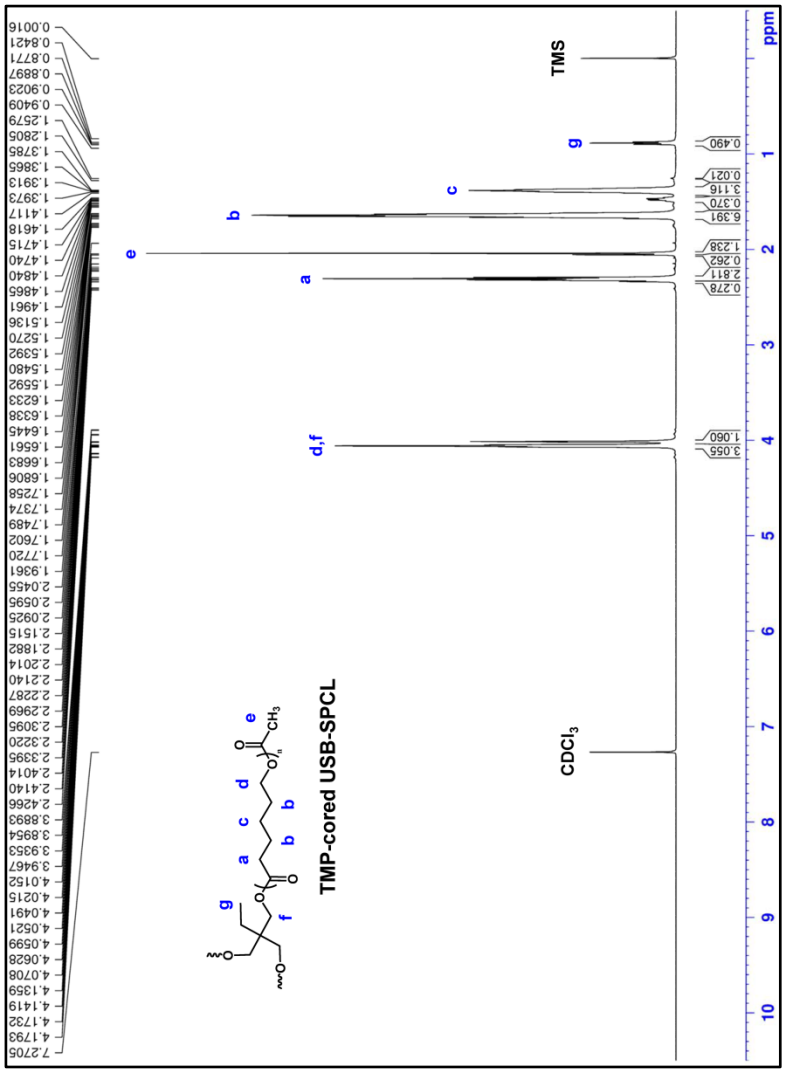

(a) USB-SPCL3-3

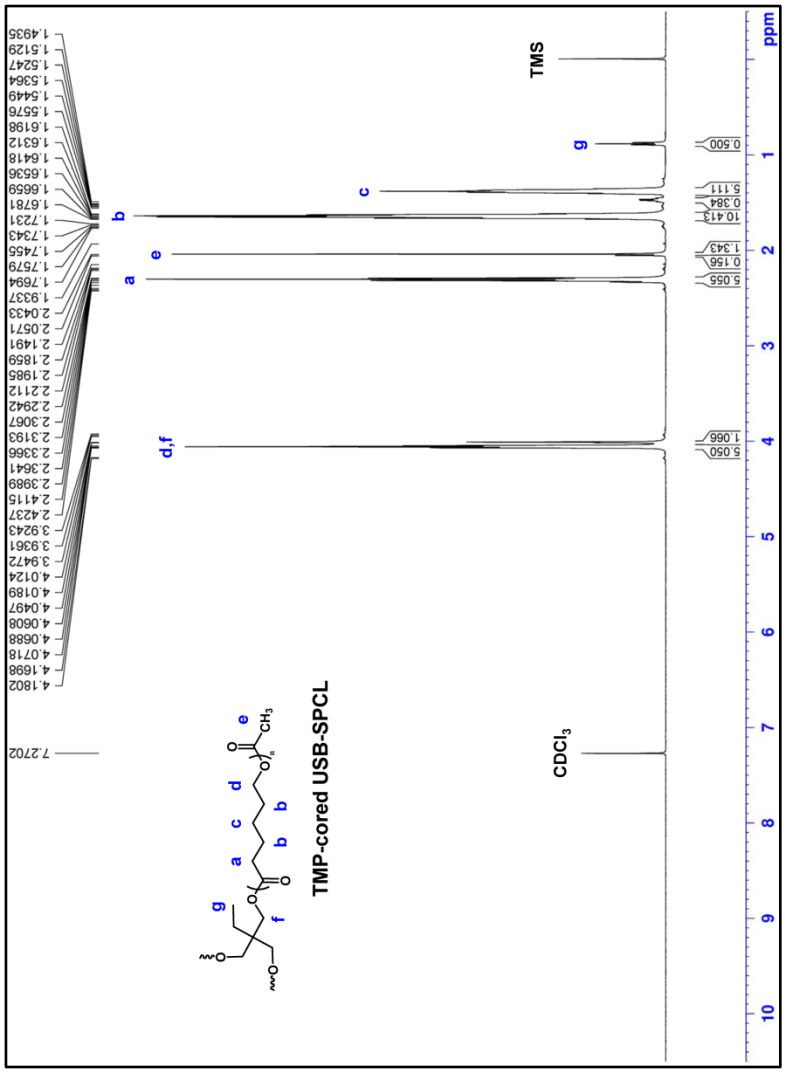

(b) USB-SPCL3-5

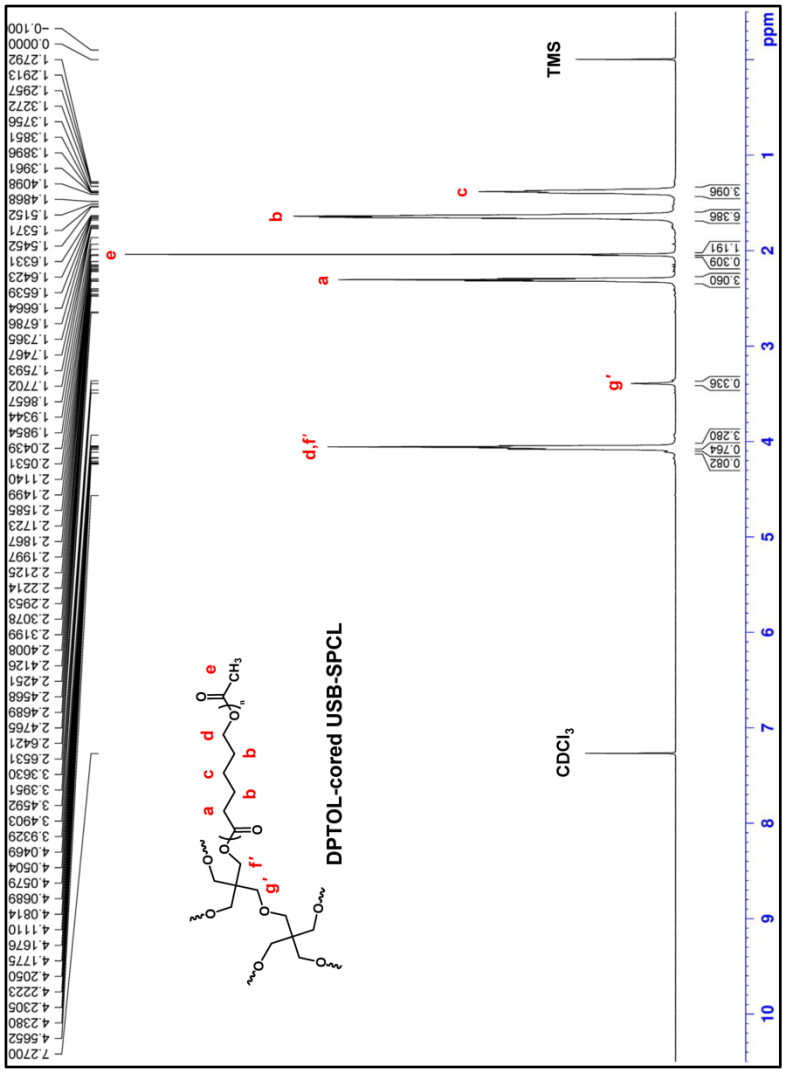
DPTOL-cored USB-SPCL
TMS
CDCl3
ppm
a
b
c
d,f'
e
g'
3.096
6.386
1.191
0.309
3.060
0.336
0.082
0.764
3.280

(c) USB-SPCL6-3

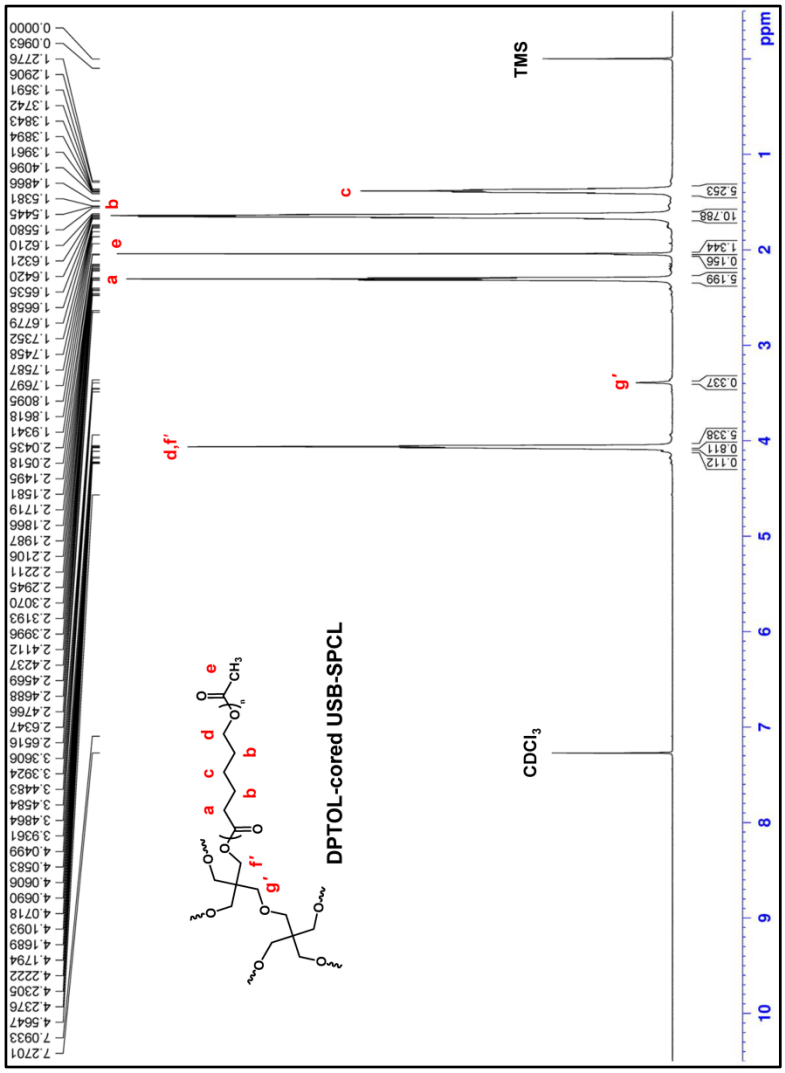

(d) USB-SPCL6-5

Figure II-2. ^{1}H NMR spectra of (a) USB-SPCL3-3, (b) USB-SPCL3-5, (c) USB-SPCL6-3, and (d) USB-SPCL6-5.

Table II-1. The numbers and lengths of branched segments and molecular weights for USB-SPCLs.

Sample	1H NMR			MALDI-TOF	
	N_{number}	N_{length}	$M_{n,NMR}$ (g mol^{-1})	$M_{n,MALDI}$ (g mol^{-1})	MWD
USB-SPCL3-3	2.94	3.09	1300	1310	1.22
USB-SPCL3-5	3.00	5.06	1990	2110	1.23
USB-SPCL6-3	6.06	3.06	2620	2470	1.07
USB-SPCL6-5	6.06	5.20	4100	3610	1.09

We note that adjusting monomer-to-polymer conversion and end-capping the terminal hydroxyl groups were crucial for the synthesis of USB-SPCLs with precisely controlled architectures. Figure II-3 is the ^{1}H NMR spectra of the as-polymerized uncapped USB-SPCL3-3 (before purification) at different reaction times for a given quantity of catalyst and reaction temperature. As shown in Figure II-3, the peaks corresponding to the unreacted CL monomer reduced as the reaction time increased, and eventually disappeared over the reaction time of 3 h, indicating that CL monomers was fully converted to USB-SPCL3-3 over the reaction of 3 h. The quantitative monomer-to-polymer conversion efficiency was calculated based on the ratio of ^{1}H NMR peak integrals corresponding to the methylene protons in the unreacted CL monomer and the branched segments of USB-SPCL3-3 (see Figure II-4). As expected, we found that the monomer-to-polymer conversion efficiency over 99.9% was accomplished over the reaction time of 3 h. In addition, as CL monomers were converted to USB-SPCL3-3, *i.e.*, as the reaction time progressed, the N_{length} values of USB-SPCL3-3 gradually increased. The targeted N_{length} value (DP = 3) was observed in the 3 h sample with a 96% monomer-to-polymer conversion efficiency. On the other hand, the N_{length} values exceeded the targeted value over the reaction time of 3 h, although there were no longer any CL monomers to react with USB-SPCL3-3. The excess N_{length} values can be explained by the formation of undesired cyclic PCLs attributed to the backbiting transesterification side reaction because the

cyclization of PCLs by the backbiting transesterification side reaction readily occurred during the ROP of the CL monomer as the monomer-to-polymer conversion approached completion.[7,8] These results obviously showed that the control of the monomer-to-polymer conversion played an important role in the synthesis of USB-SPCLs with the mono-dispersed branches, in other words, the monomer-to-polymer conversion should be carefully controlled to synthesize USB-SPCLs with well-defined architecture through cooperatively tuning up the reaction conditions, such as quantity of catalyst, reaction temperature, and reaction time. The control of the monomer-to-polymer conversion to prevent the backbiting transesterification side reaction during the ROP of the CL monomer, however, has not been reported before in the literature for the synthesis of well-defined PCLs. Many researchers have carried out the ROP of the CL monomer with a rough amount of catalyst and reaction time without considering the monomer-to-polymer conversion, and such ROP can result in the failure of obtaining SPCLs with desired architectures, which may further lead to a lack of properties of SPCLs. Hence, we adjusted the monomer-to-polymer conversion of the as-polymerized uncapped USB-SPCLs to 95−97% in this study.

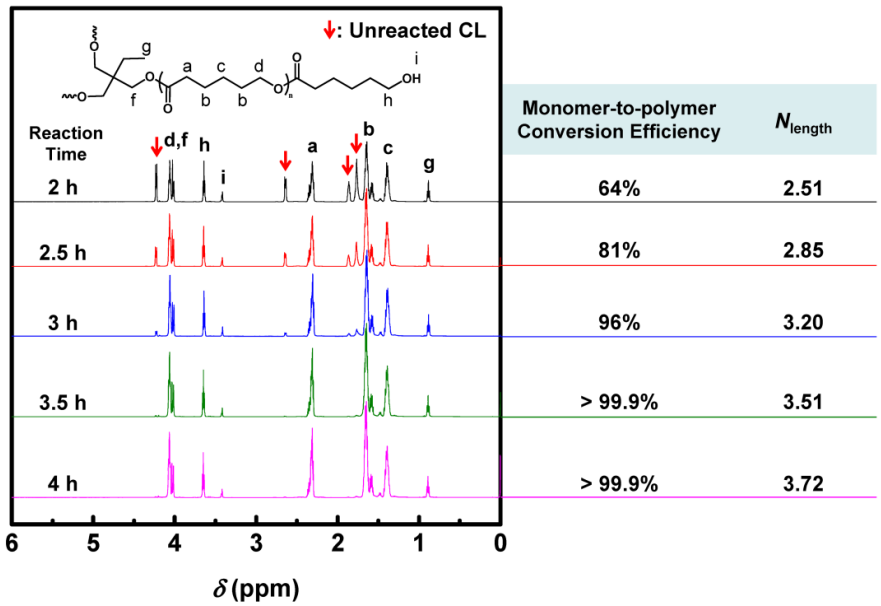

Figure II-3. ^{1}H NMR spectra of the as-polymerized uncapped USB-SPCL3-3 (before purification) at different reaction times.

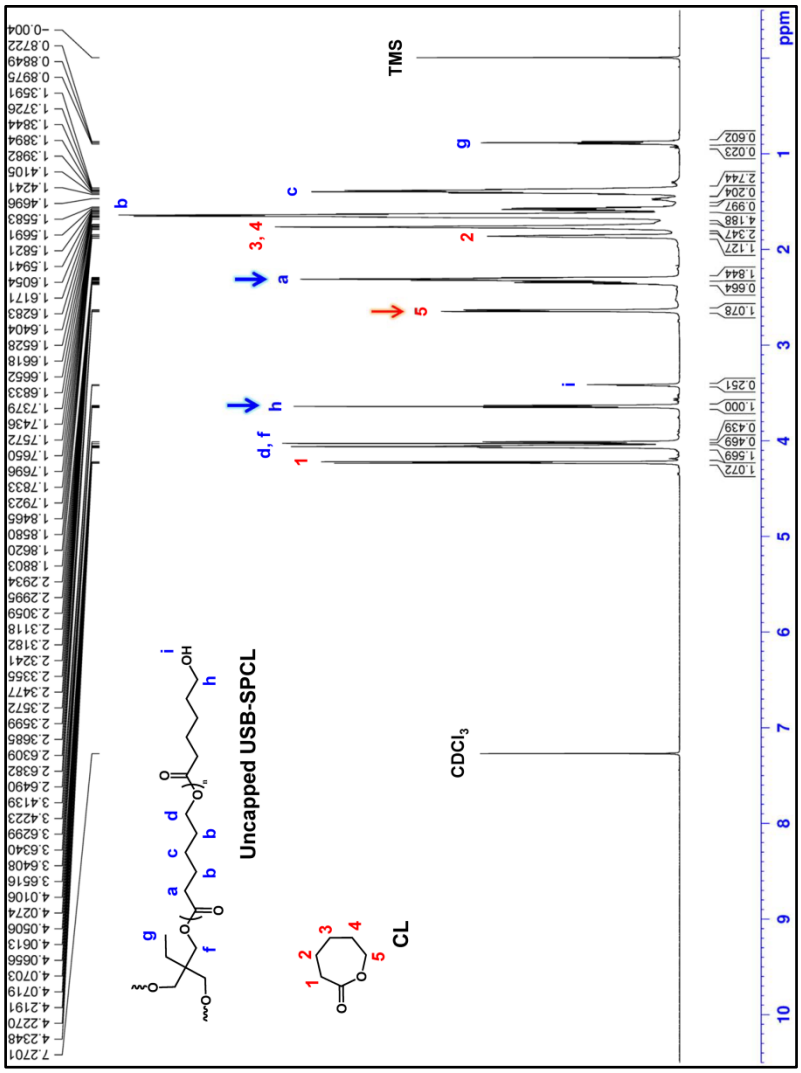

(a) 2 h of reaction time

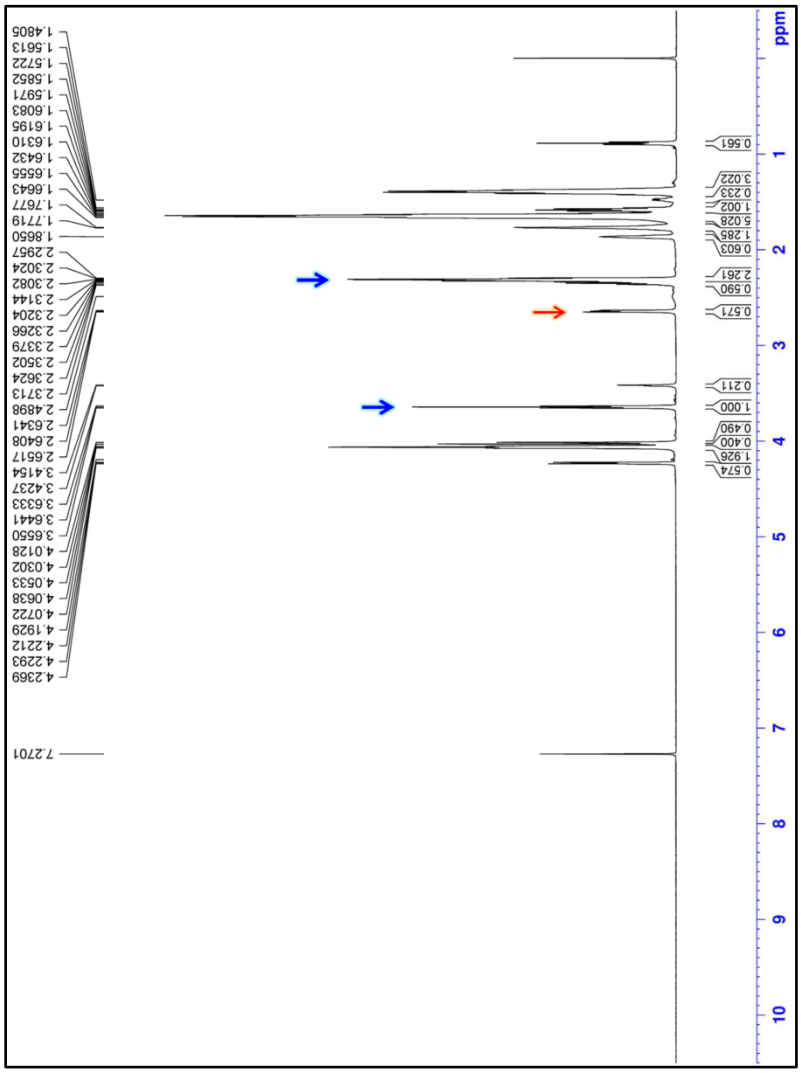

(b) 2.5 h of reaction time

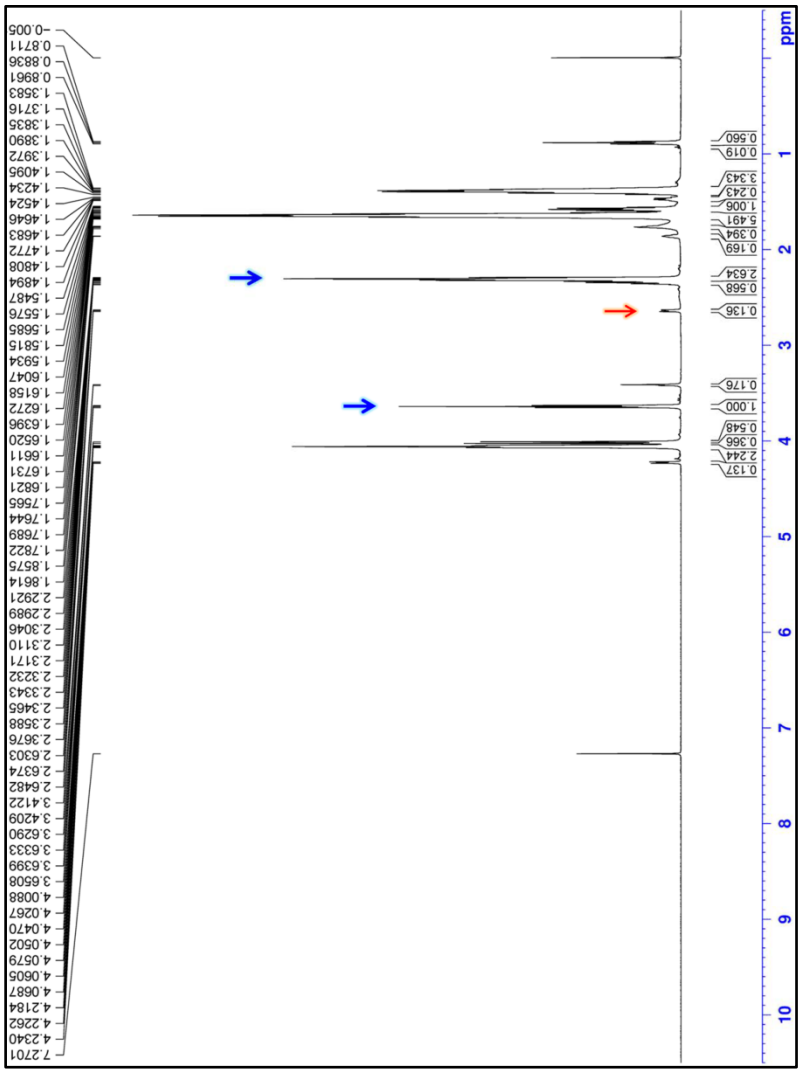

(c) 3 h of reaction time

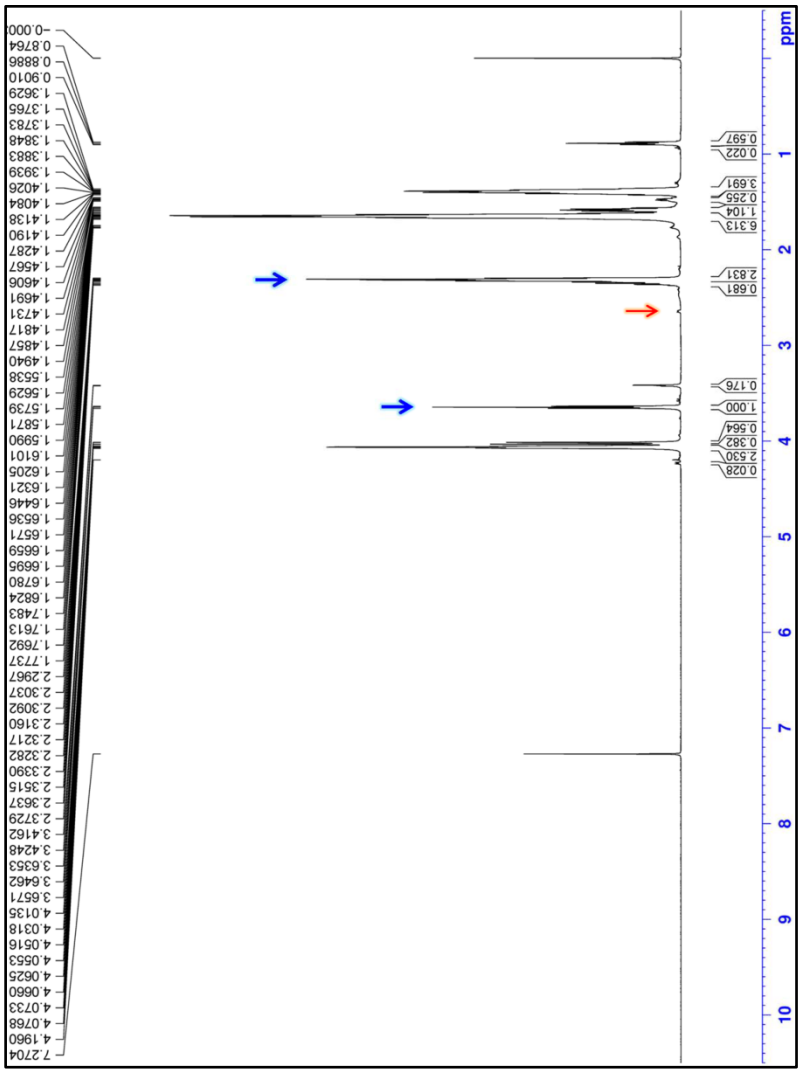

(d) 3.5 h of reaction time

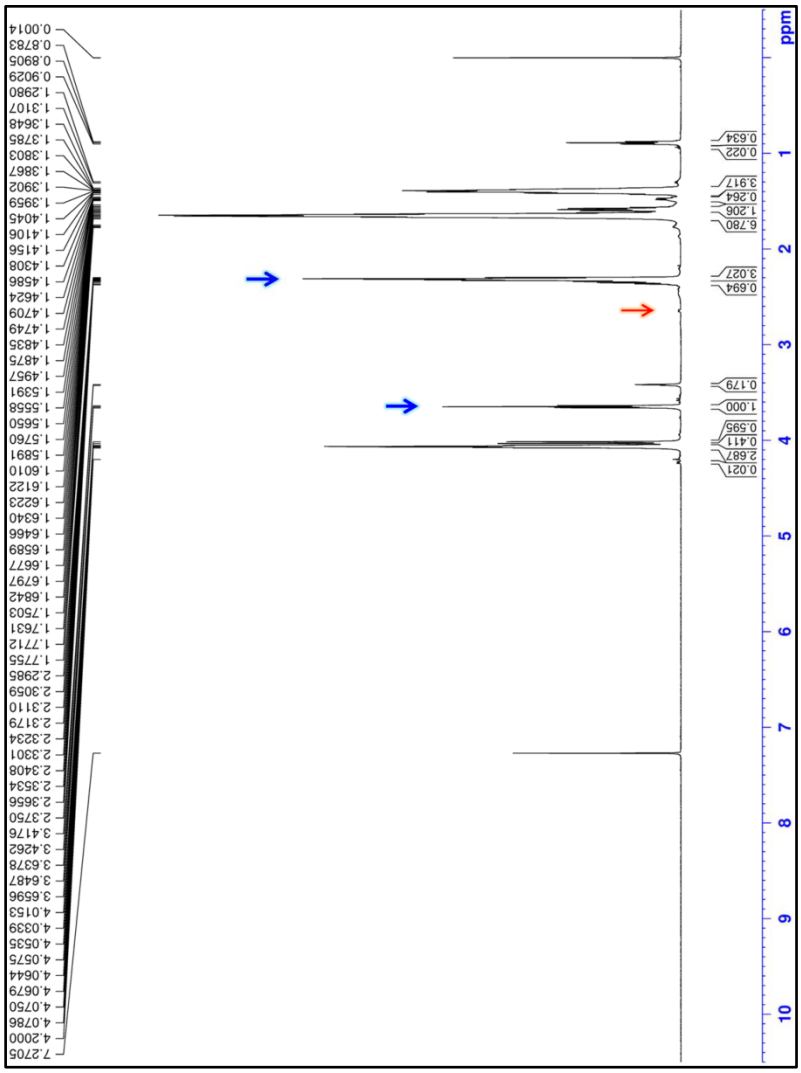

(e) 4 h of reaction time

Figure II-4. ^{1}H NMR raw data of the as-polymerized uncapped USB-SPCL3-3 (before purification) at different reaction times.

Since the resulting as-polymerized USB-SPCLs were transparent viscous liquids (or soft waxy) (see Figure II-5) and their solubilities were similar to that of the unreacted CL monomer, the precipitation and filtering methods commonly used to purify and collect typical PCLs were not available for USB-SPCLs. Other purifying and collecting techniques, such as extraction, chromatography and centrifugation, were also inefficient or unavailable. Indeed, a similar purification problem exists in a commercially available SPCL comprising a TMP core and short branches (PCL-T). The ^{1}H NMR and MALDI-TOF mass data obtained from PCL-T definitely revealed that the PCL-T contained many impurities and undesired structures, such as the unreacted TMP core materials, the unreacted CL monomers, and the cyclic PCLs corresponding to the molar mass of '$n \times MW_{CL}$' (see Figure II-6). These results indirectly illustrated the difficulties associated with the production (including purification and collection) of SPCLs with extremely small branches. Thus, we used a vacuum evaporation technique with heating to purify the as-polymerized USB-SPCLs by eliminating unreacted CL monomers and to collect the purified USB-SPCLs in a high yield. As shown in Figure II-7(a), the unreacted CL monomer peaks in the ^{1}H NMR spectrum of the as-polymerized uncapped USB-SPCL3-3 prior to vacuum purification disappeared after vacuum purification, indicating the successful removal of unreacted CL monomers. The N_{length} values, however, increased from 3.20 to 4.02 after vacuum purification of the as-polymerized uncapped USB-

SPCL3-3 (see Figure II-8), indicating that an undesired reaction occurred in the as-polymerized USB-SPCL3-3 during the vacuum purification. The MALDI-TOF mass spectrum of the as-polymerized uncapped USB-SPCL3-3 prior to vacuum purification shown in Figure II-7(b) displayed the targeted number-average molecular weight and narrow MWD. After vacuum purification, however, the number-average molecular weight and MWD increased, and the undesired mass peaks corresponding to the cyclic PCLs were observed (Figure II-7(b)). These results supported that the well-controlled structure of the uncapped USB-SPCL3-3 collapsed during the vacuum purification by the formation of undesired cyclic PCLs attributed to the backbiting transesterification side reaction. To solve the problems on the vacuum purification of the as-polymerized USB-SPCLs, we completely end-capped the terminal hydroxyl groups in the as-polymerized USB-SPCLs by small acetate groups. End-capping the branches of the as-polymerized USB-SPCLs resulted in the removal of unreacted CL monomers without inducing any changes in the molecular structure of USB-SPCLs during the vacuum purification because the terminal acetate groups inherently blocked the backbiting transesterification side reaction of USB-SPCLs. A schematic diagram of the reaction mechanism associated with the end-capping effects during the vacuum purification of USB-SPCLs is shown in Figure II-9. Finally, we could synthesize molecularly well-defined three- and six-branched

star PCLs with ultra-small-branched segments (DP = 3 or 5), as confirmed by FT-IR, ^{1}H NMR, and MALDI-TOF mass measurements.

From a scientific and commercial perspective, our synthetic protocol via manipulating monomer-to-core ratio, adjusting monomer-to-polymer conversion, end-capping the terminal hydroxyl groups, and vacuum purification offers a promising method for the production of USB-SPCLs with a precisely controlled architecture and a high yield exceeding 93%. Furthermore, this method is straightforward (pilot-scale pseudo-one-pot process) and enables the accurate analysis and interpretation of the structure−property relationships in PCLs with extremely small branches.

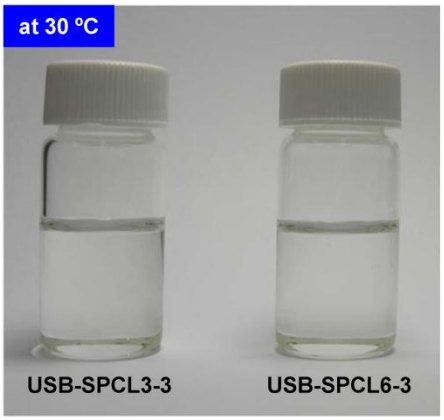

Figure II-5. Images of USB-SPCL3-3 and USB-SPCL6-3 at room temperature.

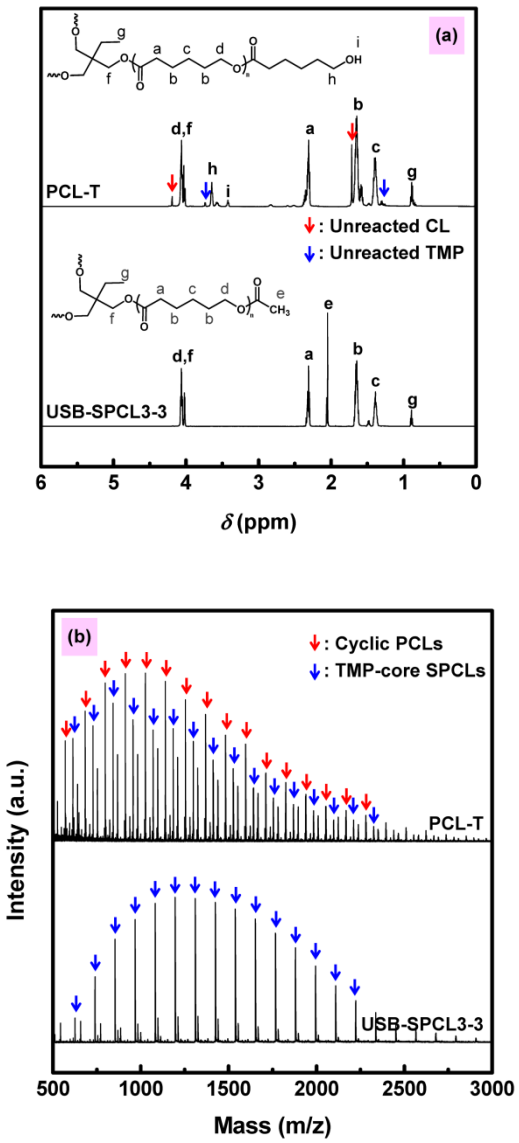

Figure II-6. (a) ^{1}H NMR spectra of PCL-T and USB-SPCL3-3 and (b) MALDI-TOF mass spectra of PCL-T and USB-SPCL3-3.

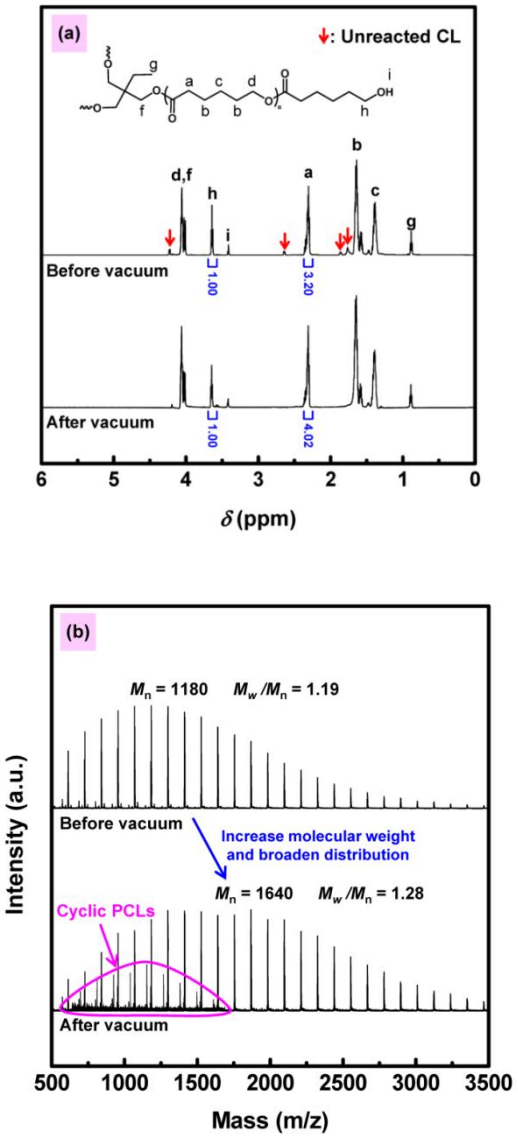

Figure II-7. (a) ^{1}H NMR spectra of the as-polymerized uncapped USB-SPCL3-3 before and after vacuum purification. (b) MALDI-TOF mass spectra of the as-polymerized uncapped USB-SPCL3-3 before and after vacuum purification.

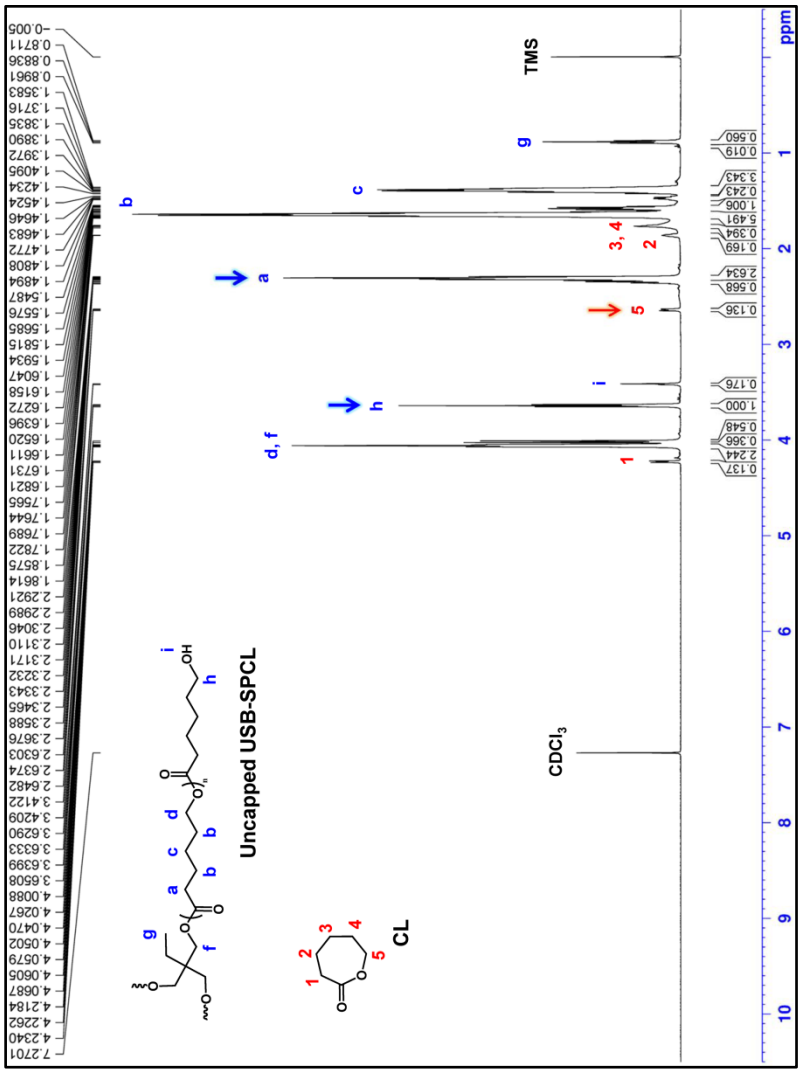

(a) Before vacuum purification

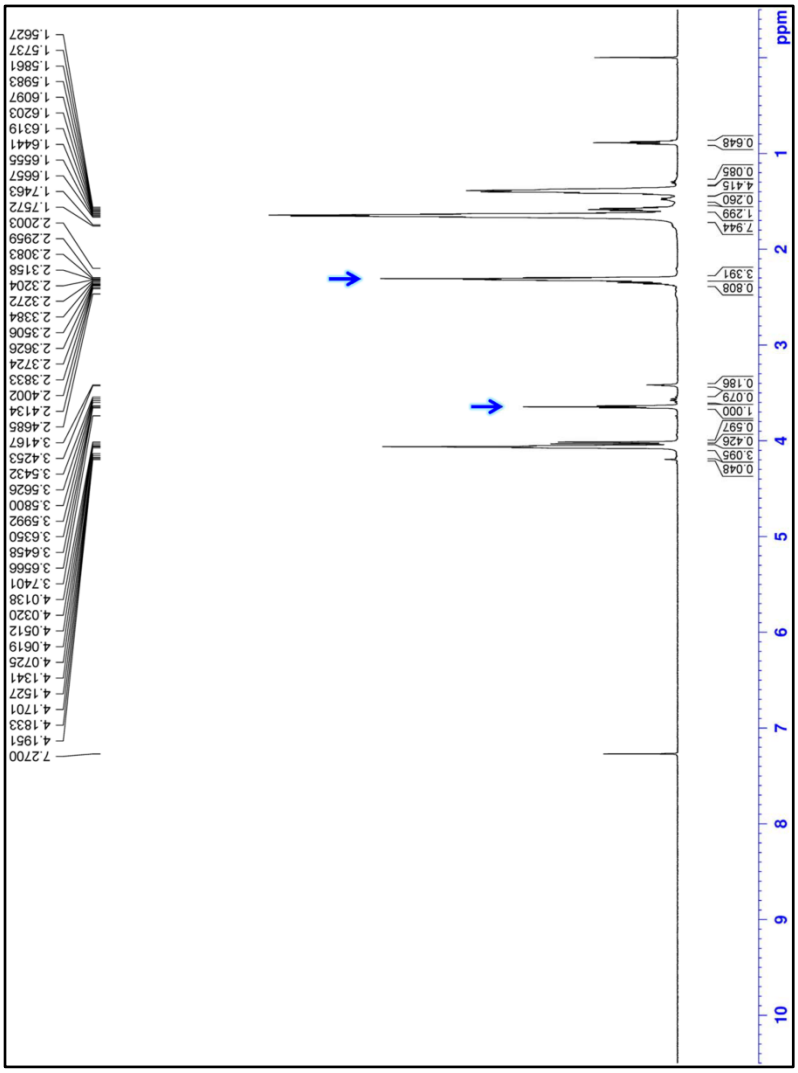

(b) After vacuum purification

Figure II-8. ^{1}H NMR spectra of the as-polymerized uncapped USB-SPCL3-3 (a) before and (b) after vacuum purification.

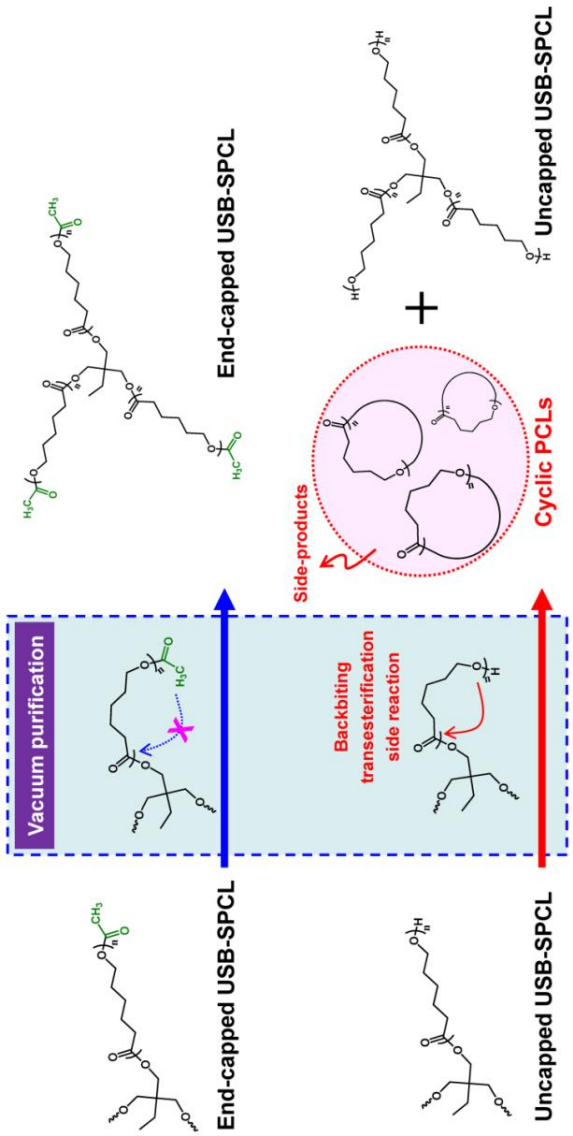

Figure II-9. Schematic diagram showing the reaction mechanism associated with the end-capping effects during the vacuum purification of USB-SPCLs.

II-3-2. Crystallization behaviors of USB-SPCLs

The DSC 2nd heating thermograms of all USB-SPCLs exhibited broad double-melting peaks, as shown in Figure II-10(a). The low-temperature endotherm of USB-SPCLs corresponded to the melting of the original crystals formed during the DSC 1st cooling process, and the high-temperature endotherm of USB-SPCLs resulted from the melting of the recrystallized crystals formed during the DSC 2nd heating process.[9,10] The exotherm corresponding to the recrystallization of USB-SPCLs during the DSC 2nd heating process was hidden under the double endotherm peaks.[9,10] By contrast, LPCL1-10 (with a total molecular weight similar to that of USB-SPCL3-3) and SPCL3-10 (with the same number of branched segments as USB-SPCL3-3) exhibited sharp single-melting peak at higher temperature (> 45 ℃), as shown in Figure II-10(b). These results suggested that the extremely small branched segments hindered the molecular packing of USB-SPCLs. Moreover, the crystallization behaviors of USB-SPCLs appeared to depend on not the molecular weight and the number of branched segments but the branched segment length. Choi et al. reported that the defects among free chain ends disrupted the orderly folding pattern of the crystals and reduced interchain cooperativity.[11] Hence, the apparent end group concentrations of USB-SPCLs were calculated based on the number of branched segments per molecule divided by the number-average molecular

weight.[12] The end group concentration values increased with decreasing N_{length} and with increasing N_{number}, and the order was USB-SPCL3-5 (14.22×10^{-4}) < USB-SPCL6-5 (16.62×10^{-4}) < USB-SPCL3-3 (22.90×10^{-4}) < USB-SPCL6-3 (24.29×10^{-4}). The values obtained from LPCL1-10 and SPCL3-10, on the other hand, were 8.13×10^{-4} and 8.11×10^{-4}, respectively. The end group concentration values for USB-SPCLs were quite higher than those for LPCL1-10 and SPCL3-10 because USB-SPCLs had extremely small branches. This result supported that low melting temperatures and broad double-melting peaks of USB-SPCLs were attributed to their high end group concentrations. Additionally, USB-SPCLs were thought to have low crystallizability, small crystal size, and broad crystallite size distribution because their high end group concentrations disturbed the crystallization of USB-SPCLs due to a higher degree of hindrance in the chain ordering by increasing the end group concentration.[11] Figure II-10(c) revealed that the melting temperatures of USB-SPCLs at the maximum endotherm intensity were inversely proportional to the end group concentration values. In particular, USB-SPCL3-3 and USB-SPCL6-3, which had higher end group concentrations, showed lower melting temperatures than the others. Thus, USB-SPCL3-3 and USB-SPCL6-3 were liquids, even at room temperature (Figure II-5).

The effects of the extremely small branched architecture (with high end group concentration) on the ordered chain arrangement and packing of USB-SPCLs were explored in greater detail by analyzing the crystallization parameters. The crystallization parameters of USB-SPCLs were obtained from the crystallization exotherms during non-isothermal crystallization at a cooling rate of −5 ℃ min^{-1} (Figure II-10(d)). The crystallization parameters correspond to the maximum peak temperature, T_p, the temperature at the intercept between the tangents to the baseline and to the high-temperature side of the curve, T_c, the initial slope at the inflection point on the high-temperature side of the curve, $|S_i|$, and the peak width at half-height, ΔW.[13,14] A schematic diagram of these four crystallization parameters is shown in the inset in Figure II-10(d). The other crystallization parameters were the enthalpy of crystallization, ΔH_c, and the degree of crystallinity, X_c. All crystallization parameters of USB-SPCLs are listed in Table II-2, including the $T_c - T_p$ values. The T_p, T_c, $|S_i|$, ΔH_c, and X_c values of USB-SPCLs decreased with increasing end group concentration, whereas the $T_c - T_p$ and ΔW values of USB-SPCLs increased with increasing end group concentration. These results indicated that USB-SPCLs with higher end group concentrations had a slow rate of nucleation (low $|S_i|$ value), and the nuclei were created over a wider temperature range. The slow rate of nucleation led to a low overall rate of crystallization (high $T_c - T_p$ value) and a broad crystallite size

distribution (high ΔW value), resulting in a small degree of crystallinity (low X_c). Thus, USB-SPCL6-3 with the highest end group concentration showed the smallest degree of crystallinity (28.2%) among USB-SPCLs, and the crystallization exotherm obtained from USB-SPCL6-3 was extraordinarily broad and low compared to those obtained from other USB-SPCLs, as shown in Figure II-10(d). These crystallization behaviors agreed well with the melting behaviors of USB-SPCLs. On the other hand, the order of the glass transition temperature, T_g, values for USB-SPCLs was USB-SPCL3-3 < USB-SPCL3-5 ≃ USB-SPCL6-3 < USB-SPCL6-5, in disagreement with the order of their end group concentrations (Figure II-10(a) and Table II-2). The T_g values of USB-SPCLs interestingly were proportional to the total molecular weights, regardless of the molecular architecture, such as the number and length of branched segments. Such T_g values of USB-SPCLs appeared to result from their extremely small branches. We are investigating these unique behaviors in detail using dynamic analysis techniques, which will be dealt in our next publications.

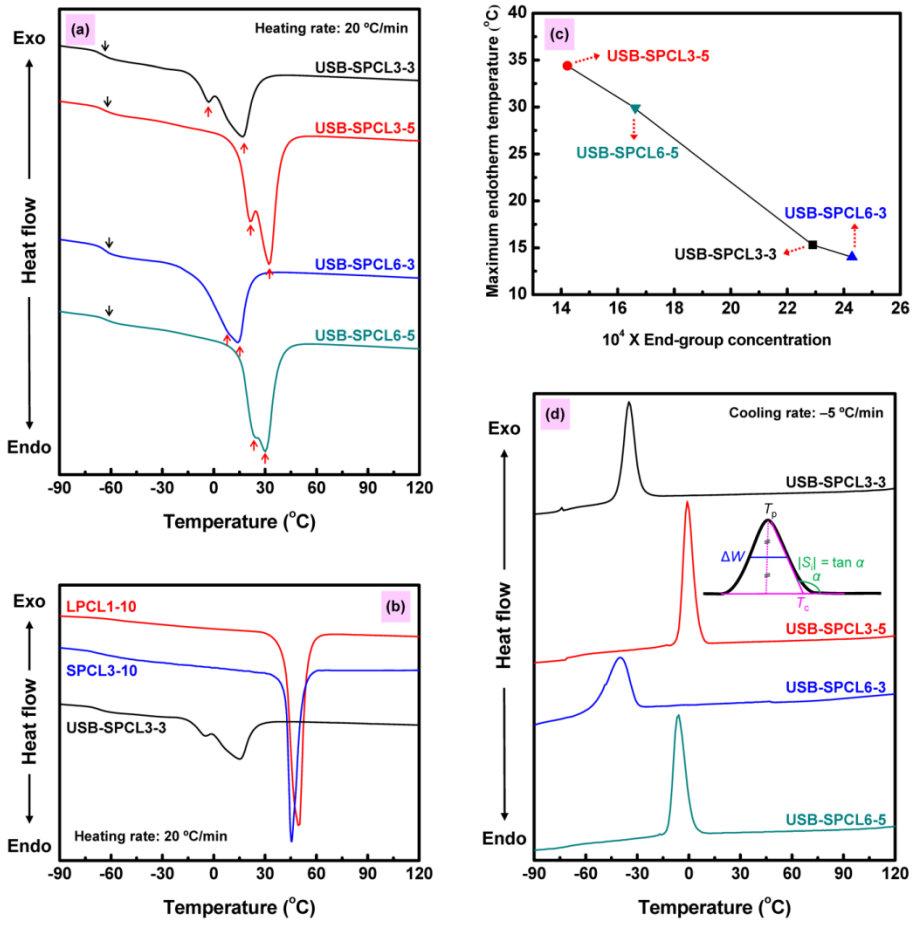

Figure II-10. (a) DSC thermograms of USB-SPCLs during the heating scan. (b) DSC thermograms of LPCL1-10, SPCL3-10, and USB-SPCL3-3 during the heating scan. (c) The maximum endotherm temperature values of USB-SPCLs as a function of the end group concentration. (d) DSC thermograms of USB-SPCLs during the cooling scan.

Table II-2. Thermal properties of USB-SPCLs.

Sample	USB-SPCL3-3	USB-SPCL3-5	USB-SPCL6-3	USB-SPCL6-5
T_c (℃)	−27.2	5.4	−31.6	1.6
T_p (℃)	−34.5	−1.6	−40.9	−6.2
T_c–T_p (℃)	7.3	7	9.3	7.8
ΔH_c (J g^{-1})[a]	39.1	48.3	38.4	47.1
X_c (%)[a]	28.7	35.4	28.2	34.5
$\lvert S_i \rvert$	0.066	0.077	0.026	0.063
ΔW	6.54	6	12.49	6.68
T_g (℃)	−67.2	−64.6	−64.0	−62.7

[a]The ΔH_c value was determined from the peak area of the crystallization exotherm peak, and the X_c value was calculated according to $X_c = (\Delta H_c / \Delta H_c^{\infty}) \times 100$, where ΔH_c^{∞} is the heat of crystallization for a 100% crystalline homo-poly(ε-caprolactone), 136.4 J g^{-1}.[15,16]

II-4. Conclusion

This study provided a facile synthesis of ultra-small-branched star poly(ε-caprolactone)s (USB-SPCLs) using a pilot-scale pseudo-one-pot process. We showed that the monomer-to-core ratio, the monomer-to-polymer conversion, end-capping the terminal hydroxyl groups and vacuum purification should be significantly considered in order to synthesize USB-SPCLs with the well-defined architecture. This synthetic method solved a chronic backbiting problem associated with PCLs and prevented the collapse of USB-SPCL structures during the synthesis and purification process, resulting in precisely controlled USB-SPCLs having mono-dispersed small branches with a high yield. USB-SPCLs were transparent viscous liquids (or soft waxy) even at room temperature, and had low melting temperatures, broad double-melting peaks, and low crystallizability due to the extremely small branches. We believe that the synthetic method introduced here will enable the synthesis of a variety of PCL architectures with extremely small branched segment lengths. This study opens up a route to the development of new types of PCLs with unique properties and to an understanding of the effects of extremely small branched segments on molecular behaviors.

References and Notes

1. Shibita, A.; Takase, H.; Shibata, M. *Polymer* **2014**, *55*, 5407−5416.

2. Nakamura, T.; Chu, X.; Shimasaki, T.; Shibata, M. *J. Colloid Interface Sci.* **2013**, *404*, 8−15.

3. Shibata, M.; Teramoto, N.; Hoshino, K.; Takase, H.; Shibita, A. *J. Appl. Polym. Sci.* **2013**, *130*, 4229−4236.

4. Bilgin, A.; Yağcı, Ç. *Eur. Polym. J.* **2014**, *61*, 240−252.

5. Choi, W.; Chung, J. W.; Kwak, S.−Y. *J. Polym. Sci., Part A: Polym. Chem.* **2015**, *53*, 1134−1142.

6. Choi, J.; Kim, I.−K.; Kwak, S.−Y. *Polymer* **2005**, *46*, 9725−9735.

7. Kricheldorf, H. R.; Berl, M.; Scharnagl N. *Macromolecules* **1988**, *21*, 286−293.

8. Martin, E.; Dubois, P.; Jérôme, R. *Macromolecules* **2000**, *33*, 1530−1535.

9. Rim, P. B.; Runt, J. P. *Macromolecules* **1983**, *16*, 762−768.

10. Lee, Y.; Porter, R. S. *Macromolecules* **1987**, *20*, 1336−1341.

11. Choi, Y. K.; Bae, Y. H.; Kim, S. W. *Macromolecules* **1998**, *31*, 8766−8774.

12. Roovers, J. E. L.; Toporowski, P. M. *J. Appl. Polym. Sci.* **1974**, *18*, 1685−1691.

13. Chen, C.; Fei, B.; Peng, S.; Zhuang, Y.; Dong, L.; Feng, Z. *Eur. Polym. J.* **2002**, *38*, 1663−1670.

14. Chung, J. W.; Son, S.−B.; Chun, S.−W.; Kang, T. J.; Kwak, S.−Y. *J. Polym. Sci., Part B: Polym. Phys.* **2008**, *46*, 989−999.

15. Xu, J.; Shi, W. *Polymer* **2006**, *47*, 5161−5173.

16. Choi, J.; Kwak, S.−Y. *Macromolecules* **2004**, *37*, 3745−3754.

CHAPTER III

TOTAL-MOLECULAR-WEIGHT-DEPENDENT ROUSE DYNAMICS OF ULTRA-SMALL-BRANCHED STAR POLY(*ε*-CAPROLACTONE)S AS A SINGLE COARSE-GRAIN UNIT

III-1. Introduction

The structure–property relationships of polymers have been thoroughly investigated using comparing viscoelastic properties between star-shaped and linear polymers. Kraus et al. first reported that the increase in the viscosity of star polymers with molecular weight did not occur according to a power law, as observed in linear polymers, but instead occurred exponentially.[1] Quack et al. showed that the viscosity of star polymers did not depend on the total molecular weight but only on the molecular weights of individual branched segments.[2] Similar findings were made by Mykhaylyk et al., who observed that the zero-shear-rate viscosity of hydrogenated star polybutadienes was exponentially dependent on the molecular weights of the arms rather than on the total molecular weights of the stars.[3] Acebo et al.

also reported that the viscosity of multiarm star block copolymers (hyperbranched poly(ethyleneimine)-*b*-poly(ε-caprolactone)) increased exponentially as the arm length (or arm molecular weight) of the star block copolymer increased.[4] These phenomena were attributed to the fact that star polymers are not able to reptate as linear polymers because of their central tie point that suppresses the translational motion of the branched segments.[5] Instead, star polymers can relax by contour-length fluctuations of branched segments. This contour-length fluctuation allows the branched segments to retract some distance down the confining tube toward the central tie point and then explore a new path by extending back in another direction.[5,6] Since deep retractions of branched segments in star polymers are not favored entropically and are exponentially unlikely, thus the viscoelastic properties of star polymers depend exponentially on the molecular weights of individual branching segments.[5,6] These studies clearly showed that the dynamics of star polymers were determined by the individual branched length and the central tie point. However, most of these previous studies addressed the dynamic behaviors of star polymers with polymeric large branches. Star polymers with extremely small branches and their dynamic behaviors have not been studied sufficiently although star polymers with extremely small branches are highly attractive due to the ease of control over degradation, low softening point, and good miscibility with other materials, compared with typical star polymers.[7–10] Thus, from both the scientific and industrial point

of view, the various investigations into dynamic phenomena in star polymers with extremely small branches are positively necessary to use these highly attractive advantages in an extremely small branched system.

In this study, we investigated the effects of extremely small branches on the dynamic behavior of a star polymer using well-defined ultra-small-branched star poly(ε-caprolactone)s (USB-SPCLs) as a model system.[11] The glass transition, viscoelasticity, flow activation energy, and longest Rouse relaxation time of USB-SPCLs interestingly depended on total molecular weight regardless of molecular architecture parameters, such as the number and length of branched segments. Moreover, these dynamic phenomena of USB-SPCLs followed the modified Mark–Houwink power law and the Bueche-modified Rouse model for unentangled linear polymers rather than traditional star polymer models that depend exponentially on the individual branched molecular weight. This suggests that a whole USB-SPCL molecule acts as a dynamically-equivalent single coarse-grain unit with one Rouse-segmental motion. These results broaden and deepen the understanding of the molecular dynamic behaviors of star polymers with extremely small branches, and further this enables new applications for star polymers as well as more complex branched polymers with unique dynamic properties.

III-2. Experimental Section

III-2-1. Materials

USB-SPCLs were synthesized by ring-opening polymerization (ROP) of ε-caprolactone (CL) monomers via manipulating the monomer-to-core ratio, adjusting the monomer-to-polymer conversion, end-capping the terminal hydroxyl groups, and vacuum purification in a facile pseudo-one-pot bulk process without organic solvents.[7,8] Eight different USB-SPCLs were synthesized in which the number of branches, N_{number}, and the average lengths of the individual branches (the average DP per branch) , N_{length}, were varied. These polymers are denoted as USB-SPCLN_{number}-N_{length}, and the specific polymers treated here are named USB-SPCL3-3 (where N_{number} = 3 and N_{length} = 3), USB-SPCL3-5 (N_{number} = 3 and N_{length} = 5), USB-SPCL6-3 (N_{number} = 6 and N_{length} = 3), and USB-SPCL6-5 (N_{number} = 6 and N_{length} = 5). The chemical structures of the synthesized USB-SPCLs, including N_{number} and N_{length}, were analyzed using ^{1}H nuclear magnetic resonance (NMR) spectroscopy. The number-average molecular weights, M_n, the weight-average molecular weights, M_w, and the molecular weight distributions (MWDs) were measured using matrix-assisted laser desorption/ionization time-of-flight mass spectrometry (MALDI-TOF-MS). More detailed information about the syntheses and general characterizations of USB-SPCLs

are provided in our previous publications.[7,8]

III-2-2. Characterization

The glass transitions of USB-SPCLs were measured by differential scanning calorimetry (DSC) using a Netzsch DSC 200 F3 with a heating rate of 20 ℃ min^{-1} over the temperature range of −110 to 140 ℃ under a nitrogen atmosphere. The glass transition temperature, T_g, was determined in each case according to the inflection point in the second DSC curve. The viscoelastic behaviors of USB-SPCLs were observed by dynamic mechanical spectrometry using a stress-controlled rheometer (TA Instruments Inc. AR2000). The AR2000 was operated in a cone-and-plate geometry with a 1° angle and a 60-mm-diameter cone. The gap between the cone and the plate was 80 μm in all measurements. Dynamic frequency sweeps were performed over an angular frequency range of 0.5−100 rad s^{-1} and the temperature range 30−90 ℃, measured in 10 ℃ intervals. The strain values were determined using a dynamic strain sweep to lie within the linear viscoelastic region.

III-3. Results and Discussion

III-3-1. Glass transition behaviors of USB-SPCLs

Three- and six-branched USB-SPCLs were prepared with various number of CL repeating units (DP = 3 or 5) in each individual branch initiated from trimethylolpropane (TMP) and dipentaerythritol (DPTOL) cores (Figure III-1). From ^{1}H NMR and MALDI-TOF-MS measurements (Table III-1), it was confirmed that the USB-SPCLs were well synthesized with the desired N_{number}, N_{length}, and narrow MWDs ($M_w/M_n \leq 1.2$). Then, the glass transitions of the resulting USB-SPCLs were observed through DSC. As shown in Figure III-2(a), the lowest T_g was recorded for USB-SPCL3-3 (−67.2 ℃), followed by similar intermediate values for USB-SPCL3-5 (−64.6 ℃) and USB-SPCL6-3 (−64.0 ℃), and finally the highest T_g for USB-SPCL6-5 (−62.7 ℃). It is generally accepted that a star polymer with a greater number of branches is known to yield a smaller pervaded volume ($V \approx R^3$) and faster molecular mobility at a given total molecular weight.[12,13] In addition, Roovers et al. reported that the T_g value of a star polymer decreased as the end-group concentration increased due to an increase in the free volume.[14,15] Thus, the end-group concentrations of USB-SPCLs were evaluated by determining 'N_{number}/M_n'.[15] Among USB-SPCLs with the same N_{number}, Figure III-2(a) shows that USB-SPCLs with the shorter branched length had

higher end-group concentrations than USB-SPCLs with the longer branched length, and, indeed, that USB-SPCLs with the higher end-group concentrations had lower T_g values than USB-SPCLs with the lower end-group concentrations. These results were consistent with the report by Roovers. However, USB-SPCL3-3 displayed lower T_g value than USB-SPCL6-3, even though the end-group concentration of USB-SPCL3-3 is lower than that of USB-SPCL6-3. USB-SPCL3-5 also exhibited a lower T_g value than USB-SPCL6-5 despite the lower end-group concentration for USB-SPCL3-5 compared with that of USB-SPCL6-5. Moreover, USB-SPCL3-5 and USB-SPCL6-3 exhibited similar T_g values despite the end-group concentration of USB-SPCL6-3 being about 70% greater than that of USB-SPCL3-5 and despite USB-SPCL6-3 being expected to form a smaller pervading volume due to a high N_{number} and a low N_{length} compared with USB-SPCL3-5. These unusual results revealed that the 'traditional' relationship between glass transition behavior and end-group concentration apparently does not apply to our SPCL system with extremely small branches. Instead, Figure III-2(b) shows interestingly that the glass transition behaviors of USB-SPCLs depend on their total molecular weights, not on the molecular architecture features such as N_{number} and N_{length}. These results revealed that the extremely small branches in USB-SPCLs cause a new type of molecular dynamic that differs from that of typical star polymers. Actually, Kisliuk et al. reported that star polybutadiene (PB) with unentangled and relatively large

arm length (1,950 g/mol) exhibited unexpected behaviors, which were T_g, segmental and fast dynamics depending on the total molecular weight but not on its molecular architecture, yet this report did not show the explanation for why such dynamics of PB are manifested.[16] Hence, we investigated the dynamics of USB-SPCLs in more detail by observing their viscoelastic behaviors and molecular motions.

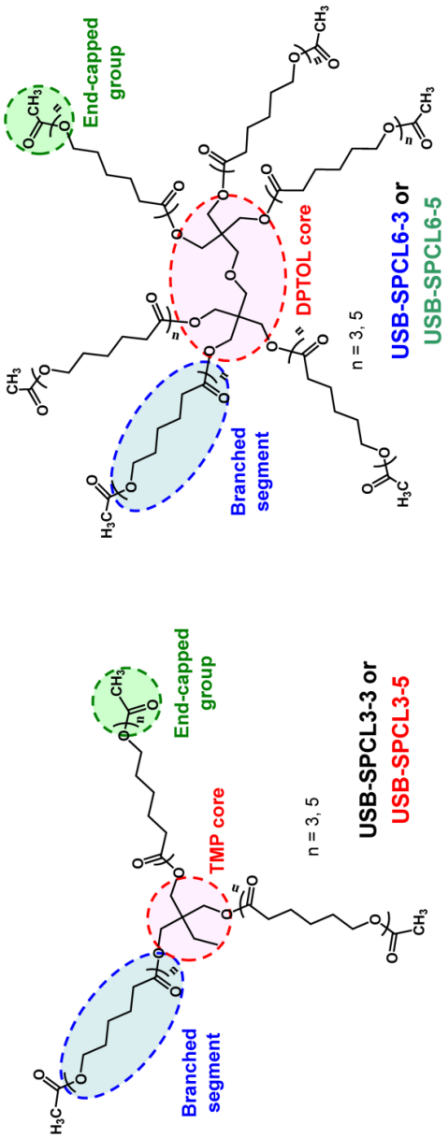

Figure III-1. Molecular architectures of USB-SPCLs that have TMP or DPTOL as the core.

Table III-1. General characteristics of USB-SPCLs.

Sample	N_{number}	N_{length}	M_n (g mol^{-1})	M_w (g mol^{-1})	MWD
USB-SPCL3-3	2.94	3.09	1310	1600	1.22
USB-SPCL3-5	3.00	5.06	2110	2600	1.23
USB-SPCL6-3	6.06	3.06	2470	2640	1.07
USB-SPCL6-5	6.06	5.20	3610	3930	1.09

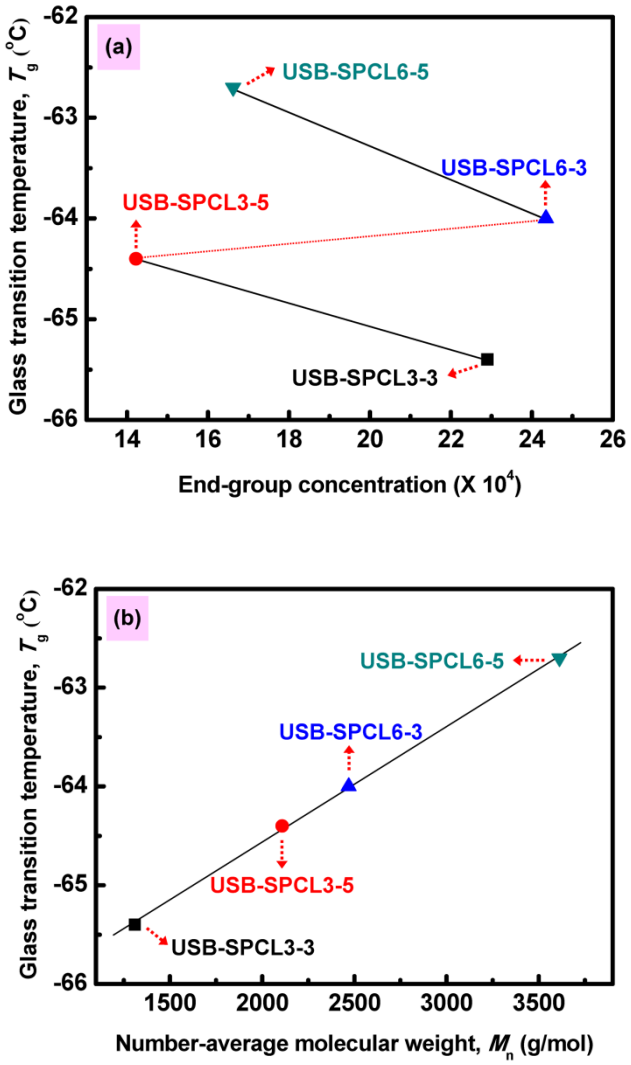

Figure III-2. The T_g values of USB-SPCLs as a function of (a) the end-group concentration or (b) the total M_n.

III-3-2. Viscoelastic behaviors and molecular motions of USB-SPCLs

Figure III-3(a) shows the loss tangent, tan δ, curves for USB-SPCLs in a given angular frequency, ω, range at the reference temperature T_r = 60 ℃. In general, purely viscous behavior (Newtonian viscous liquid) exhibits infinite tan δ and purely elastic behavior (Hookean elastic solid) exhibits zero tan δ.[17−19] As shown in Figure III-3(a), the order of the tan δ curves for USB-SPCLs from the upper-right to the lower-left was USB-SPCL3-3 > USB-SPCL3-5 ≃ USB-SPCL6-3 > USB-SPCL6-5. The tan δ curves for USB-SPCLs in the other temperature range (30−90 ℃) showed the same trends (data not shown). Thus, USB-SPCL3-3 was thought to be the most viscous and USB-SPCL6-5 was thought to be the least viscous among them. USB-SPCL3-5 and USB-SPCL6-3 showed intermediate viscous properties with a similar tan δ values. Interestingly, this order of the tan δ curves for USB-SPCLs was reversely consistent with the order for their total molecular weights. This indicated that the viscoelasticity of USB-SPCLs depended on their total molecular weights, regardless of the structural factors of USB-SPCLs such as N_{number} and N_{length}. Such total-molecular-weight-dependent viscoelasticity of USB-SPCLs is a very distinctive observation when considering that the viscoelasticity of typical star polymers with relatively long branches has a dependency on the length of branch.[1−6] Thus, the degree

of viscoelasticity for USB-SPCLs was investigated using modified double-logarithmic Cole−Cole plots of the shear loss modulus (viscous behavior), $G''(\omega)$, versus the shear storage modulus (elastic behavior), $G'(\omega)$, in a given frequency range at temperatures varying between 30 and 90 ℃ (Figure III-3(b)). The modified Cole−Cole plots of all USB-SPCLs were located above and to the left of a 45°-sloped straight line drawn at $G''(\omega) = G'(\omega)$, that is, $G''(\omega) > G'(\omega)$, indicating that all USB-SPCLs exhibited a viscous response-dominant feature.[20−22] The modified Cole−Cole plots of each USB-SPCL did not vary with temperature in the range measured and the slopes for these plots were 0.5, indicating that structural changes of USB-SPCL, such as melting, crystallization and aggregation, did not occur in this temperature range.[23] These results from Cole−Cole plots were considered that USB-SPCLs had terminal flow behaviors from room temperature.[20−23] In addition, the order of the modified Cole−Cole plots from the upper-left to the lower-right was USB-SPCL3-3 > USB-SPCL3-5 ≃ USB-SPCL6-3 > USB-SPCL6-5, following the reverse order of their total molecular weights. This showed that the degree of viscoelasticity of USB-SPCLs in the terminal flow condition also followed the total molecular weights regardless of the structural factors, consistent with the results from the tan δ curves for USB-SPCLs.

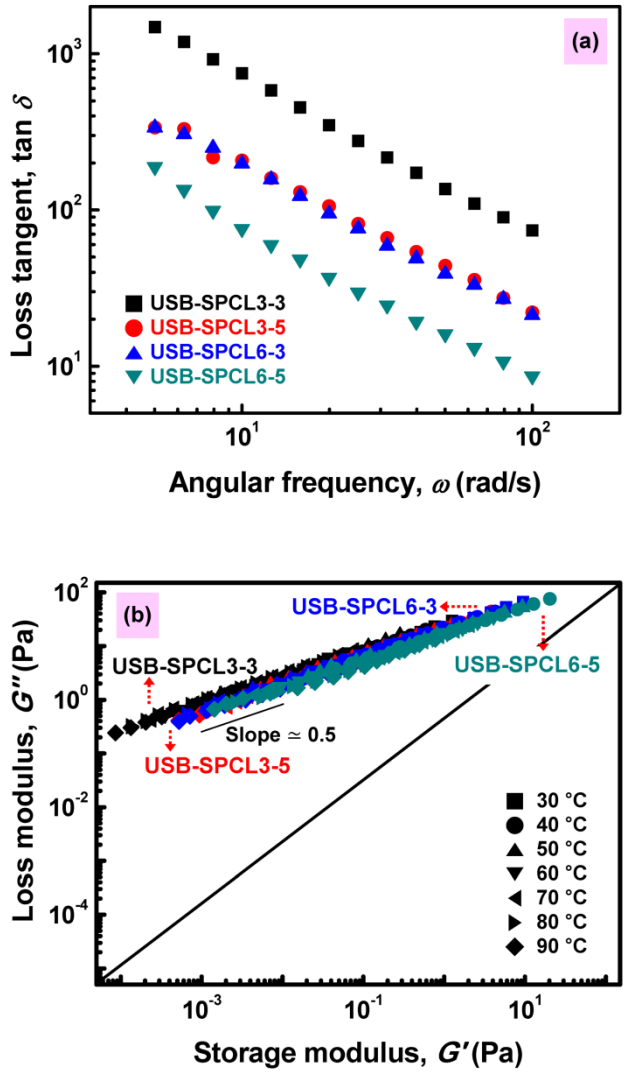

Figure III-3. (a) The tan δ values of USB-SPCLs as a function of ω at the reference temperature T_r = 60 ℃. (b) Modified Cole–Cole plots: logarithmic plots of $G''(\omega)$ versus $G'(\omega)$ for USB-SPCLs in a given frequency range at various temperatures.

The viscoelastic master curves for USB-SPCLs were obtained from the viscoelastic curves of USB-SPCLs in a given frequency range at various temperatures (see Figure III-4) using the time−temperature superposition (TTS) principle over the entire temperature range measured.[23] As shown in Figure III-5, all of the $G'(\omega)$ or $G''(\omega)$ data for USB-SPCLs in the measured temperature range were superposed fairly well at the reference temperature T_r = 60 ℃ using only horizontal shift factors, a_T, that were obtained based on the zero-shear-rate viscosity at each temperature divided by the zero-shear-rate viscosity at the reference temperature $(\eta_0(T)/\eta_0(T_r))$. All of the viscoelastic master curves for USB-SPCLs increased linearly with increasing frequency, and the superposed $G'(\omega)$ curves were observed to remain below the superposed $G''(\omega)$ curves without crossover over the entire frequency range. Moreover, the slopes of the superposed $G'(\omega)$ and $G''(\omega)$ curves versus the reduced angular frequency, $a_T\omega$, were determined to be 2 and 1, respectively. Therefore, it was considered that USB-SPCLs exhibited unentangled chain dynamics even at room temperature.[20−23]

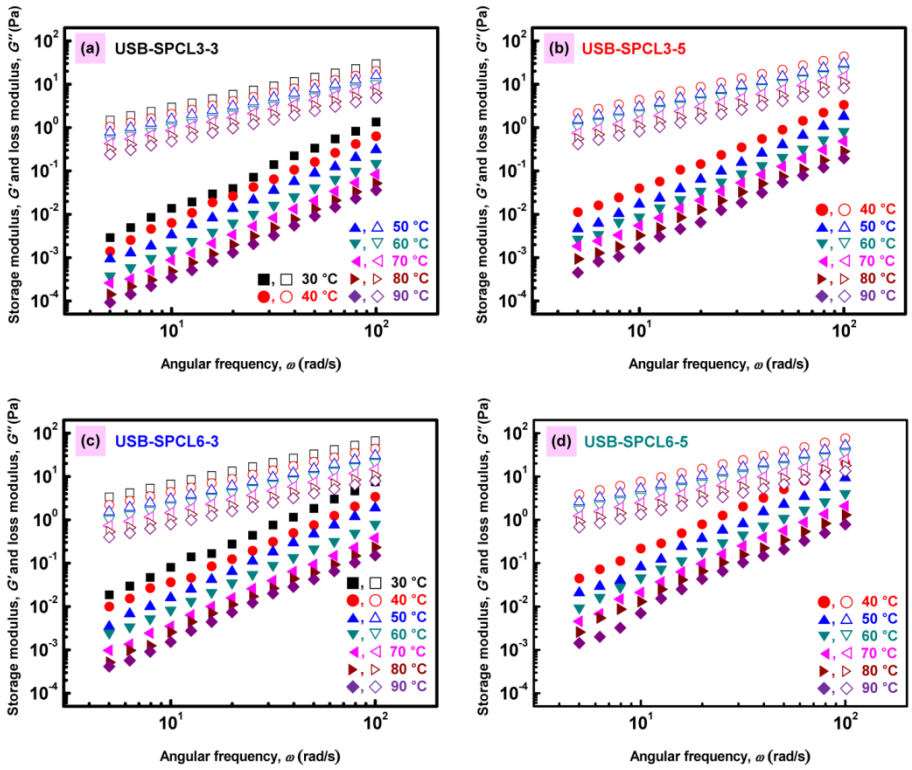

Figure III-4. The viscoelastic curves of dynamic moduli $G'(\omega)$ (filled symbol) and $G''(\omega)$ (open symbol) as a function of ω at different temperatures for (a) USB-SPCL3-3, (b) USB-SPCL3-5, (c) USB-SPCL6-3, and (d) USB-SPCL6-5.

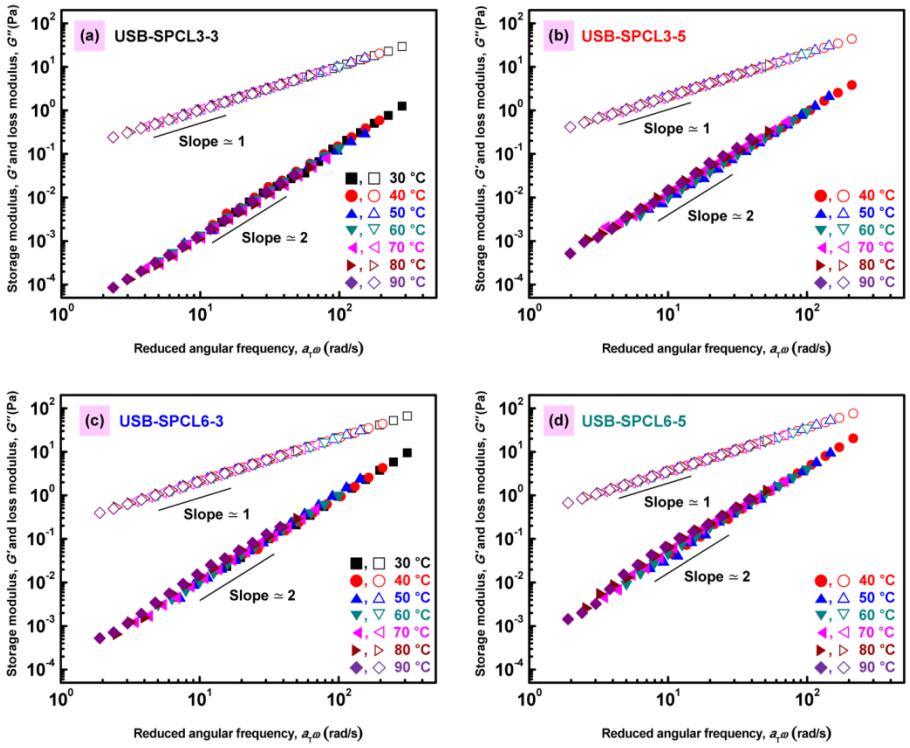

Figure III-5. Viscoelastic master curves plotting the dynamic moduli $G'(\omega)$ (filled symbol) and $G''(\omega)$ (open symbol) as a function of $\alpha_T\omega$ at 60 ℃, for (a) USB-SPCL3-3, (b) USB-SPCL3-5, (c) USB-SPCL6-3, and (d) USB-SPCL6-5.

The viscoelastic behaviors of USB-SPCLs were investigated in further detail by separating viscosity and elasticity. The complex viscosities, η^*, of all USB-SPCLs at a given temperature were independent of the angular frequency (Figure III-6), indicating a Newtonian fluid without chain entanglement.[24] According to the limiting values of the dynamic moduli ($\eta_0 = \lim_{\omega \to 0} G''(\omega)/\omega$), the ω-independent η^* values of USB-SPCLs could change into the zero-shear-rate viscosity, η_0.[25,26] Fetters et al. described that the η_0 value of a star polymer depends on the molecular weight of an individual branched segment without considering the total molecular weight and the number of branched segments, following Equation (1):[25,27,28]

$$\eta_0 \propto \left(\frac{M_b}{M_e}\right)^b \exp\left(v' \frac{M_b}{M_e}\right) \qquad (1)$$

where M_b is the molecular weight of an individual branched segment, M_e is the entanglement molecular weight, and b and v' are parameters on the order of 1. In Equation (1), the η_0 values of star polymers are determined by M_b, irrespective of their total molecular weights and N_{number}, and they increase "exponentially" with increasing M_b (see Figure III-7). However, as shown in Figure III-8(a), USB-SPCLs yielded different η_0 values at a given temperature even if USB-SPCLs had the same M_b (same N_{length}); USB-SPCL3-3 exhibited a lower η_0 value than USB-SPCL6-3, and USB-SPCL3-

5 displayed a lower η_0 value than USB-SPCL6-5. These results reveal that the η_0 values of USB-SPCLs did not follow Equation (1). Instead, the η_0 values of USB-SPCLs increased linearly with increasing total M_w at a given temperature (see Figure III-8(b)). Since total-molecular-weight-dependent η_0 behaviors of polymers are generally represented in the dynamics of typical linear polymers, the resulting η_0 values of USB-SPCLs were applied to the modified Mark–Houwink equation (Mark–Houwink–Sakurada/Berry–Fox relation) for linear polymer melts, as follows:[25–30]

$$\eta_0 = K{M_w}^a \qquad (2)$$

where K and a are empirical parameters obtained from the slope and intercept of the power law plot, respectively. In general, the a value is 3.4−3.6 for M_w greater than M_e and 1−2.5 for M_w less than M_e. In the case of USB-SPCLs, the a values at a given temperature were determined to be 1.12−1.62 without considering their molecular architecture, suggesting that the η_0 behaviors of USB-SPCLs can be represented by the dynamics of typical unentangled linear polymers. This indicated the total molecular weights of USB-SPCLs were smaller than M_e, in good agreement with the results from the viscoelastic master curves for USB-SPCLs. Therefore, the combined results from the zero-shear-rate viscosity and modified Mark–Houwink equation analyses showed that the viscosity behaviors for USB-SPCLs did not follow the model

for a typical star polymer but instead followed the model for an unentangled linear polymer, even though USB-SPCLs are star polymers. These unusual dynamics of USB-SPCLs associated with the unentangled-linear-polymer viscosity behaviors were thought to be attributable to the extremely small branches in USB-SPCLs, and thereby the dynamic behaviors of USB-SPCLs can be explained by the Rouse model for linear polymers.

The elastic properties of USB-SPCLs were investigated by the elasticity coefficient and steady-state compliance using the following equations in the Rouse model:[12,31–33]

$$A_G = \lim_{\omega \to 0} \frac{G'(\omega)}{\omega^2} \qquad (3)$$

$$J_e{}^0 = \lim_{\omega \to 0} \frac{G'(\omega)}{G'(\omega)^2 + G''(\omega)^2} = \frac{A_G}{{\eta_0}^2} \qquad (4)$$

where A_G is the elasticity coefficient and $J_e{}^0$ is the steady-state compliance, corresponding to the permanent elasticity. Figure III-8(c) shows that the logarithmic A_G and $J_e{}^0$ values of USB-SPCLs at the reference temperature (T_r = 60 ℃) depended linearly on the total M_w, as represented in typical linear polymers, regardless of the molecular architecture parameters such as N_{number} and N_{length}. The plots at other temperatures had similar curves (data not shown). According to the Bueche-modified Rouse model for linear

polymers, the slope value of A_G versus total M_w curve exhibits 3−4.3 for an unentangled linear polymer and 7.5 for an entangled linear polymer.[32,33] In the case of USB-SPCLs, the slopes of A_G versus total M_w curves at a given temperature were 3.38−4.18, indicating their unentangled-linear-polymer behaviors of A_G. In addition, the J_e^0 curves for USB-SPCLs were proportional to total M_w without affecting their branched segments. This indicated that USB-SPCLs exhibited unentangled J_e^0 behaviors, whereas the J_e^0 curves for entangled linear polymers are independent of M_w.[12,34,35] Thus, we thought that the elasticity of USB-SPCLs also followed the Rouse dynamic behaviors of unentangled linear polymers.

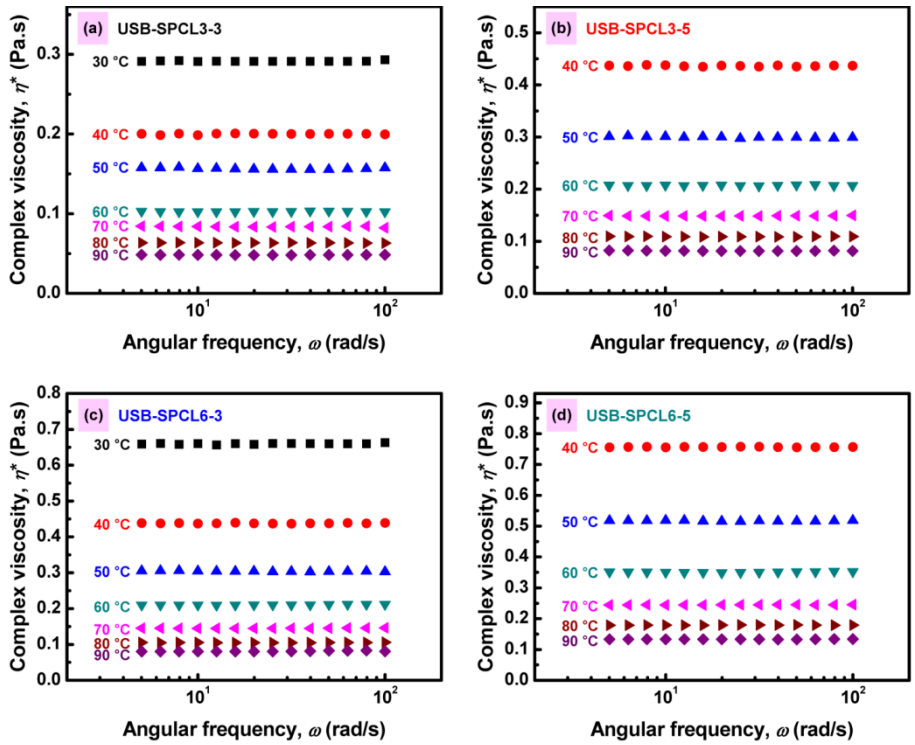

Figure III-6. The η^* values as a function of ω at different temperatures for (a) USB-SPCL3-3, (b) USB-SPCL3-5, (c) USB-SPCL6-3, and (d) USB-SPCL6-5.

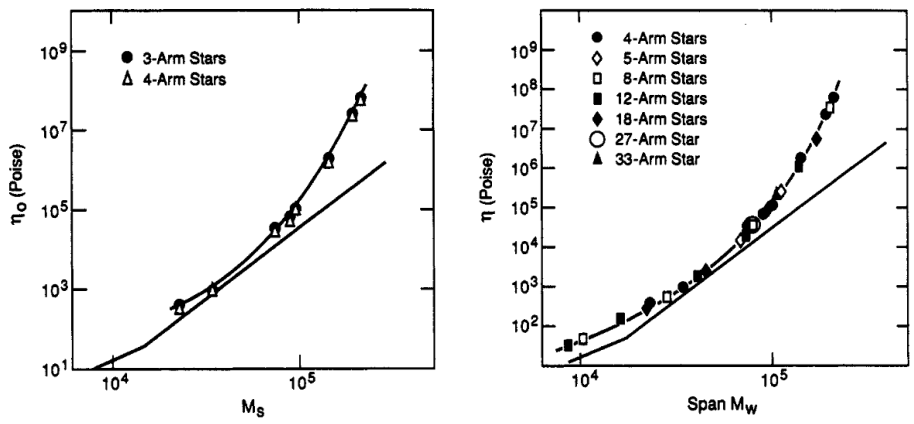

Figure III-7. Logarithmic plot of the viscosity of star polymers with functionalities of three or more versus span molecular weight, M_s. M_s is the molecular weight of the longest linear span in the molecule and is equal to twice the arm molecular weight of a star. The lower line applies to linear polymers. The difference among the viscosities of star polymers with different arm number is hardly noticeable.[25]

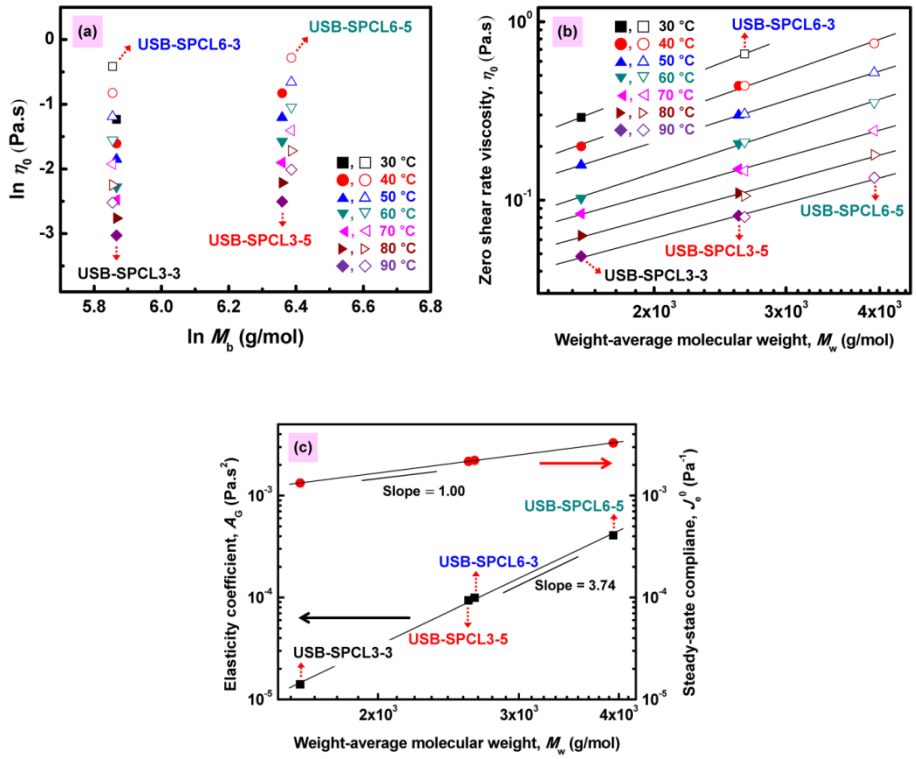

Figure III-8. (a) Logarithmic plots of η_0 versus M_b for USB-SPCLs at various temperatures. (b) Logarithmic plots of η_0 versus total M_w for USB-SPCLs at various temperatures. (c) Logarithmic plots of A_G and J_e^o versus total M_w for USB-SPCLs at the reference temperature T_r = 60 ℃.

The molecular motions of USB-SPCLs were investigated to demonstrate their unusual total-molecular-weight-dependent Rouse dynamic behaviors through their flow activation energies and longest Rouse relaxation times. Figure III-9(a) shows the plots of $\ln \eta_0$ versus 1000/T for each of USB-SPCLs. In Figure III-9(a), the measured temperature ranges were far above T_g (> T_g + 100 ℃), and the plots were quite good straight lines. The flow activation energies of USB-SPCLs could therefore be derived from the slopes of these plots using the following Arrhenius equation:[36,37]

$$\eta_0 = A \exp\left(\frac{E_a}{RT}\right) \qquad (5)$$

where E_a is the flow activation energy, R is the gas constant, T is the absolute temperature, and A is a constant. The flow activation energy is the energy required to overcome the potential barrier to flow and provides information about the cooperative diffusional motion of polymer segments.[38–40] The order of the determined E_a values for USB-SPCLs was USB-SPCL6-5 (33.1 kJ mol^{-1}) > USB-SPCL6-3 (32.9 kJ mol^{-1}) > USB-SPCL3-5 (31.8 kJ mol^{-1}) > USB-SPCL3-3 (28.0 kJ mol^{-1}), indicating that the cooperative diffusional motions of USB-SPCL segments became more rapid as their total molecular weights decreased. In addition to the flow activation energy, the longest Rouse relaxation time, which is associated with the coordinated motion of the whole polymer molecule, of each USB-SPCL was obtained by multiplying the

viscosity and elasticity, as follows:[12,32,41-43]

$$\tau_R \equiv \eta_0 \cdot {J_e}^0 \qquad (6)$$

where τ_R is the longest Rouse relaxation time. As shown in Figure III-9(b), the τ_R values of USB-SPCLs were linearly proportional to the total M_w at a given temperature, and the slopes of τ_R curves were determined to be between 2.25 and 2.56, corresponding to the a+1 values derived from the relationships mentioned above for unentangled linear polymers: $\eta_0 \propto {M_w}^a$ and ${J_e}^0 \propto M_w$. Such total-molecular-weight-dependent relaxation of a whole USB-SPCL molecule suggests that the coordinated motion of a whole USB-SPCL molecule was not affected by the individual branched motion. It was thought that the individual branches in a USB-SPCL molecule were dynamically equivalent and that a whole USB-SPCL molecule moved with a simple uni-motion, because the extremely small branches on the scale of 20–40 atoms were smaller than the Kuhn length of their linear counterparts and existed within one dynamic unit.[44] If several dynamic boundaries were involved in the individual branch and the branches in a USB-SPCL molecule were not dynamically equivalent, USB-SPCL might show the molecular motion depending on the branching length not the total molecular weight, as is represented in typical star polymers.[45] Thus, we presumed that a whole USB-SPCL molecule acts as a dynamically-equivalent unit, *i.e.*, a single

coarse-grain unit. In our presumption, the interesting dynamic phenomena of USB-SPCL can be demonstrated by comparison with a typical star polymer with polymeric large branched segments. In Figure III-10, the typical star polymer has several branches, conceptually divided into multiple coarse-grain units, each of which is composed of several monomeric segments. The monomeric segments in a coarse-grain unit are dynamically equivalent and do not represent a valid dynamic motion, and the coarse-grain unit displays an individual Rouse-segmental motion. Thus, the individual branched motion in the typical star polymer is determined by the assembly of individual Rouse-segmental motions, and hence the whole molecular motion of the typical star polymer depends on the several branches moving individually of each other with one central tie point. On the other hand, an individual branch of USB-SPCL is extremely small with only 20–40 atoms and is composed of several monomeric segments without a valid dynamic unit. Instead, a whole USB-SPCL molecule is regarded as a single coarse-grain unit with dynamically-equivalent branches. Therefore, the whole molecular motion of USB-SPCL represents one Rouse-segmental motion of a single coarse-grain unit, resulting in the total-molecular-weight-dependent Rouse dynamics of USB-SPCL.

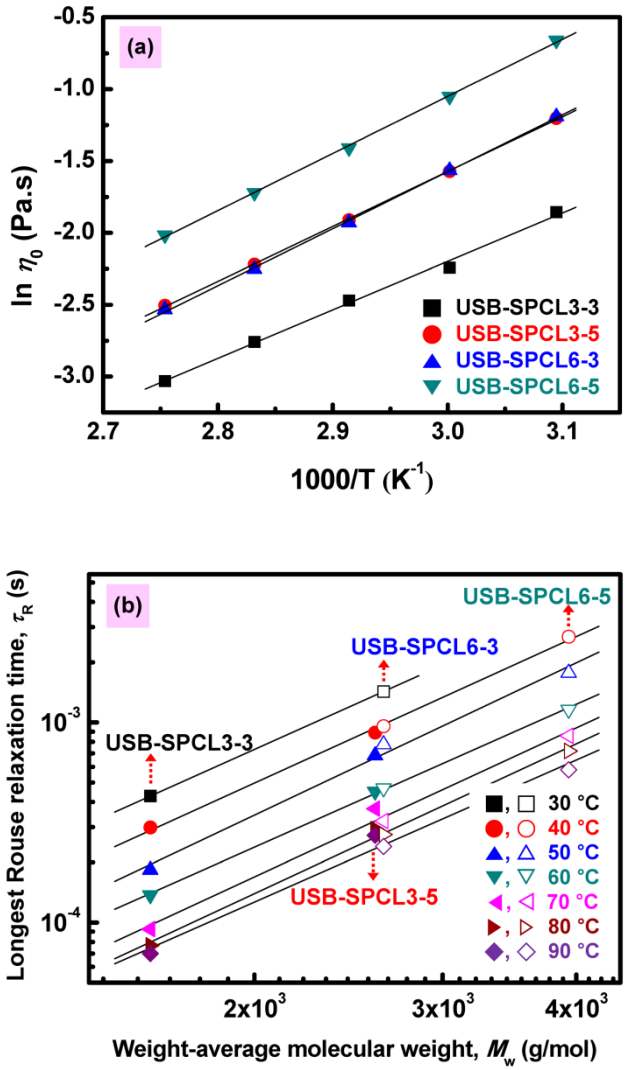

Figure III-9. (a) Arrhenius plot of $\ln \eta_0$ versus the inverse temperature for the USB-SPCLs. (b) Logarithmic plots of τ_R versus the total M_w for USB-SPCLs at various temperatures.

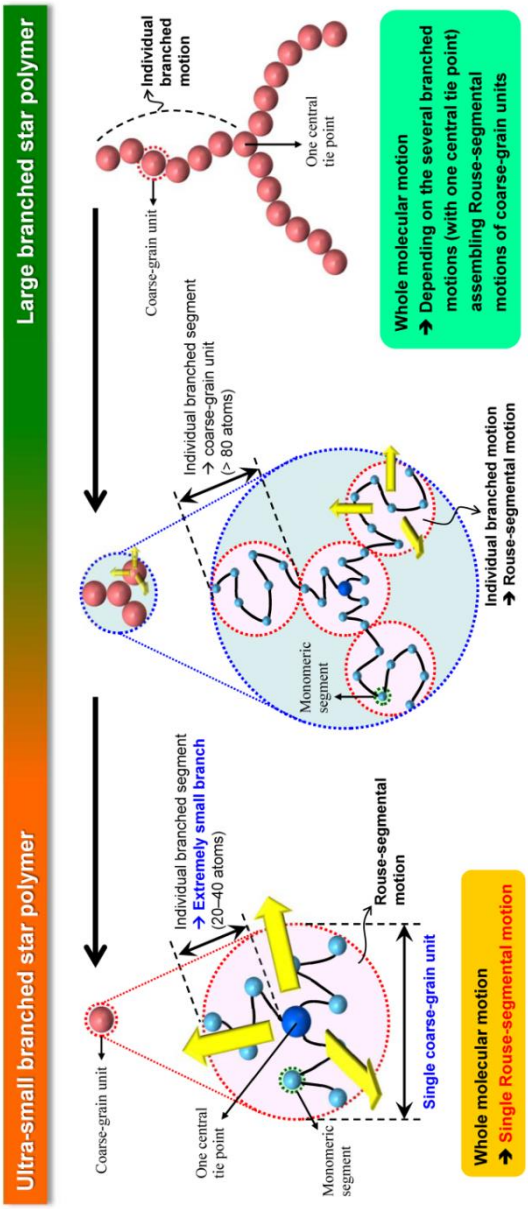

Figure III-10. Schematic illustration of the proposed molecular behavior for a star polymer with extremely small branches.

III-4. Conclusion

This study demonstrated the unique molecular dynamic behaviors of USB-SPCLs used as model star polymers with extremely small branches. The glass transition, viscoelasticity, viscosity, elasticity, flow activation energy, and longest Rouse relaxation time of USB-SPCLs exhibited the total-molecular-weight-dependent Rouse dynamic behaviors that followed unentangled linear polymer models, instead of typical star polymer behaviors being affected by the number and length of branched segments. This suggests that an extremely small branch in USB-SPCLs is composed of several monomeric segments without a valid dynamic unit and that a whole USB-SPCL molecule represents one Rouse-segmental motion of a single coarse-grain unit with dynamically-equivalent branches. We believe that the unusual results from this study provide new insights into the molecular dynamic behaviors in an extremely small branched system, and this may pave the way for designing new types of branched polymers with unique dynamic behaviors as well as with attractive advantages of high end-group concentration, such as controlling polymer degradation, lowering softening point, and providing miscibility.

References and Notes

1. Kraus, G.; Gruver, J. T. J. *Polym. Sci., Part A: Gen. Pap.* **1965**, *3*, 105−122.

2. Quack, G.; Fetters, L. J. *Polym Prepr (Am Chem Soc Div Polym Chem)* **1977**, *18*, 558−565.

3. Mykhaylyk, O. O.; Fernyhough, C. M.; Okura, M.; Fairclough, J. P. A.; Ryan, A. J.; Graham, R. *Eur Polym J* **2011**, *47*, 447−464.

4. Acebo, C.; Fernández−Francos, X.; Ferrando, F.; Serra, À .; Salla, J. M.; Ramis, X. *React. Funct. Polym.* **2013**, *73*, 431−441.

5. Frischknecht, A. L.; Milner, S. T.; Pryke, A.; Young, R. N.; Hawkins, R.; McLeish, T. C. B. *Macromolecules* **2002**, *35*, 4801−4820.

6. Milner, S. T.; McLeish, T. C. B. *Macromolecules* **1998**, *31*, 7479−7482.

7. Choi, W.; Chung, J. W.; Kwak, S.−Y. *ACS Appl. Mater. Interfaces* **2014**, *6*, 11118−11128.

8. Choi, W.; Chung, J. W.; Kwak, S.−Y. *J. Polym. Sci., Part A: Polym. Chem.* **2015**, *53*, 1134−1142.

9. Fukuzaki, H.; Yoshida, M.; Asano, M.; Kumakura, M.; Mashimo, T.; Yuasa, H.; Imai, K.; Yamanaka, H. *Polymer* **1990**, *31*, 2006−2014.

10. Lin, S.−Y.; Chen, K.−S.; Teng, H.−H.; Li, M.–J. *J. Microencapsul.* **2000**, *17*, 577−586.

11. Choi, W.; Chung, J. W.; Kwak, S.−Y. *Polymer* **2015**, *79*, 91−98.

12. Ferry, J. D. *Viscoelastic Properties of Polymers*, 3rd ed.; Wiley: New York, 1980.

13. Sun, C.; Ritchie, J. E. *J. Phys. Chem.* **2011**, *115*, 8381−8389.

14. Fox, T. G.; Flory, P. J. *J. Appl. Phys.* **1950**, *21*, 581−591.

15. Roovers, J. E. L.; Toporowski, P. M. *J. Appl. Polym. Sci.* **1974**, *18*, 1685−1691.

16. Kisliuk, A.; Ding, Y.; Hwang, J.; Lee, J. S.; Annis, B. K.; Foster, M. D.; Sokolov, A. P. *J. Polym. Sci. Part B: Polym. Phys.* **2002**, *40*, 2431−2439.

17. Walberer, J. A.; McHugh, A. J. *J. Rheol.* **2001**, *45*, 187−201.

18. Macosko, C. M. *Rheology: principles, measurements and applications*; Wiley-VCH Publishers: New York, 1994.

19. Barnes, H. A.; Hutton, J. F.; Walters, K. *An Introduction to Rheology*; Elsevier: Amsterdam, 1989.

20. Harrell, E. R.; Nakajima, B. F. *J. Appl. Polym. Sci.* **1984**, *29*, 995−1010.

21. Kwak, S.−Y.; Choi, J.; Song, H. J. *Chem. Mater.* **2005**, *17*, 1148−1156.

22. Chung, J. W.; Oh, K. S.; Kwak, S.−Y. *Macromol. Mater. Eng.* **2007**, *292*, 627−633.

23. Yang, Z.; Han, C. D. *Macromolecules* **2008**, *41*, 2104−2118.

24. Uppuluri, S.; Keinath, S. E.; Tomalia, D. A.; Dvornic, P. R. *Macromolecules* **1998**, *31*, 4498−4510.

25. Fetters, L. J.; Kiss, A. D.; Pearson, D. S.; Quack, G. F.; Vitus, F. J. *Macromolecules* **1993**, *26*, 647−654.

26. Gupta, R. K. *Polymer and Composite Rheology*, 2nd ed., Revised and Expanded ed.; Marcel Dekker, Inc.: New York, 2000.

27. Auhl, D.; Stadler, F. J.; Münstedt, H. *Macromolecules* **2012**, *45*, 2057−2065.

28. Claesson, H.; Malmström, E.; Johansson, M.; Hult, A. *Polymer* **2002**, *43*, 3511−3518.

29. Koopmans, R.; den Doelder, J.; Molenaar, J. *Polymer Melt Fracture*; CRC press, Taylor & Francis Group: Boca Raton, FL, 2011.

30. Berry, G. C.; Fox, T. G. *Adv. Polym. Sci.* **1968**, *5*, 261−357.

31. Graessley, W. W.; Roovers, J. *Macromolecules* **1979**, *12*, 959−965.

32. Onogi, S.; Masuda, T.; Kitagawa, K. *Macromolecules* **1970**, *3*, 109−116.

33. Masuda, T.; Kitagawa, K.; Inoue, T.; Onogi, S. *Macromolecules* **1970**, *3*, 116−125.

34. Rouse, P. E. *J. Chem. Phys.* **1953**, *21*, 1272−1280.

35. Bueche, F. *J. Chem. Phys.* **1952**, *20*, 1959−1964.

36. Lomellini, P. *Polymer* **1992**, *33*, 4983−4989.

37. Liu, C.−Y.; He, J.; Keunings, R.; Bailly, C. *Macromolecules* **2006**, *39*, 8867−8869.

38. Siline, M.; Leonov, A. I. *Polymer* **2002**, *43*, 5521−5525.

39. Ratna, D.; Divekar, S.; Samui, A. B.; Chakraborty, B. C.; Banthia, A. K. *Polymer* **2006**, *47*, 4068−4074.

40. Shinzawa, H.; Nishida, M.; Kanematsu, W.; Tanaka, T.; Suzuki, K.; Noda, I. *Analyst* **2012**, *137*, 1913−1921.

41. Rubinstein, M.; Colby, R. H. *Polymer Physics*; Oxford Univ. Press: New York, 2003.

42. Roovers, J. *Macromolecules* **1991**, *24*, 5895−5896.

43. Dealy, J. M.; Larson, R. G. *Structure and Rheology of Molten Polymers*; Hanser: Munich, 2006.

44. The estimated Kuhn length values were 8.00 nm for LPCL1-17 and 4.34 nm for LPCL1-32, indicating that PCL has one dynamic unit in at least 9 monomers for 2,110 g mol^{-1} PCL and 5 monomers for 3,610 g mol^{-1} PCL. The USB-SPCL counterparts for the same total molecular weight of LPCL1-17 and LPCL1-32, *i.e*, USB-SPCL3-5 and USB-SPCL6-5, have ca. 4.65 nm branched segment lengths in a fully extended conformation and have only 5 monomers in an individual branched segment.

45. Liu, L. *Multiscale Simulations of Star Polymer Melts*; Ph.D. Thesis, University of Twente, The Netherlands, 2014.

CHAPTER IV

ULTRA-SMALL-BRANCHED STAR POLY(ε-CAPROLACTONE)S AS PHTHALATE-FREE PVC PLASTICIZERS DESIGNED FOR NON-TOXICITY AND IMPROVED MIGRATION RESISTANCE

IV-1. Introduction

Star-shaped poly(ε-caprolactone)s (SPCLs) with extremely small branches provide higher biocompatibility, lower melting point, higher free volume, and better miscibility with other polymers, compared with a linear analogue with the same molecular weight.[1–5] Furthermore, they have smaller degrees of entanglement and shorter relxation times, thus they are attractive alternatives to phthalate plasticizers for flexible poly(vinyl chloride)s (PVCs).[6–8]

Here, we developed an unentangled SPCLs with extremely short branched segments capable of providing excellent flexibility to PVC and improving the migration resistance from PVC using a facile pilot-scale pseudo-one-pot process.[9] These ultra-small-branched SPCLs (USB-SPCLs) were transparent viscous liquids at room temperature and exhibited Newtonian behaviors.

USB-SPCLs were biologically safe without producing an acute toxicity response, and they displayed good processability and high miscibility with PVC. The flexible PVCs prepared using USB-SPCLs exhibited good flexibility and transparency properties that were comparable to those obtained from DEHP. Most of all, the migration of USB-SPCLs from the flexible PVCs was negligible, whereas considerable quantities of DEHP migrated out of the flexible PVCs. Thus, we anticipate that USB-SPCLs can be used as a non-toxic alternative plasticizer for the preparation of phthalate-free flexible PVCs, which are tremendously attractive for applications in medical devices, food packaging, and infant care products.

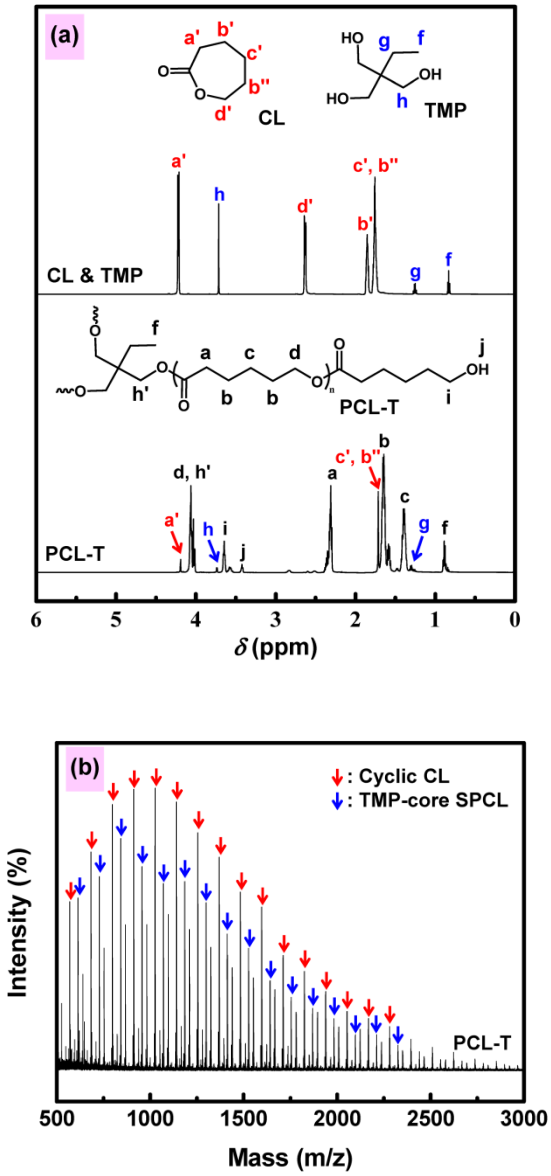

Figure IV-1. (a) ^{1}H NMR spectra of CL, TMP, and PCL-T. (b) MALDI-TOF mass spectrum of PCL-T.

IV-2. Experimental Section

IV-2-1. Materials

ε-Caprolactone (CL) and trimethylolpropane (TMP) were purchased from Alfa Aesar Co., Ltd., USA and Tokyo Chemical Industry Co., Ltd., Japan., respectively. Dipentaerythritol (DPTOL), ethylene glycol (EG), tin(II) 2-ethylhexanoate ($Sn(Oct)_2$), and acetic anhydride (Ac_2O) were purchased from Sigma-Aldrich Ltd., Korea. Di-(2-ethyl-hexyl) phthalate (DEHP) was obtained from Junsei Chemical Co., Ltd., Japan. The suspension-grade poly(vinyl chloride) (PVC) resin P-1000 ($\eta_0 \approx$ 300,000 cP at 220 °C) was kindly provided by Hanwha Chemical Co., Ltd., Korea. The secondary plasticizer E-700 (epoxidized soybean oil) was supplied by Songwon Co., Ltd., Korea. The thermal stabilizer ADK STAB RUP-110 was obtained from Adeka Korea Co., Ltd., Korea. All chemicals were used without further purification.

IV-2-2. Synthesis and characterization of USB-SPCLs

Four USB-SPCLs with molecular architectures that varied with respect to the number of branches, N_{number}, and the average length of the individual branches (the average DP per branch), $N_{<length>}$, were synthesized using a previously

developed method.[10] These USB-SPCLs are denoted by USB-SPCLN_{number}-$N_{<\text{length}>}$: USB-SPCL3-3, USB-SPCL3-5, USB-SPCL6-3, and USB-SPCL6-5. The number of branched segments was controlled according to the hydroxyl functionalities of the core materials, 3 (TMP) or 6 (DPTOL). The degree of polymerization of the individual branched segments, referred to as the length of branched segments, was controlled by the molar ratio of CL to the hydroxyl groups on the core material ([CL]/[core-OH]).

The chemical architectures of USB-SPCLs were analyzed by ^{1}H NMR spectroscopy using a Bruker Avance spectrometer 600, with chloroform-*d* ($CDCl_3$-*d*) as the solvent. The number and average length of branched segments (N_{number} and $N_{<\text{length}>}$) in USB-SPCLs were determined from the integral ratio of ^{1}H NMR peaks between the core moiety peak and the end-capping moiety peaks and between the end-capping moiety peak and the methylene proton peak of the CL repeating unit in the branched segment, respectively. The number-average molecular weights of USB-SPCLs were calculated using N_{number} and $N_{<\text{length}>}$, denoted $M_{\text{n,NMR}}$. The molecular weights of USB-SPCLs were also measured using matrix-assisted laser desorption/ionization time-of-flight mass spectrometry (MALDI-TOF-MS), denoted $M_{\text{n,MALDI}}$, using an Applied Biosystems Voyager-DE STR spectrometer with a nitrogen laser (337 nm, 3 ns pulse width) operated in the linear mode. The matrix solution was prepared using dihydrobenzoic acid

(DHB) dissolved in a tetrahydrofuran (THF) matrix, and the samples were mixed with the matrix solution in volumetric ratios of 1:1. The glass transition temperature, T_g, and melting temperature, T_m, of USB-SPCLs were measured by differential scanning calorimetry (DSC) using a Netzsch DSC 200 F3 with a heating rate of 20 ℃/min over the temperature range of −100 to 100 ℃ under a nitrogen atmosphere. The complex viscosities of USB-SPCLs were measured by dynamic mechanical spectrometry using a stress-controlled rheometer TA instruments Inc. AR2000. The AR2000 was operated in a cone-and-plate geometry with a 1° angle and a 60 mm diameter cone, and the gap between the cone and the plate was 80 μm in all measurements. Dynamic frequency sweeps were performed over the angular frequency range 0.5–100 rad s^{-1} and the temperature range 30–90 ℃, measured in 10 ℃ intervals. The strain values were determined, using a dynamic strain sweep, to lie within the linear viscoelastic region. The thermal resistance of USB-SPCLs was observed using thermogravimetric analysis (TGA) measurements collected on a TA Instruments Q500 with a heating rate of 10 ℃/min over the temperature range 25–600 ℃ under a nitrogen flow.

IV-2-3. Acute toxicity test of USB-SPCLs

The biological safety profiles of USB-SPCLs were evaluated by performing acute toxicity tests, based on the OECD 423 guidelines, at the Korea Institute of Toxicology (KIT), Korea. Briefly, the experimental rats (Crl: CD (SD)) were divided into four groups, each of which contained five males and five females. A single dose of 500, 1,000, and 2,000 mg USB-SPCLs/kg body weight was given to three experimental groups, and the remaining group served as a control group. The three experimental and one control groups were observed 1, 2, and 4 h after dosing, and once daily thereafter, for a total of 15 days. All rats were sacrificed at the end of the observation period and subjected to a necropsy analysis.

IV-2-4. Processing properties of USB-SPCLs

The absorption and fusion properties were measured by mixing PVC with USB-SPCLs using conventional manufacturing methods for fabricating flexible PVC sheet products. The formulations of the flexible PVCs were 100 parts per hundred (phr) PVC resin (65 wt%), 50 phr USB-SPCL plasticizer (32 wt%), 2 phr E-700 as a secondary plasticizer (1 wt%), and 3 phr ADK STAB RUP-110 as a thermal stabilizer (2 wt%). The absorption properties of USB-SPCLs into the PVC resin were observed by measuring the

dry time based on the American Standard Testing Methods (ASTM) D2396-94 using a C.W. Brabender planetary mixer heated at 80 ℃ and operated at 30 rpm. The fusion properties of PVC/USB-SPCLs were investigated by measuring the fusion time according to the ASTM D2538-02 procedure using a C.W. Brabender measuring mixer heated at 90 ℃ and operated at 30 rpm. Prior to the fusion time measurements, the PVC/USB-SPCL compounds were produced using a Henschel mixer, heated to 120 ℃ and operated at 2,000 rpm, in order to completely absorb USB-SPCLs into the PVC resin. Given the measured absorption and fusion properties, flexible PVC sheets were prepared with dimensions of 250 × 250 × 2 mm^3 using a hot press operated at 180 ℃ for 10 min. Neat PVC, PVC/DEHP, and PVC/LPCL sheets were prepared according to the same procedure, and their properties were compared to those of PVC/USB-SPCLs. The miscibility properties of PVC and USB-SPCLs were measured using solid-state ^1H NMR spectroscopy methods performed on a Bruker minispec mq 20 spectrometer operated at 40 ℃, with a proton resonance frequency of 19.95 MHz.

IV-2-5. Characterization of the flexible PVCs

The plasticizing efficiency of USB-SPCLs was evaluated based on the lowering of the T_g in PVC/USB-SPCLs relative to the corresponding values of

PVC/DEHP and PVC/LPCL. The T_g values were measured by DSC using a heating rate of 10 ℃/min over the temperature range −100 to 100 ℃ under a nitrogen atmosphere. The flexibility properties of PVC/USB-SPCLs were investigated by measuring their Shore A and D hardness values according to the ASTM D2240 procedures. The mechanical properties of PVC/USB-SPCLs were determined by measuring the tensile strength, elongation at break, and tear strength according to the ASTM D638 and ASTM D624 procedures. The measurements were conducted using an Instron 4204 universal testing machine at a crosshead speed of 500 mm/min. The optical properties of PVC/USB-SPCLs were investigated by measuring the transmittance and haze values using a BYK Gardner Haze-Gard Plus hazemeter.

IV-2-6. Migration resistance test of the flexible PVCs

The migration resistance values of USB-SPCLs were evaluated by immersing flexible PVC sheet samples in n-hexane at 50 ℃ for 2 h, according to the Food and Drug Administration (FDA) procedure 21 CFR 177.1520, performed in the Société Générale de Surveillance (SGS) Korea Co., Ltd. The degree of plasticizer migration was measured under harsher conditions: the quantities of USB-SPCLs that migrated out of the PVC/USB-SPCL

samples and into the liquid, solid, and gas phases were measured and compared to the corresponding values measured for PVC/DEHP. Flexible PVC sheet samples were prepared with dimensions of $20 \times 20 \times 2$ mm^3. The extractability properties of USB-SPCLs were tested according to the ASTM D5227-95 procedure, in which the samples were immersed in 1 L n-hexane (liquid phase) and stirred at 50 ℃ for 7 days. The exudability of USB-SPCLs was tested according to the ASTM D2199-82 procedure, in which the samples were placed between two unplasticized poly(methyl-methacrylate) (PMMA) sheets (solid phase) and then pressed under 10 tons with heating at 50 ℃ for 7 days. The volatility of USB-SPCLs was tested according to the ASTM D1203-94 procedure, in which the samples were positioned at the center of activated carbons (granular, 4−14 mesh) in a glass Petri dish. The assembly was then placed in an oven, and air was circulated (gas phase) at 80 ℃ for 7 days.

IV-3. Results and Discussion

IV-3-1. Synthesis and characterization of USB-SPCLs

As shown in Table IV-1, the N_{number} values of USB-SPCLs were consistent with the number of hydroxyl functionalities present in the core materials, 3 (TMP) or 6 (DPTOL), and the $N_{<length>}$ values of USB-SPCLs were consistent with the molar ratio of CL to the hydroxyl groups on the core material (DP = 3 or 5). The values of $M_{n,NMR}$ and $M_{n,MALDI}$ differed to a small degree, but both values approached the theoretical number-average molecular weights of USB-SPCLs, $M_{n,theory}$. MALDI-TOF mass spectra of USB-SPCLs also provided narrow molecular weight distributions (M_w/M_n = 1.06−1.17). These findings supported the conclusion that USB-SPCLs were obtained with well-controlled molecular architectures and without impurities, such as unreacted CL monomers or side-products.

The T_g values of USB-SPCLs appeared to be proportional to their respective total molecular weights, rather than to their molecular architecture parameters N_{number} and N_{length}. By contrast, the T_m values of USB-SPCLs decreased with decreasing N_{length} and increasing N_{number}, *i.e.*, increasing end group concentration (see Table IV-1).[11,12] Thus, USB-SPCL3-3 and USB-SPCL6-3, which featured relatively high end group concentrations, formed

transparent viscous liquids, even at room temperature, with significantly low T_m values.

The rheological properties of USB-SPCLs were observed by measuring the complex viscosities, η^*, at various temperatures as a function of the angular frequency. Figure IV-2 shows the master curves of the complex viscosities for USB-SPCLs according to the time-temperature superposition principle.[13] The reduced complex viscosities (η^*/a_T) and the reduced angular frequencies ($a_T\omega$) for USB-SPCLs were determined using a shift factor a_T, where the shift factor a_T is defined as the viscosity at temperature T divided by the viscosity at 60 ℃. As shown in Figure IV-2, all of the master curves were perfectly superposed and were independent of the angular frequency, indicative of a Newtonian fluid. This result suggested that USB-SPCLs did not display chain entanglement, even at room temperature, due to the presence of short branched segments. The lack of chain entanglement can lead to fast molecular motions and provide PVC chains with a high flexibility.[14]

The temperatures that corresponded to the onset weight loss, T_{do}, in each of USB-SPCLs were measured using TGA and are listed in Table IV-1. USB-SPCL3-3 and USB-SPCL6-3 (with small values of $N_{<length>}$) showed lower T_{do} values than USB-SPCL3-5 and USB-SPCL6-5 (longer $N_{<length>}$). This result indicated that the thermal stabilities of USB-SPCLs also depended on their

end group concentration. The decomposition of conventional PCLs was influenced by a syn *Ei* mechanism and an unzipping mechanism.[15] The unzipping reactions proceeded from the end groups after water had been generated through the syn *Ei* reactions.[15] Thus, USB-SPCLs with smaller $N_{<length>}$ values had higher end group concentrations and resulted in lower T_{do} values relative to USB-SPCLs prepared with larger $N_{<length>}$ values. Meanwhile, the T_{do} values of USB-SPCLs were 313–323 ℃, whereas that of DEHP was 242 ℃. This result indicated that the weight loss of USB-SPCLs was negligible during heating up to 300 ℃, whereas the weight loss of DEHP began at 242 ℃ (Figure IV-3). This result suggested that USB-SPCLs should display better thermal resistance properties than DEHP in the context of conventional flexible PVC manufacturing processes, which are generally conducted at 200 ℃.

Table IV-1. General characteristics of USB-SPCLs.

Sample	USB-SPCL3-3	USB-SPCL3-5	USB-SPCL6-3	USB-SPCL6-5
N_{number}	3.09	3.01	6.04	6.05
$N_{<\text{length}>}$	3.00	5.03	3.08	5.05
$M_{\text{n,NMR}}$ (g/mol)[a]	1320	1990	2630	4000
$M_{\text{n,MALDI}}$ (g/mol)	1480	2000	2360	3770
$M_{\text{n,theory}}$ (g/mol)	1287	1972	2561	3931
T_{g} (℃)	−66.4	−64.8	−64.4	−62.0
T_{m} (℃)	15.3	34.4	14	29.9
T_{do} (℃)	320	323	321	313

[a]Number-average molecular weights are determined by ^{1}H NMR spectra:

$$M_{n,NMR} = MW_{core} + MW_{CL} \times N_{<length>} \times N_{number} + MW_{end-cap} \times N_{number} - MW_H \times N_{number}$$

where MW_{core}, MW_{CL}, MW_{H}, and $MW_{\text{end-cap}}$ are the molar masses of the core material (TMP or DPTOL), CL monomer, hydrogen, and end-capping moiety (–$COCH_3$), respectively.

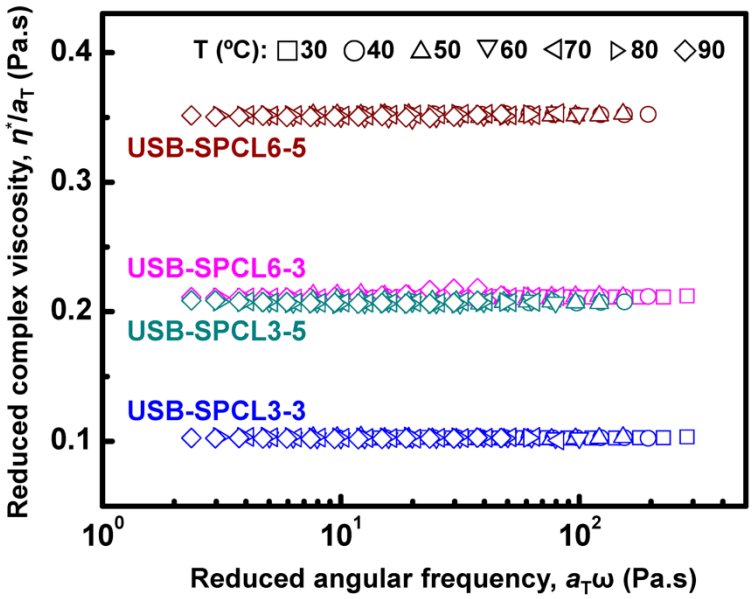

Figure IV-2. Master curves of the complex viscosities for USB-SPCLs as a function of the reduced angular frequency, at 60 ℃.

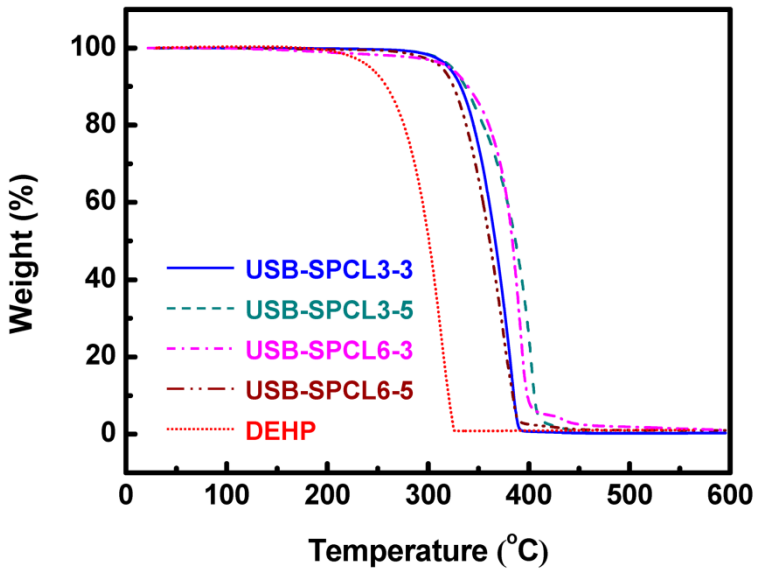

Figure IV-3. TGA thermograms of USB-SPCLs and DEHP.

IV-3-2. Biological safety of USB-SPCLs

The acute toxicities of USB-SPCLs were tested using a predictive model for biological safety (non-toxicity). The results provided by KIT revealed that none of the treated (experimental) rats died during the 15 day observational period after a single dose of USB-SPCLs. No significant weight changes were observed in any of the treated rats. Additionally, no pathological changes were observed on the skin, fur, or eyes, and the rats' behaviors remained unchanged except for the experimental group that received to a single dose of 2,000 mg kg^{-1} USB-SPCL3-5. In this group of five males and five females, two males and two females displayed a prone position and moderately irregular respiration at 4 h after dosing, but they returned to baseline thereafter. These behavioral changes may have resulted from the relatively high value of T_m for USB-SPCL3-5, which was assumed a soft waxy phase at room temperature. After conducting observations over 15 days, all animals, including those in the control group, were sacrificed and dissected to collect blood from the heart and remove internal organs for gross and histopathologic observations. The three experimental groups displayed no histopathological changes in the liver, kidney, heart, spleen, ovaries, testes, or intestines relative to the control group. The acute oral toxicity tests revealed that USB-SPCLs yielded toxic doses of over 2,000 mg kg^{-1}, whereas

USB-SPCL3-5 yielded a toxic dose of 1,000 mg kg^{-1}. These doses suggested that USB-SPCLs are biologically safe and non-toxic.

IV-3-3. Processing properties of PVC/USB-SPCLs

The absorption and fusion properties of materials are important for preparing powdered mixtures of polymer resins and liquid additives, such as plasticizers. We prepared a series of phthalate-free flexible PVC samples using USB-SPCLs as alternative plasticizers. The absorption and fusion properties of these samples were investigated by determining the dry time and fusion time, respectively. The absorption and fusion properties of the flexible PVC prepared using DEHP were also measured for comparison to the properties of the phthalate-free flexible PVCs prepared using USB-SPCLs. The dry times of PVC/USB-SPCLs were measured by analyzing the torque curves during mixing of the powdered PVC resin (100 phr, 65 wt%), USB-SPCLs (50 phr, 32 wt%), and other additives in a planetary mixer heated at 80 ℃ and operated at 30 rpm, according to the ASTM D2396-94 procedure. As shown in Figure IV-4(a), the torque curves of the mixtures increased immediately after the addition of USB-SPCLs and additives, indicating that USB-SPCLs wetted and solvated the surfaces of the PVC powders. The torque curves then gradually decreased as the mixtures flowed more freely

due to the permeation of USB-SPCLs into the PVC powders. After USB-SPCLs had been completely absorbed into the PVC powders, the torque curves of the mixtures stopped falling and slowly began to rise again. The minimum value of the torque curves is called the dry point. We determined the dry times of PVC/USB-SPCLs by measuring the time between the addition of USB-SPCLs and achievement of the dry point in the sample. As listed in Table IV-2, the dry times of PVC/USB-SPCLs were ordered as follows: PVC/USB-SPCL3-3 < PVC/USB-SPCL3-5 < PVC/USB-SPCL6-3 < PVC/USB-SPCL6-5. Typically, the viscosity of a plasticizer will affect the dry time of the flexible PVC.[16,17] Thus, we measured the viscosities of USB-SPCLs using a Brookfield DV-II+ viscometer heated at the mixing temperature (80 ℃). The resulting viscosities were ordered as follows: USB-SPCL3-3 (65 (cP)) < USB-SPCL3-5 (112 (cP)) < USB-SPCL6-3 (127 (cP)) < USB-SPCL6-5 (210 (cP)), which corresponded to the ordering of the PVC/USB-SPCLs dry times. These results clearly indicated that the low viscosities of USB-SPCLs facilitated absorption into the PVC powders and resulted in a shorter dry time for PVC/USB-SPCLs. We noted that the viscosities of USB-SPCLs followed the total molecular weights of USB-SPCLs (Table IV-1) rather than their molecular architecture parameters, N_{number} and $N_{<\text{length}>}$. Thus, the dry times of PVC/USB-SPCLs appeared to depend on the total molecular weights of USB-SPCLs, regardless of their architectures. Meanwhile, the dry times and torque loads of PVC/USB-

SPCLs were higher than the corresponding values obtained from PVC/DEHP because the viscosities of PVC/USB-SPCLs were much higher than the viscosity of DEHP (7 (cP) at 80 ℃).

The fusion time measurements were conducted by preparing the PVC/USB-SPCL compounds in which USB-SPCLs were completely pre-adsorbed. We then analyzed the torque curves of the PVC/USB-SPCL compounds at 90 ℃, 30 rpm according to the ASTM D2538-02 procedure (Figure IV-4(b)). The fusion times of PVC/USB-SPCLs were determined by measuring the time between the addition of the PVC/USB-SPCL compounds and achievement of the maximum value of the torque curve (the fusion point).[18] The fusion properties of the PVC/DEHP compound were also observed. As listed in Table IV-2, the fusion times of PVC/USB-SPCLs were ordered as follows: PVC/USB-SPCL3-3 < PVC/USB-SPCL3-5 < PVC/USB-SPCL6-3 < PVC/USB-SPCL6-5. Paul et al. reported that the fusion time of PVC tended to shorten as the plasticizer viscosity decreased.[17] PVC/USB-SPCLs followed this general relationship between the fusion time and the viscosity; USB-SPCLs with a low viscosity yielded a short PVC/USB-SPCLs fusion time. All of PVC/USB-SPCLs, however, displayed fast fusion times compared to PVC/DEHP, although DEHP displayed a much lower viscosity than USB-SPCLs. Presumably, these results were attributed to an increase

in the miscibility of USB-SPCLs with PVC due to the relatively large number of carbonyl groups in USB-SPCLs.[18]

The solubility parameters of USB-SPCLs were used to evaluate the theoretical miscibility between PVC and USB-SPCLs based on the chemical architectures of USB-SPCLs. The solubility parameter was calculated with consideration for the contributions of the dispersion forces, permanent dipoles, and hydrogen bonds, called the Hansen solubility parameter (see Table IV-3).[19,20] Then, the interaction radius between PVC and USB-SPCLs was 8.13–8.26 $((J/cm^3)^{1/2})$, and that between PVC and DEHP was 7.20 $((J/cm^3)^{1/2})$, indicating that USB-SPCLs and DEHP were miscible with PVC.

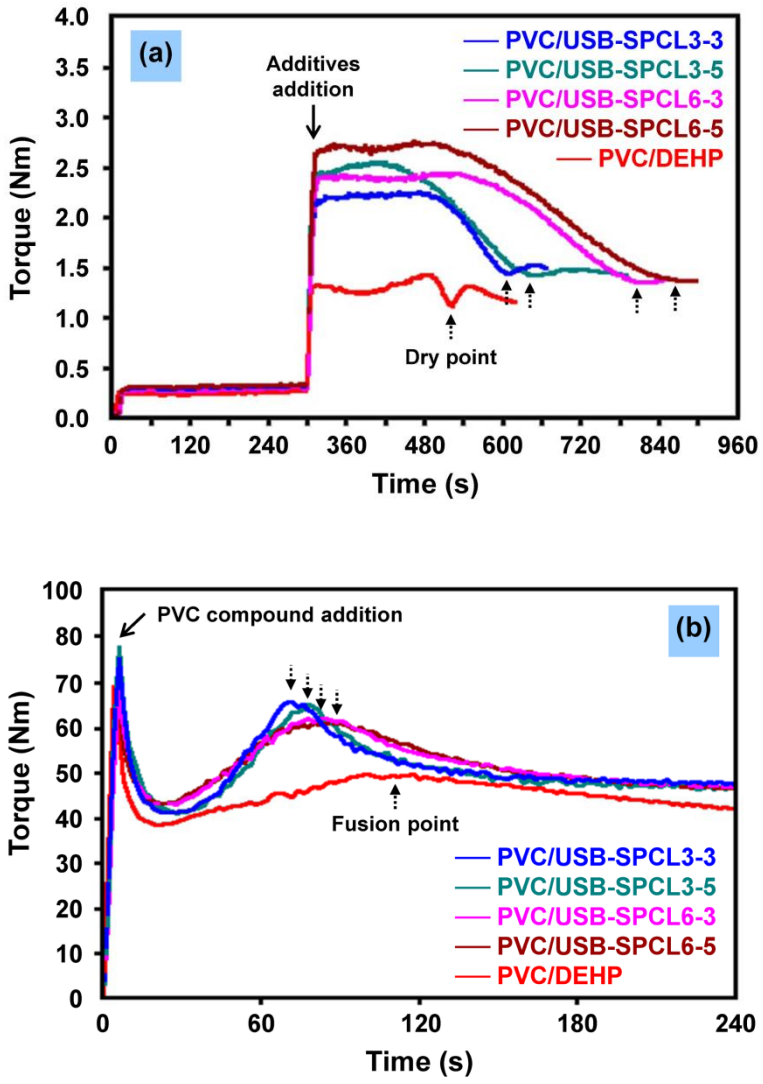

Figure IV-4. Torque–time curves of the PVC/USB-SPCLs and PVC/DEHP blends corresponding to the (a) absorption behaviors, and (b) fusion behaviors.

Table IV-2. Dry times and fusion times.

Sample	Dry time (s)	Fusion time (s)
PVC/USB-SPCL3-3	308	66
PVC/USB-SPCL3-5	348	72
PVC/USB-SPCL6-3	520	76
PVC/USB-SPCL6-5	566	80
PVC/DEHP	222	110

Table IV-3. Hansen solubility parameter terms and interaction radii for PVC, USB-SPCLs, and DEHP

Sample	δ $((J/cm^3)^{1/2})^a$	δ_v $((J/cm^3)^{1/2})$	δ_h $((J/cm^3)^{1/2})$	IR $((J/cm^3)^{1/2})^b$
PVC	25.04	24.83	3.20	—
USB-SPCL3-3	19.33	17.86	7.39	8.13
USB-SPCL3-5	19.24	17.79	7.33	8.16
USB-SPCL6-3	19.38	17.83	7.59	8.26
USB-SPCL6-5	19.26	17.76	7.45	8.25
DEHP	18.63	17.90	5.17	7.20

[a]The Hansen solubility parameter (δ) for each compound is calculated from the chemical structures according to the methods of Van Krevelen:

$$\delta = \left(\delta_d{}^2 + \delta_p{}^2 + \delta_h{}^2\right)^{0.5}$$

where δ_d, δ_p, δ_h are the contributions of the dispersion forces, permanent dipoles, and hydrogen bonding, respectively.

[b]The interaction radius (IR) is calculated as:

$$\text{IR} = \left(\left(\delta_{v,PVC} - \delta_{v,plasticizer}\right)^2 + \left(\delta_{h,PVC} - \delta_{h,plasticizer}\right)^2\right)^{0.5}$$

where δ_v is a combination of the dispersion and polar forces, (δ_v=($\delta_v{}^2$+ $\delta_p{}^2$)$^{0.5}$).

The actual miscibility between PVC and USB-SPCLs were measured experimentally to investigate the influence of USB-SPCL architectures on the miscibility of PVC/USB-SPCLs. We characterized the spin-lattice relaxation times of neat PVC, USB-SPCLs, and PVC/USB-SPCLs to evaluate the miscibility between PVC and USB-SPCLs on length scales of less than 10 nm.[21] As shown in Figure IV-5, the values of $\ln[(M_\infty - M(\tau))/(2M_\infty)]$ in all samples (neat PVC, USB-SPCLs, and PVC/USB-SPCLs) decreased linearly as τ increased over the range of τ values tested, indicating that all samples were characterized by single T_1 values. USB-SPCLs with small N_{number} displayed lower T_1 values than USB-SPCLs with larger N_{number}, and it appeared that T_1 was not significantly affected by the value of $N_{<length>}$ for USB-SPCLs. Blending USB-SPCLs with the PVC, however, increased the T_1 values of PVC/USB-SPCLs as the values of $N_{<length>}$ and N_{number} for USB-SPCLs increased. These effects were attributed to the polar interactions between the PVC chains and the carbonyl groups of the USB-SPCL molecules, which slowed the spin-lattice relaxation times of the protons in the PVC/USB-SPCL blends. PVC/USB-SPCLs exhibited single T_1 values that fell between the T_1 values of their corresponding neat components, indicating that PVC and USB-SPCLs were dynamically homogeneous in the PVC/USB-SPCLs blends and that the average domain sizes of their neat components in the blends were smaller than the proton diffusive path length within the

timescale T_1.[22] The upper limits of USB-SPCL and PVC domain sizes in PVC/USB-SPCLs were determined by estimating the average diffusive path length using the following equation:[21,22]

$$< L >= (6DT_1)^{1/2} \qquad (1)$$

where <*L*> is the average diffusive path length for the effective spin diffusion and *D* is the spin-diffusion coefficient, typically around 100 $nm^2\ s^{-1}$ for a solid. The calculated <*L*> values for the PVC/USB-SPCL3-3, PVC/USB-SPCL3-5, PVC/USB-SPCL6-3, and PVC/USB-SPCL6-5 samples were 7.25, 7.52, 7.59, and 7.85 nm, respectively, and these values increased with increasing $N_{<length>}$ and N_{number} for USB-SPCLs. These results indicated that the upper limit on the average domain size for the USB-SPCLs and PVC blends increased with increasing $N_{<length>}$ and N_{number} for USB-SPCLs. Thus, all USB-SPCLs apparently provided molecular-level miscibility with an average domain size of less than 8 nm in the PVC/USB-SPCLs blends, indicating that USB-SPCLs displayed excellent miscibility with PVC.

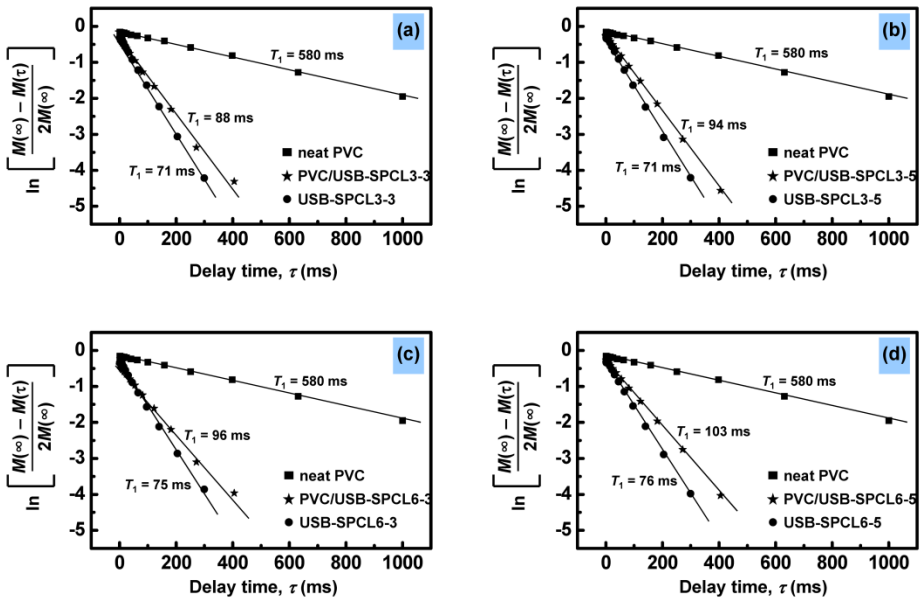

Figure IV-5. Logarithmic plots of the resonance intensity versus the delay time for PVC/USB-SPCLs and their neat components: (a) PVC/USB-SPCL3-3, (b) PVC/USB-SPCL3-5, (c) PVC/USB-SPCL6-3, and (d) PVC/USB-SPCL6-5.

IV-3-4. Physical properties of the flexible PVCs

We evaluated the flexibility of PVC/USB-SPCLs indirectly by calculating the plasticizing efficiencies of USB-SPCLs based on the glass transition behaviors of neat PVC, PVC/USB-SPCLs, PVC/DEHP, and PVC/LPCL. As shown in Figure IV-6, single glass transitions were observed for each PVC/USB-SPCL DSC thermogram. These transitions occurred between the transitions of the corresponding neat components, and the glass transitions of the neat components themselves were absent from the blend curves, indicating that PVC and USB-SPCLs were miscible. The single T_g values for PVC/USB-SPCLs were determined by the inflection points of the glass transition curves and are listed in Table IV-4. As shown in Table IV-4, the T_g values of PVC/USB-SPCLs fell below 2 ℃, indicating that the samples were sufficiently flexible at room temperature. The plasticizing efficiencies of USB-SPCLs were calculated using the following equation:[23,24]

$$E_{\Delta T_g}(\%) = \frac{\Delta T_{g,plasticizer}}{\Delta T_{g,DEHP}} \times 100 \qquad (2)$$

where $E_{\Delta Tg}$ is the plasticizing efficiency of the plasticizer and ΔT_g represents the reduction in T_g from neat PVC to flexible PVC. All USB-SPCLs exhibited $E_{\Delta Tg}$ values that exceeded 87.3% of the value of DEHP. In particular, USB-SPCL3-3 yielded a value of 92.9% (Table IV-4). These

results showed that USB-SPCLs were as good as DEHP in providing excellent flexibility to the PVC. The ordering of the USB-SPCL $E_{\Delta Tg}$ values corresponded to the inverse ordering of the T_g values, as shown in Table IV-1 and IV-4. It should be noted that the T_g values of USB-SPCLs were proportional to their respective total molecular weights, irrespective of the molecular architecture. Thus, the $E_{\Delta Tg}$ values, *i.e.*, the degree of flexibility in USB-SPCLs, were found to be inversely proportional to the total molecular weight rather than to the molecular architecture parameters. On the other hand, LCPL exhibited relatively high T_g and low $E_{\Delta Tg}$ values compared to USB-SPCL6-3, which had a similar total molecular weight (Table IV-4), indicating that the branched architecture of USB-SPCL6-3 improved the plasticizing efficiency.

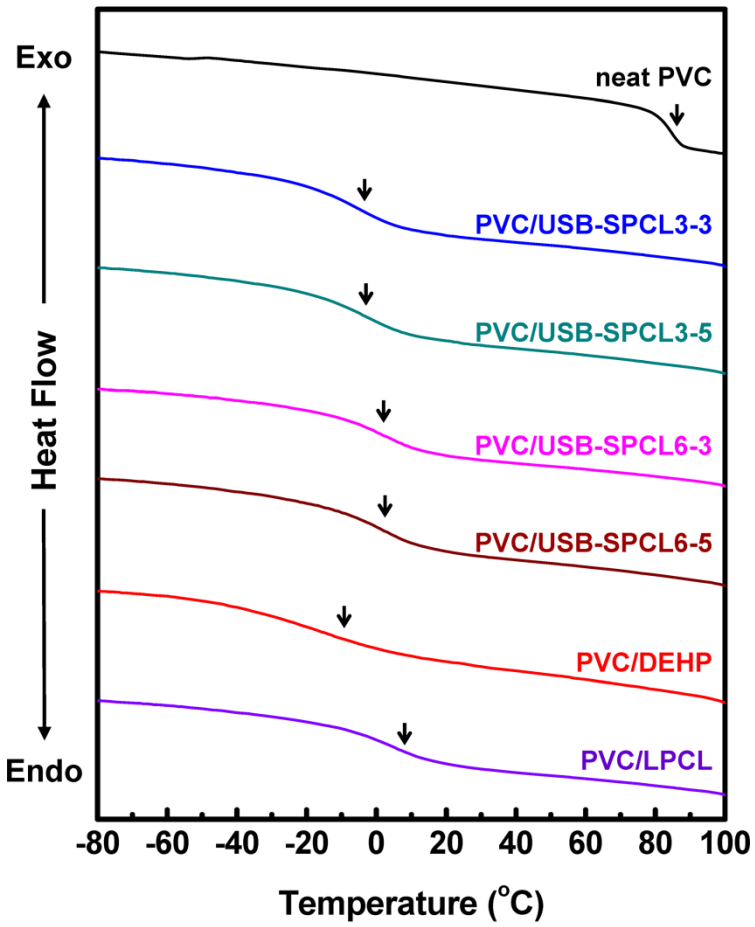

Figure IV-6. DSC thermograms of neat PVC, PVC/USB-SPCLs, PVC/DEHP, and PVC/LPCL recorded during a second heating step.

Table IV-4. Glass transition temperatures and percentage plasticizing efficiencies.

Sample	T_g (℃)	E_{Tg} (%)
PVC	84.8	0
PVC/USB-SPCL3-3	−3.3	92.9
PVC/USB-SPCL3-5	−2.5	92.1
PVC/USB-SPCL6-3	1.9	87.4
PVC/USB-SPCL6-5	2	87.3
PVC/DEHP	−10.0	100
PVC/LPCL	7	82.1

The Shore hardness offers a direct measurement of the flexibility of a material. The Shore hardness values of the samples prepared here were measured using two types of indenters: type A and type D Durometers. As shown in Figure IV-7(a), PVC/USB-SPCL3-3 and PVC/USB-SPCL3-5 yielded Shore A and D hardness values that were similar to those of PVC/DEHP, although PVC/USB-SPCL6-3 and PVC/USB-SPCL6-5 yielded slightly higher Shore A and D hardness values compared to the values of PVC/DEHP. These results revealed that PVC/USB-SPCLs had excellent flexibilities that were similar to the flexibility properties of PVC/DEHP. Taken together and considering the flexibility properties, USB-SPCL3-3, which showed the highest $E_{\Delta Tg}$ value and the lowest Shore hardness value, was thought to be the most suitable plasticizer for preparing phthalate-free flexible PVC products.

The mechanical properties of PVC/USB-SPCLs were investigated based on the stress−strain behaviors and the tear strength. As shown in Figure IV-8, all PVC/USB-SPCLs exhibited typical ductile stress−strain behaviors with shapes that resembled the curve obtained from PVC/DEHP. All of PVC/USB-SPCLs, however, displayed a higher tensile strength and a larger elongation at break value compared to PVC/DEHP. PVC/USB-SPCL6-5 displayed an elongation at break value that was 23% greater than the value obtained from PVC/DEHP. The elongation at break values of PVC/USB-

SPCLs increased as the total molecular weight increased, whereas PVC/USB-SPCLs displayed comparable tensile strength values across the series (see Table IV-5). These results indicated that USB-SPCLs conveyed a larger degree of stretchability to the PVC than did DEHP. The tear strength values of PVC/USB-SPCLs increased in the order PVC/USB-SPCL3-3 < PVC/USB-SPCL3-5 < PVC/USB-SPCL6-3 < PVC/USB-SPCL6-5 (Figure IV-7(b)), indicating that the toughness values of USB-SPCLs increased with increasing $N_{<\text{length}>}$ and N_{number}. Furthermore, PVC/USB-SPCL6-5 exhibited a 30% greater toughness compared to PVC/DEHP. Thus, an increase in the stretchability of PVC/USB-SPCLs was attributed to an improved toughness due to the introduction of USB-SPCLs with a total molecular weight exceeding that of DEHP. These properties allow USB-SPCLs to provide excellent stretchability and fracture toughness to the PVCs, to much greater effect than DEHP. PVC/LPCL displayed a ductile stress−strain curve, higher tensile strength, and larger elongation at break compared to PVC/DEHP (Figure IV-8); however, the stretchability and fracture toughness of LPCL was lower than the values obtained from USB-SPCL6-3 for similar total molecular weights. As a result, we found that star-shaped polymers have a better overall plasticizing performance than linear polymers because of their branching architecture.

Figure IV-7(c) shows images of flexible PVC sheets prepared using either USB-SPCLs or DEHP. As shown in Figure IV-7(c), the PVC/USB-SPCL and PVC/DEHP samples were transparent and did not differ in appearance, suggesting that all samples displayed similar optical properties. The optical properties were evaluated quantitatively by measuring the transmittance and haze values of the PVC/USB-SPCLs and PVC/DEHP samples. As shown in Figure IV-7(d), the transmittance values of PVC/USB-SPCLs were similar to the values obtained from PVC/DEHP. The haze values of PVC/USB-SPCLs were also similar to the value obtained from PVC/DEHP, although PVC/USB-SPCL3-5 had a slightly higher haze value and PVC/USB-SPCL6-3 had a slightly lower haze value. The similarities between the optical properties of PVC/USB-SPCLs and PVC/DEHP proposed that USB-SPCLs can be useful in transparent flexible PVC products.

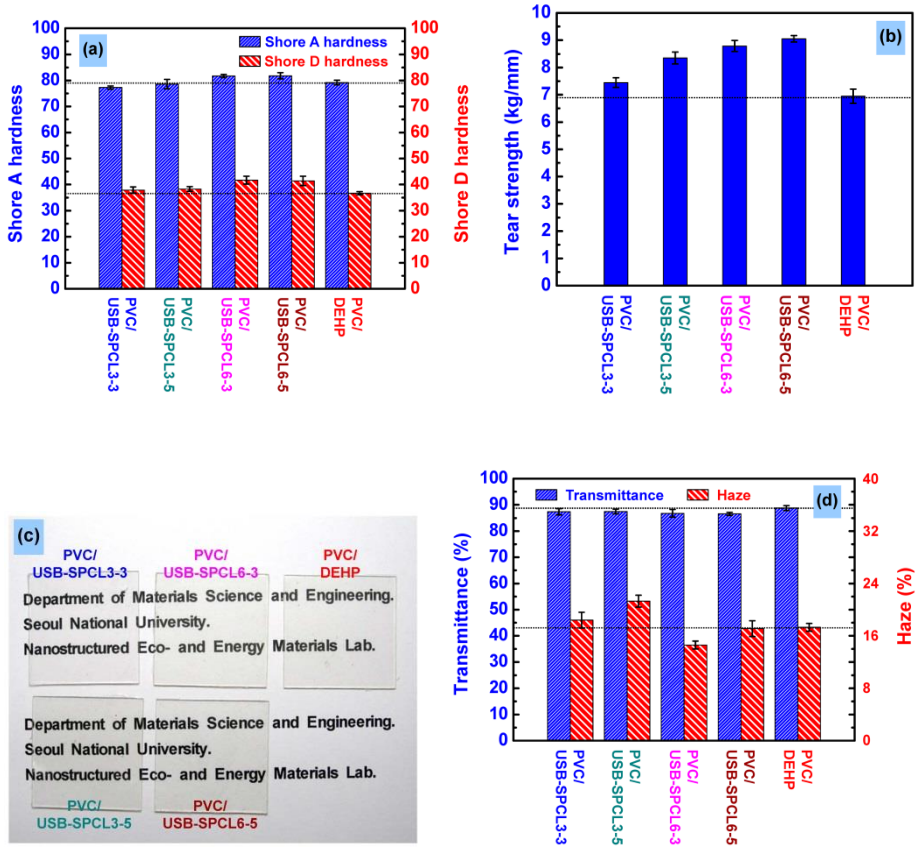

Figure IV-7. (a) Shore A and D hardness values, (b) tear strength values, (c) images of various blend sheets, (d) % transmittance and haze values for PVC/USB-SPCLs and PVC/DEHP.

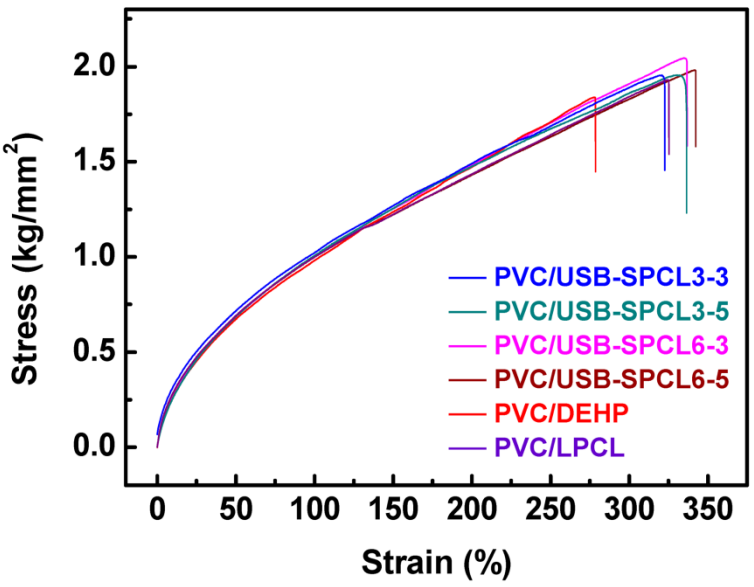

Figure IV-8. Tensile stress−strain curves for PVC/USB-SPCLs, PVC/DEHP, and PVC/LPCL.

Table IV-5. Tensile strengths and elongations at break.

Sample	Tensile strength (kg/mm^2)	Elongation at break (%)
PVC/USB-SPCL3-3	1.96	322
PVC/USB-SPCL3-5	1.96	336
PVC/USB-SPCL6-3	2.04	338
PVC/USB-SPCL6-5	2	343
PVC/DEHP	1.83	278
PVC/LPCL	1.95	326

IV-3-5. Migration resistance of USB-SPCLs

The migration resistance of USB-SPCLs was tested according to FDA procedures for simulating plasticizer migration from food packaging products into oily foods. n-Hexane was used as a extraction medium because the solubility profile of n-hexane is similar to that of cooking oil. The weight loss attributed to the loss of the plasticizer from a PVC product heated in n-hexane at 50 ℃ for 2 h must not exceed 5.5% if it is to be used in contact with foods, *e.g.* in plastic food wrap, food bags, or food storage containers. As shown in Figure IV-9(a), the weight losses of PVC/USB-SPCLs were negligible during the test period, whereas PVC/DEHP showed a weight loss of nearly 10%. These results indicated that USB-SPCLs can be useful for manufacturing flexible PVC products for use in the food packaging industry, whereas DEHP is prohibited from use in products that come in contact with food. The degree of plasticizer migration was determined according to ASTM procedures conducted under three different environmental conditions to approximate common PVC product use situations. The extractability test measured plasticizer migration into a liquid medium, such as an oily food or drink. The exudability test measured plasticizer migration in a food packaging or PVC leather product in contact with another solid substrate, such as a food or cloth. The volatility test measured plasticizer migration from a PVC flooring or wallpaper product into the ambient atmosphere (gas phase).

The simulation conditions were intensified to accelerate plasticizer migration within the experimental timeframe. The degree of plasticizer migration was calculated by measuring the specimen weight loss during the test period:

$$\text{Degree of Plasticizer Migration (\%)} = \frac{W_1 - W_2}{W_1 \times x} \times 100 \qquad (3)$$

where W_1 and W_2 represent the specimen weights before and after the tests, respectively, and x is the weight fraction of plasticizer in the specimens. Here, we assumed that the weight losses of the specimens were due only to USB-SPCLs or DEHP (32 wt%), although the secondary plasticizer (1 wt%) and the thermal stabilizer (2 wt%) also migrated during the tests. As shown in Figure IV-9(b), a trace quantity of USB-SPCLs migrated out of the PVC/USB-SPCL specimens under all conditions examined, whereas a considerable quantity of DEHP migrated out of the PVC/DEHP specimens. Particularly, more than 80% of DEHP present in the specimen migrated into the liquid phase, 25 times the degree of migration of USB-SPCLs. These results indicated that the migration of USB-SPCLs from the flexible PVCs was markedly reduced. It should be noted that the migration of USB-SPCLs decreased as the total molecular weight increased. This trend was observed under other migration conditions as well (exudability and volatility) and clearly revealed that the drastically high migration resistance of USB-SPCLs was attributed to an increase in the total molecular weight of USB-SPCLs.

The migration of USB-SPCLs was also thought to be restricted by the numerous carbonyl groups present in the branched segments, which formed attractive interactions with the PVC chains. These effects quite reduced the degree of USB-SPCL migration, even under harsh conditions. Consequently, our non-toxic USB-SPCLs can be useful for fabricating phthalate-free flexible PVC products designed for close contact with the human body, such as medical devices, infant care products, or food packaging products. Such products would avoid potential health risks and environmental concerns based on the migration properties of the phthalates currently in use.

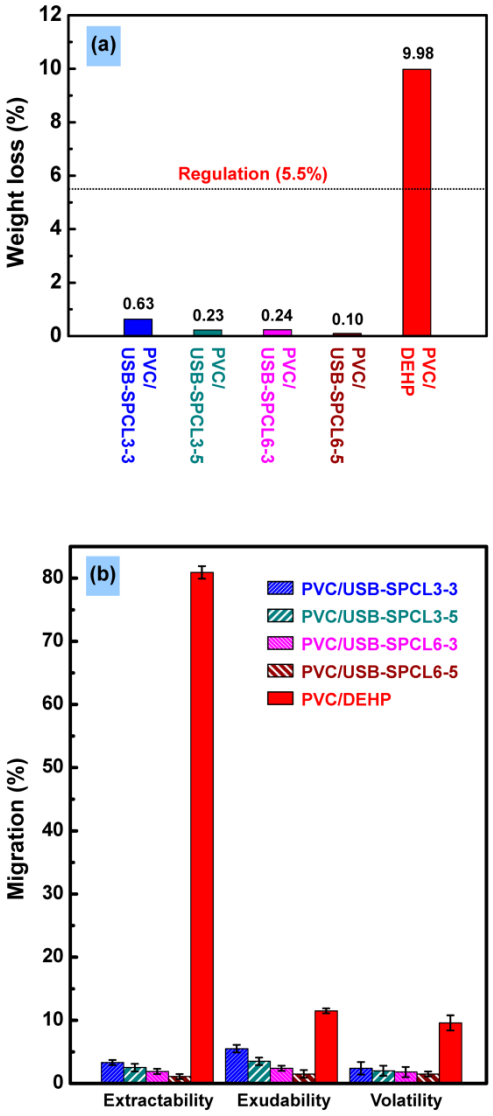

Figure IV-9. (a) Weight loss of PVC/USB-SPCLs and PVC/DEHP heated in n-hexane at 50 ℃ for 2 h, and (b) the degree of plasticizer migration for USB-SPCLs and DEHP, determined from the extractability, exudability, and volatility tests.

IV-4. Conclusion

We developed USB-SPCLs as non-toxic alternative plasticizers for use in phthalate-free flexible PVC products. USB-SPCLs were synthesized and purified to have a precisely controlled architecture through a facile pilot-scale pseudo-one-pot process combined with the end-capping and the vacuum treatment techniques. USB-SPCLs were transparent viscous liquids with unentangled Newtonian behaviors due to their extremely short branched segments. The compounds were found to be biologically safe without inducing acute toxicity. PVC/USB-SPCLs exhibited good processability with a fast fusion rate and a high miscibility with an average domain size of less than 8 nm. Moreover, USB-SPCLs provided excellent flexibility, transparency, stretchability, and fracture toughness to its PVC mixture, and the mixture properties were comparable to those conveyed by DEHP. USB-SPCLs were nearly resistant to migration from the flexible PVCs into a liquid phase, whereas considerable quantities of DEHP migrated out of the flexible PVC under identical circumstances. USB-SPCLs are, therefore, tremendously attractive as non-toxic alternative plasticizers for use in phthalate-free flexible PVC products ranging from medical devices to food packaging products.

References and Notes

1. Sanda, F.; Sanada, H.; Shibasaki, Y.; Endo, T. *Macromolecules* **2002**, *35*, 680−683.

2. Choi, J.; Kim, I.−K.; Kwak, S.−Y. *Polymer* **2005**, *46*, 9725−9735.

3. Fréchet, J. M. J. *Science* **1994**, *263*, 1710−1715.

4. Fukuzaki, H.; Yoshida, M.; Asano, M.; Kumakura, M. *Polymer* **1990**, *31*, 2006−2014.

5. Lin, S.−Y.; Chen, K.–S.; Teng, H.–H.; Li, M.–J. *J. Microencapsulation* **2000**, *17*, 577–586.

6. Noroozi, N.; Thomson, J. A.; Noroozi, N.; Schafer, L. L.; Hatzikiriakos, S. G. *Rheol. Acta.* **2012**, *51*, 179−192.

7. Nair, L. S.; Laurencin, C. T. *Prog. Polym. Sci.* **2007**, *32*, 762−798.

8. Ferry, J. D. *Viscoelastic Properties of Polymers*, 3rd ed; Wiley: New York, 1980.

9. Choi, W.; Chung, J. W.; Kwak, S.−Y. *ACS Appl. Mater. Interfaces* **2014**, *6*, 11118−11128.

10. Choi, W.; Chung, J. W.; Kwak, S.−Y. *J. Polym. Sci., Part A: Polym. Chem.* **2015**, *53*, 1134−1142.

11. Roovers, J. E. L.; Toporowski, P. M. *J. Appl. Polym. Sci.* **1974**, *18*, 1685−1691.

12. Choi, Y. K.; Bae, Y. H.; Kim, S. W. *Macromolecules* **1998**, *31*,

8766−8774.

13. Yang, Z.; Han, C. D. *Macromolecules* **2008**, *41*, 2104−2118.

14. Uppuluri, S.; Keinath, S. E.; Tomalia, D. A.; Dvornic, P. R. *Macromolecules* **1998**, *31*, 4498–4510.

15. Persenaire, O.; Alexandre, M.; Degée, P.; Dubois, P. *Biomacromolecules* **2001**, *2*, 288–294.

16. Schwab, P. A.; Wingrave, J. A. *J. Macromol. Sci., Part B: Phys.* **1981**, *20*, 429−440.

17. Paul, D.H. *J. Vinyl Technol* **1979**, *1*, 92−97.

18. Chen, C.H.; Wesson, R.D.; Collier, J.R.; Lo, Y.W. *J. Appl. Polym. Sci.* **1995**, *58*, 1107−1115.

19. Van Krevelen, D. W. *Properties of Polymers*; Elsevier: New York, 2003.

20. Greco, A.; Brunetti, D.; Renna, G.; Mele, G.; Maffezzoli, A. *Polym. Degrad. Stab.* **2010,** *95*, 2169−2174.

21. Huang, J.−M.; Yang, S.−J. *Polymer* **2005**, *46*, 8068−8078.

22. Yi, J. Z.; Goh, S. H. *Polymer* **2001**, *42*, 9313−9316.

23. Choi, J.; Kwak, S.−Y. *Environ. Sci. Technol.* **2007**, *41*, 3763−3768.

24. Yu, B. Y.; Chung, J. W.; Kwak, S −Y. *Environ. Sci. Technol.* **2008**, *42*, 7522−7527.

CHAPTER V

PHOTON CORRELATION DYNAMICS OF ULTRA-SMALL-BRANCHED POLY(ε-CAPROLACTONE)S AND ITS INTERACTION WITH PLASTICIZATION IN MISCIBLE BLEND SYSTEM

V-1. Introduction

Ultra-small-branched star poly(ε-caprolactone)s (USB-SPCLs) interestingly follow Rouse dynamic model for unentangled linear polymers although USB-SPCLs are star polymers, resulting in total-molecular-weight-dependent Rouse dynamics regardless of the molecular architecture parameters (*e.g.*, degree of branching and branching length).[1] This showed that a whole USB-SPCL molecule acts as a dynamically-equivalent single coarse-grain unit because of the extremely small branches. Such dynamic and structural features (including fast motion and high end-group concentration) of USB-SPCLs can provide high free volume in a miscible polymer blend, and thus we further investigated USB-SPCLs as nontoxic plasticizers for flexible poly(vinyl chloride)s (PVCs).[2] It was found that PVC/USB-SPCL blends

have a good miscibility with migration resistance and exhibit excellent flexibility, stretchability, and fracture toughness, indicating a high plasticizing efficiency of USB-SPCLs. Now, it is supposed to investigate how the total-molecular-weight-dependent Rouse dynamics of USB-SPCLs affects the plasticization of miscible PVC/USB-SPCL blends through the dynamic interplay between PVC and USB-SPCLs.

Rouse dynamics of unentangled USB-SPCLs in the pure state is modified in miscible PVC/USB-SPCL blends because of the interchain dynamic constraints and intermolecular interactions with entangled linear PVC matrix, whereas the Rouse theory ignores local intermolecular interactions and the surrounding chains are described as a continuum that provide only a heat bath.[3–6] Such modified dynamic behaviors in the miscible PVC/USB-SPCL blends can be analyzed using time-resolved scattering of photon correlation spectroscopy (PCS) in concentrated solution system.[7–10] Wide frequency capability of PCS covers a dynamic range of a few or many decades of delay time, which allows quantitative determination of various types of polymer molecular motions.[7–9,11,12] High sensitivity of PCS, in the blend system, enables observation of two separate relaxation modes, indicating distinct motional characteristics of the individual components. Several previous PCS studies have found that the individual component dynamic processes are observed even in the miscible blends, resulting from a significant difference

between the component segmental relaxation rates.[8,9,12–15] In addition, PCS in concentrated solution system provides the time-resolved scattering profiles in the pure and blend states under the same conditions (including the same temperature in the same phases), and thus the dynamic changes before and after blending are directly comparable even though USB-SPCLs are liquid phase and PVC is solid phase above room temperature. The dynamics in the concentrated polymer solutions, so-called pseudo-bulk dynamics, does not essentially vary from the dynamic properties in bulk polymers because a concentrated polymer solution in a good solvent contains a three-dimensional fluctuating network with overlapping neighboring polymer coils (the individual polymer segments belonging to different chains and/or distant parts of the same chain are packed very closely to one another and solvent molecules are distributed uniformly among them) and has stronger polymer−polymer interactions than polymer−solvent interactions.[16–20] Actually, Lai et al. reported the time-resolved scattering of PCS in both concentrated polymer solution and polymer melt using polystyrene.[21,22] They showed that the relaxation times of the polymer motion in both concentrated solution and melt systems have the same order of magnitude as chain mobility, although the concentrated solution system has much lower relaxation time and narrower relaxation time distribution due to the solvent effect. It is therefore expected that the pseudo-bulk dynamics of PVC, USB-SPCLs, and their miscible blends shows the dynamic changes of PVC and

USB-SPCLs in the blends and reflects plasticizing effects of unentangled USB-SPCLs on entangled linear PVC matrix.

The pseudo-bulk dynamics using PCS basically quantifies the relaxation time as a function of the magnitude of the scattering vector, *i.e.*, the scattering-vector-dependent dynamic structure factor, and obtains the correlation function of the scattered light intensity with certain delay times.[10,23,24] The obtained time variations in the scattered light intensity are analyzed to determine the autocorrelation function of the scattered light intensity. The normalized form of the intensity autocorrelation function is given as follows:[7,8,20,25,26]

$$g_2(t) = \frac{G_2(\tau)}{\langle I(t)\rangle^2} = \frac{\langle I(t)I(t+\tau)\rangle}{\langle I(t)\rangle^2} \qquad (1)$$

where $g_2(t)$ is the normalized intensity autocorrelation function, $G_2(\tau)$ is the intensity autocorrelation function, $I(t)$ is the intensity fluctuation function, τ is the delay time, and the brackets indicate a time average. The $g_2(t)$ is correlated with the theoretical normalized field autocorrelation function, according to the Siegert relationship as follows:[7,8,20,25,26]

$$g_2(t) = 1 + f|g_1(t)|^2 \qquad (2)$$

where $g_1(t)$ is the normalized field autocorrelation function, and f is an instrumental parameter accounting for deviation from the ideal correlation. In the polymer blend system, two relaxation modes of the autocorrelation function can be fitted to the double Kohlrausch–Williams–Watts (KWW) equation:[8,9,27]

$$g_1(t) = \alpha_f \exp\left[-\left(\frac{t}{\tau_f}\right)^{\gamma}\right] + \alpha_s \exp\left[-\left(\frac{t}{\tau_s}\right)^{\beta}\right] \qquad (3)$$

where the parameters α_f and α_s are the amplitudes of the fast and slow relaxation modes, respectively, with $\alpha_f + \alpha_s = 1$. The variables τ_f and τ_s are the effective relaxation times for the fast and the slow relaxation modes, respectively, and γ ($0 < \gamma \leq 1$) and β ($0 < \beta \leq 1$) indicate the widths of the distributions of the relaxation times. The fast relaxation mode term (first term on the right-hand side of equation (3)) represents the short-time behaviors of polymer chains related to a cooperative diffusion coefficient, which reflects a concerted motion of the polymer chains. The slow relaxation mode term (second term on the right-hand side of equation (3)) represents the long-time behaviors of polymer chains associated with disengagement relaxation of individual chains or cluster relaxation.

In this study, the pseudo-bulk dynamics of PVC, USB-SPCLs, and their miscible blends was analyzed using PCS in concentrated solution system at

around room temperature, in order to investigate the dynamic effects of USB-SPCLs on the plasticization of miscible PVC/USB-SPCL blends.[28] Photon correlation dynamics of USB-SPCLs depended on their total molecular weights regardless of the molecular architectures, in good agreement with their melt dynamic behaviors. Dynamic homogeneous behaviors of PVC/USB-SPCL blends were observed and depended on the total-molecular-weight-dependent Rouse dynamics of USB-SPCLs despite their significant mobility difference, resulting from strong intermolecular interactions between PVC and USB-SPCL molecules. These dynamic results showed that the molecular motion of USB-SPCLs is highly reduced by constraint of the entangled linear PVC matrix and, instead, PVC chain motion increases up to the same mobility level of the constrained USB-SPCLs in the PVC matrix. This clearly indicated that the entangled linear PVC matrix was plasticized by distinctive and rapid molecular mobility of USB-SPCLs, resulting in the excellent flexibility of miscible PVC/USB-SPCL blends. We believe that these findings provide further understanding of the plasticization of entangled linear polymer matrix by unentangled star-shaped polymers with extremely small branches in miscible polymer blend.

V-2. Experimental Section

V-2-1. Materials

ε-Caprolactone (CL) and trimethylolpropane (TMP) were purchased from the Alfa Aesar Co., Ltd., USA and the Tokyo Chemical Industry Co., Ltd., Japan, respectively. Dipentaerythritol (DPTOL), tin(II) 2-ethylhexanoate ($Sn(Oct)_2$), acetic anhydride (Ac_2O), and anhydrous tetrahydrofuran (THF) were purchased from Sigma-Aldrich Ltd., Korea. Suspension-grade PVC resin (P-1000) was kindly provided by the Hanwha Chemical Co., Ltd., Korea. All chemicals were used without further purification.

V-2-2. Synthesis of USB-SPCLs

We synthesized three- and six-branched USB-SPCLs with three and five CL repeating units in each individual branch (DP = 3 or 5), initiated from TMP and DPTOL cores, using a previously developed method that solved a chronic synthetic problem associated with cyclic PCLs.[3,29] The synthesis was performed by manipulating the monomer-to-core ratio, adjusting monomer-to-polymer conversion, end-capping the terminal hydroxyl groups, and vacuum purification, in a facile pseudo-one-pot bulk process without any organic solvent. Precisely controlled USB-SPCLs with molecular architectures that

varied with respect to the number of branches, N_{number}, and the average length of the individual branches (the average DP per branch), N_{length}, were synthesized; these USB-SPCLs are denoted by USB-SPCLN_{number}-N_{length}: USB-SPCL3-3, USB-SPCL3-5, USB-SPCL6-3, and USB-SPCL6-5. The molecular architectures of four different USB-SPCLs are shown in Figure V-1. The N_{number} and N_{length} values were determined using ^{1}H nuclear magnetic resonance (NMR) spectroscopy, and the number-average molecular weights, M_n, the weight-average molecular weights, M_w, and the polydispersity indexes (PDIs) were determined using matrix-assisted laser desorption/ionization time-of-flight mass spectrometry (MALDI-TOF-MS); the results confirmed that the desired molecular architectures and narrow PDIs ($M_w/M_n \leq 1.2$) had been achieved (Table V-1). The completely capped terminal hydroxyl groups with small acetate groups enable investigation of the molecular behaviors of USB-SPCLs in the absence of hydrogen-bonding effects. More detailed information on the syntheses and characterization of USB-SPCLs is available in our previous publications.[2,29]

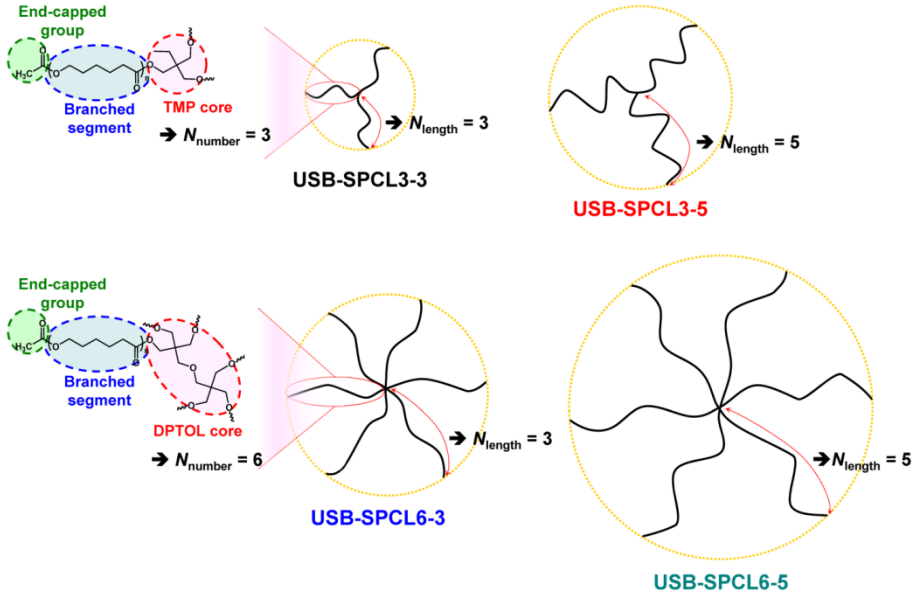

Figure V-1. Molecular architectures of four different USB-SPCLs.

Table V-1. The numbers and lengths of branches and molecular weights of USB-SPCLs.

Sample	USB-SPCL3-3	USB-SPCL3-5	USB-SPCL6-3	USB-SPCL6-5
N_{number}	2.94	3.00	6.06	6.06
N_{length}	3.09	5.06	3.06	5.2
M_n (g mol^{-1})	1310	2110	2470	3610
M_w (g mol^{-1})	1600	2600	2640	3930
PDI	1.22	1.23	1.07	1.09

V-2-3. PCS analysis

Concentrated ternary solutions of PVC/USB-SPCLs in THF were prepared at the same total solute (USB-SPCLs and PVC) concentration, *i.e.*, 0.2 g mL^{-1}. Here, THF was taken as a good solvent for both PVC and USB-SPCLs.[18,30] The PVC:USB-SPCL weight ratio in THF was accurately controlled to 100:60, which is within the maximum ratio that does not induce crystallization of PCLs in the bulk system.[31] The solutions were stirred for 24 h and then filtered several times through Millipore membranes of pore diameter 0.45 mm into dust-free cells. We also prepared concentrated binary solutions of PVC and USB-SPCLs in THF at the same solute concentration, *i.e.*, 0.2 g mL^{-1}, and these solutions were also analyzed.

PCS measurements were performed with a Photal DLS 7000 spectrometer, using a 488 nm argon ion laser operated at 70 mW. A Photal GC 1000 autocorrelator was used to determine the intensity autocorrelation function, $G_2(\tau)$, from the time variations in the scattered intensity, $I(t)$. All measurements were performed at 30–50 ℃ at scattering angles of 40°, 65°, 90°, and 115°. All calculated values were the average values for six experiments, and the experimental error was the standard deviation.

V-2-4. Differential scanning calorimetry (DSC) analysis

Bulk PVC/USB-SPCL films were prepared by solution blending, with THF as the solvent, using the method and formulation generally used for studying PVC films.[32] PVC and USB-SPCLs were dissolved in THF, at the same composition as that used in the PCS measurements, *i.e.*, a PVC:USB-SPCL weight ratio of 100:60. The mixture was stirred vigorously to ensure homogeneity, and then the THF was slowly evaporated in an oven at 40 ℃ for 24 h to eliminate all residual solvent. This gave transparent bulk PVC/USB-SPCL films. In addition, a neat PVC film without any USB-SPCL was also prepared using the same solution blending procedure.

The glass transitions of USB-SPCLs, neat PVC and PVC/USB-SPCL films were observed using DSC (Netzsch DSC 200 F3 instrument) at a heating rate of 10 ℃ min^{-1} over the temperature range –110 to 140 ℃ under a nitrogen atmosphere. The glass transition temperature, T_g, was determined in each case from the inflection point in the second DSC curve.

IV-3. Results and Discussion

Figure V-2(a) shows the intensity autocorrelation functions, plotted as $g_2(t)$–1 versus *t*, for concentrated solutions of PVC, USB-SPCL3-3, and PVC/USB-SPCL3-3 in THF, measured at 30 ℃ and a scattering angle of 40°. The other intensity autocorrelation curves, for concentrated binary (USB-SPCLs in THF) and ternary (PVC/USB-SPCLs in THF) solutions, showed the same trends (see Figure V-3). The intensity autocorrelation curves of the concentrated binary solutions (PVC in THF and USB-SPCLs in THF) were typical, and each showed a single-exponential behavior and asymptotically tended to zero as $t \rightarrow \infty$. The intensity autocorrelation curves of USB-SPCLs in THF were observed higher $g_2(t)$–1 values in the short delay time region and faster decay to zero as the delay time increased compared with that of PVC in THF. This indicates that the USB-SPCL molecules had higher relaxation strengths and faster relaxation rates than did the PVC molecules. It was notable that the intensity autocorrelation curves of the concentrated ternary systems, *i.e.*, PVC/USB-SPCLs in THF, also showed single-exponential behaviors with similar relaxation strengths to those of USB-SPCLs and similar relaxation rates to that of PVC, rather than double-exponential decay with two relaxation modes. In several previous studies, the double-exponential decay was observed even in miscible blends because of a significant difference between component segmental relaxation rates,

indicating two distinct dynamic behaviors of the individual components in the miscible blends, *i.e.*, dynamic heterogeneity of the miscible polymer blends.[8,9,12,13] Thus, the single-exponential decay for PVC/USB-SPCLs indicated that the significant different dynamic behaviors of USB-SPCL and PVC molecules changed to become the same (or almost the same) dynamic behavior on blending USB-SPCLs into PVC, *i.e.*, dynamic homogeneity of miscible PVC/USB-SPCL blends. This was attributed to the strong specific intermolecular interactions between PVC and USB-SPCL molecules (including hydrogen bonding interaction between the carbonyl group of PCL and the α-hydrogen of PVC, dipole–dipole interaction between the carbonyl group of PCL and the carbon–chlorine group of PVC, and six center interaction between the carbonyl group of PCL and the chlorine and β-hydrogen of PVC) because the dynamic heterogeneity in miscible blends can be reduced or even eliminated by strong intermolecular interactions.[6,12,14,33–35] Quantitative analysis of these intensity autocorrelation curves was performed by fitting the experimental data for PVC, USB-SPCLs, and PVC/USB-SPCLs to the single KWW equation:[7–9,20,25,26]

$$g_1(t) = \alpha_c \exp\left[-\left(\frac{t}{\tau_{\mathrm{KWW}}}\right)^{\beta}\right] \qquad (4)$$

where α_c is the relaxation strength, τ_{KWW} is the relaxation time, and β is the stretch parameter; these are treated as adjustable parameters. The

parameter β has the value 1 for a single exponential, and the value decreases as the distribution of the relaxation time becomes broader. As expected, this single KWW equation (equation (4)) successfully fitted the experimental data, shown by the solid lines in Figure V-2(a) and Figure V-3; the β values for all the samples were ca. 1. This revealed that concentrated solution systems of PVC, USB-SPCLs, and PVC/USB-SPCLs in THF had one relaxation process with narrow distributions of relaxation times, indicating that the PVC and USB-SPCL molecules both exhibited the same relaxation behaviors in their miscible blends.[9,20,25] The distribution of relaxation times can be also determined using the inverse Laplace transform (ILT), as shown below:[7–9,20,25,26]

$$g_1(t) = \int_{-\infty}^{+\infty} \exp\left(-\frac{t}{\tau}\right) L(\ln \tau)\, d \ln \tau \qquad (5)$$

where $L(\ln \tau)$ is the distribution of relaxation times. Figure V-2(b) shows the distributions of relaxation times corresponding to $L(\ln \tau)$ for PVC, USB-SPCL3-3, and PVC/USB-SPCL3-3 in THF plotted against $\log \tau$, which were obtained from ILT analyses. The single and narrow feature in these spectra clearly shows only one relaxation process for PVC, USB-SPCL3-3, and even the PVC/USB-SPCL3-3 blend. These results also indicate that the concentrated solution systems of PVC, USB-SPCLs, and PVC/USB-SPCLs in

THF were microscopically homogeneous and the molecules in these systems showed cooperative chain diffusive motion.[9,20,25]

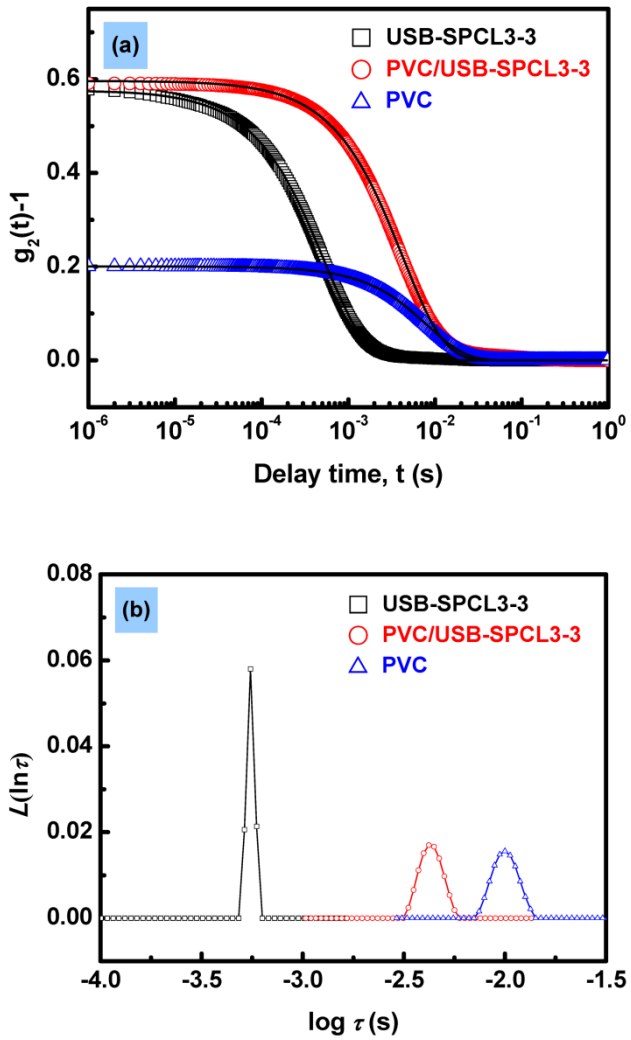

Figure V-2. (a) Intensity autocorrelation functions and solid lines fitting to KWW equation and (b) Distribution of relaxation times obtained from the ILT analyses for concentrated solutions of PVC, USB-SPCL3-3, and PVC/USB-SPCL3-3 in THF at 30 ℃ and scattering angle 40°.

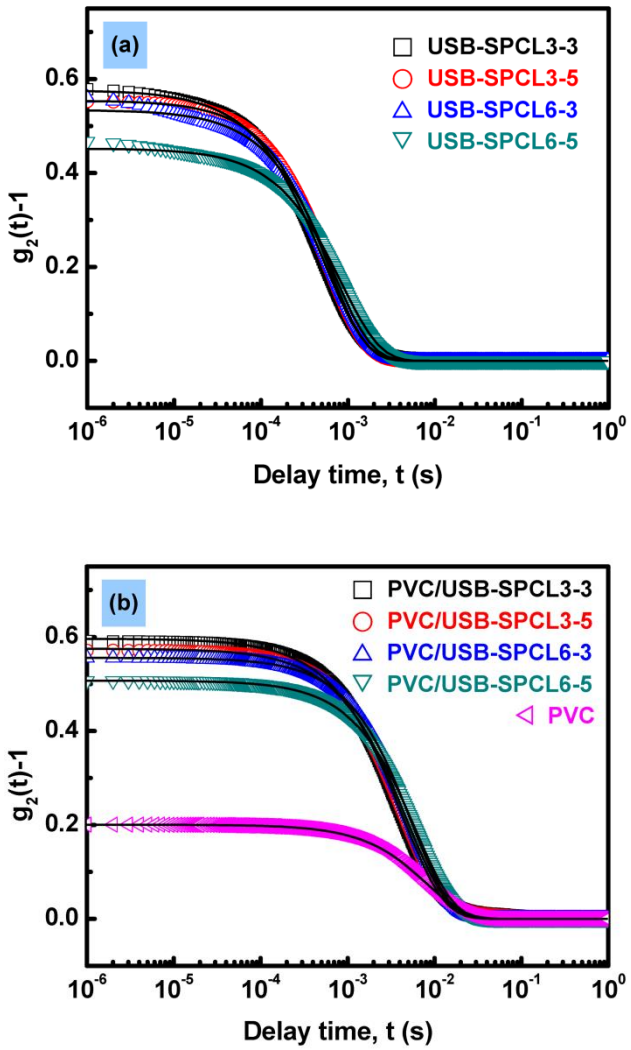

Figure V-3. Intensity autocorrelation functions and solid lines fitting to KWW equation for concentrated solutions of (a) USB-SPCLs, (b) PVC/USB-SPCLs and PVC in THF at 30 ℃ and scattering angle 40°.

Meanwhile, the relaxation rates, Γ, for all the samples at 30 ℃ were determined from the reciprocal of their τ_{KWW} values, obtained from equation (4) (both values are listed in Table V-2). The data in Table V-2 show that the Γ values of PVC/USB-SPCL samples were 8.4–7.6 times lower than those of the USB-SPCL samples and 2.2–1.6 times higher than that of the PVC sample, indicating that the relaxation motions of PVC increased after blending with USB-SPCL molecules. The relaxation rates at four scattering angles (40°, 65°, 90° and 115°) at 30 ℃ were also observed using angle-dependent PCS experiments, which can rule out the possible contribution to the relaxation processes and provide more detailed dynamic information of the cooperative chain diffusive motion. The angular dependences of the relaxation rates for PVC, USB-SPCL3-3, and PVC/USB-SPCL3-3 molecules are shown in Figure V-4(a). At all experimental scattering angles, the order of the Γ values was USB-SPCL3-3 > PVC/USB-SPCL3-3 > PVC, and all of these Γ values for PVC, USB-SPCL3-3, and PVC/USB-SPCL3-3 molecules increased with increasing scattering angle. Moreover, each of the Γ values was linearly dependent on the square of the scattering vector, q^2, indicating that the relaxation processes of the concentration fluctuation were governed by cooperative chain diffusive motion.[36,37] The other Γ values for USB-SPCL or PVC/USB-SPCL molecules showed the same trends (see Figure V-5). These results enabled us to estimate the cooperative diffusion coefficient

in the laboratory frame from the slopes of the straight lines shown in Figure V-4(a) and Figure V-5, using the following relationship:[7–9,20,25]

$$\Gamma = D_c q^2 \qquad (6)$$

where D_c is the cooperative diffusion coefficient. The determined D_c values for PVC, USB-SPCLs, and PVC/USB-SPCL molecules are shown in Figure V-4(b) as a bar graph. The D_c values in Figure V-4(b) were filled in the order of USB-SPCLs > PVC/USB-SPCLs > PVC, and USB-SPCLs had 8.5–7.9 times higher and PVC had 2.2–1.6 times lower than PVC/USB-SPCLs. This was consistent with the relationship of the relaxation rates for PVC, USB-SPCL, and PVC/USB-SPCL molecules, indicating the fast relaxation mode of all the samples in which the short-time behaviors of polymer chains relate to the cooperative chain diffusive mobility.[8,9,27] Thus, in the case of USB-SPCLs, the order of the D_c values revealed that the cooperative chain diffusive mobilities of USB-SPCL molecules were USB-SPCL3-3 > USB-SPCL3-5 > USB-SPCL6-3 > USB-SPCL6-5. It is generally accepted that a greater number of branches at a given total molecular weight, *i.e.*, high end-group concentration, are known to yield a smaller pervaded volume ($V \approx R^3$) and rapid molecular mobility.[1,5,38,39] Thus, the end-group concentrations of USB-SPCLs were determined by 'N_{number}/M_n', and the end-group concentration dependent D_c values are shown in Figure V-4(c).[39] In the case

of the same N_{number}, USB-SPCL3-3 with a higher end-group concentration had a higher D_c value than USB-SPCL3-5 with a lower end-group concentration, and USB-SPCL6-3 also had a higher D_c value than USB-SPCL6-5, in good agreement with the feature of typical star-shaped polymers. In the case of the same N_{length}, however, USB-SPCL3-3 had a higher D_c value than USB-SPCL6-3 and USB-SPCL3-5 had a higher D_c value than USB-SPCL6-5, even though the end-group concentrations of USB-SPCL3-3 and USB-SPCL3-5 are respectively lower than those of USB-SPCL6-3 and USB-SPCL6-5. Moreover, USB-SPCL6-3 with the highest relatively end-group concentration and USB-SPCL5-3 with the lowest relatively end-group concentration had intermediate D_c values among USB-SPCLs. These results indicated that the cooperative chain diffusive mobility of USB-SPCL molecules does not depend on their end-group concentrations, *i.e.*, molecular architecture variations in N_{number} and N_{length}, which differed from dynamic properties of typical star-shaped polymers. The D_c values of USB-SPCLs interestingly appeared to be proportional to their total molecular weights as shown in Figure V-4(c), which supports our previous suggestion that a whole USB-SPCL molecule acts as a single coarse-grain unit with dynamically-equivalent branches because of the extremely small branches, on the scale of 20–40 atoms.[40] This clearly showed that the cooperative chain diffusive motion of USB-SPCLs exhibited total-molecular-weight-dependent Rouse dynamic behaviors that followed unentangled linear polymer models.[40] In the

PVC/USB-SPCL blend system, the order of the D_c values was PVC/USB-SPCL3-3 > PVC/USB-SPCL3-5 > PVC/USB-SPCL6-3 > PVC/USB-SPCL6-5, and the cooperative chain diffusive mobilities of the PVC/USB-SPCL blends appeared to depend on the total-molecular-weight-dependent Rouse dynamics of USB-SPCLs. This can be thought that USB-SPCL molecular motion only slowed down but still depended on their total molecular weights, regardless of molecular architectures, in the PVC matrix and, further, strong intermolecular interactions between PVC and USB-SPCL molecules led to the chain motion of the PVC matrix following the USB-SPCL molecular motions, resulting in the homogeneous dynamic behaviors of PVC/USB-SPCL blends.

Table V-2. Relaxation times and relaxation rates for PVC, USB-SPCLs, and PVC/USB-SPCLs.

Sample	τ_{KWW} (ms)	Γ (s^{-1})
PVC	10.020 ± 0.082	100 ± 1
USB-SPCL3-3	0.553 ± 0.050	1817 ± 169
USB-SPCL3-5	0.600 ± 0.040	1672 ± 112
USB-SPCL6-3	0.630 ± 0.026	1589 ± 68
USB-SPCL6-5	0.827 ± 0.035	1211 ± 52
PVC/USB-SPCL3-3	4.603 ± 0.101	217 ± 5
PVC/USB-SPCL3-5	5.001 ± 0.130	200 ± 5
PVC/USB-SPCL6-3	5.298 ± 0.149	189 ± 5
PVC/USB-SPCL6-5	6.289 ± 0.093	159 ± 3

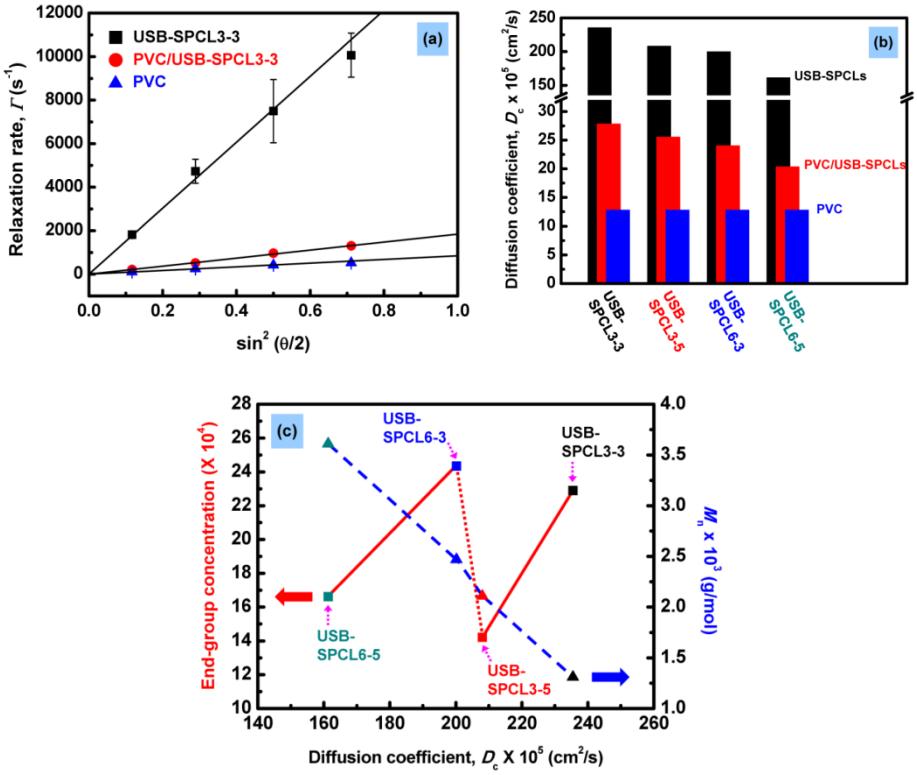

Figure V-4. (a) q^2-dependences of Γ for concentrated solutions of PVC, USB-SPCL3-3, and PVC/USB-SPCL3-3 in THF at 30 ℃ at various scattering angles; $q = (4\pi n_0/\lambda)\sin(\theta/2)$, where q is scattering vector, n_0 is refractive index, θ is scattering angle, and λ is radiation wavelength. Some error bars are smaller than symbols. (b) Determined D_c values for concentrated solutions of PVC, USB-SPCLs, and PVC/USB-SPCLs in THF. (c) Determined D_c values for concentrated solutions of USB-SPCLs in THF as function of end-group concentration and total M_n.

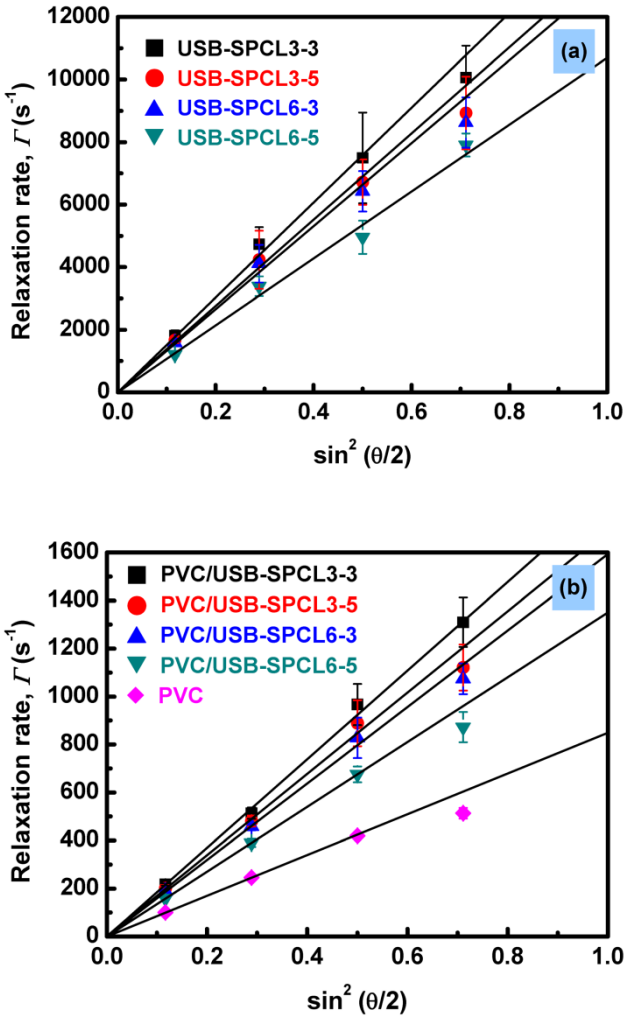

Figure V-5. q^2-dependences of Γ for concentrated solutions of (a) USB-SPCLs, (b) PVC/USB-SPCLs and PVC in THF at 30 ℃ at various scattering angles. Some error bars are smaller than symbols.

The cooperative chain diffusive motions of PVC, USB-SPCLs, and PVC/USB-SPCLs were investigated more quantitatively using the correlation time and the apparent activation energy, because the correlation time is defined as the relaxation time required for motional events and the apparent activation energy corresponds to the barrier height for potential hindering motion.[11,29] The correlation time for cooperative chain diffusive motions of PVC, USB-SPCLs, and PVC/USB-SPCL molecules were determined from the parameters, τ_{KWW} and β obtained by KWW fitting, as follows:[20,25]

$$\tau_c = \langle \tau_{\mathrm{KWW}} \rangle = \int_0^{+\infty} \exp\left[-\left(\frac{t}{\tau_{\mathrm{KWW}}} \right)^{\beta} \right] dt = \frac{\tau_{\mathrm{KWW}}}{\beta} \Gamma\left(\frac{1}{\beta} \right) \qquad (7)$$

where τ_c is the correlation time and Γ is the gamma function. Figure V-6(a) shows the determined τ_c values for PVC, USB-SPCL3-3, and PVC/USB-SPCL3-3 as a function of temperature around room temperature at a scattering angle of 40°. As shown in Figure V-6(a), the τ_c values over the entire range of experimental temperatures increased in the order USB-SPCL3-3 < PVC/USB-SPCL3-3 < PVC, and the log τ_c values for each of samples were linearly dependent on the reciprocal of the temperature and increased with decreasing temperature. The difference of the τ_c values between the pure and blend states became smaller as the temperature increased, resulting from the strong interactions between molecules at low temperature relative to the thermal fluctuation.[41] This revealed that the cooperative diffusive chain

mobility of USB-SPCL3-3 was highly reduced by the constraint of the entangled linear PVC matrix and, instead, PVC chain motion increased up to the same mobility level of the constrained USB-SPCL3-3 in the PVC matrix. Furthermore, this clearly indicated that the entangled linear PVC matrix was plasticized by distinctive and rapid molecular mobility of USB-SPCL3-3. These phenomena were also observed in other USB-SPCLs and PVC/USB-SPCL samples (see Figure V-7).

The apparent activation energies for cooperative chain diffusive motions of PVC, USB-SPCLs, and PVC/USB-SPCL molecules can be determined from the linearly dependent correlation time data in Figure V-6(a) and Figure V-7 using the Arrhenius equation, as follows:[20,25]

$$\log \tau_c = \log \tau_{c,0} + \frac{E_a}{2.303RT} \qquad (8)$$

where $\tau_{c,0}$ is the preexponential factor, E_a is the apparent activation energy, and R is the gas constant. The straight lines in Figure V-6(a) and Figure V-7 represent the fits of τ_c to equation (8), and the E_a values at around room temperature were derived from the slopes of these plots. The determined E_a values for all the samples are shown in Figure V-6(b). The E_a value of PVC was higher than those of other samples, indicating that the PVC molecules in the pure state had the highest motional barrier relative to the

cooperative chain diffusive motion. USB-SPCLs had lower E_a values than PVC/USB-SPCLs, and the E_a values of USB-SPCLs and PVC/USB-SPCLs increased with increasing the total molecular weights of USB-SPCLs. This revealed that the cooperative chain diffusive motional barrier of USB-SPCLs exhibited total-molecular-weight-dependent Rouse dynamic behaviors in both pure and blend states, resulting in decrease in the motional barrier of the PVC molecules in the blend state. These pseudo-bulk dynamic results well reflected the effects of USB-SPCL molecules on the plasticization of miscible PVC/USB-SPCL blends in the bulk system. The glass transitions of bulk PVC/USB-SPCL films and their neat components without THF solvent were observed using the DSC technique (Figure V-8), because the lowering T_g values of bulk PVC/USB-SPCL films from the neat PVC value indicate the plasticizing efficiency of USB-SPCLs.[2] The single glass transitions for each of bulk PVC/USB-SPCL films as well as their neat components were shown in Figure V-8, despite the significant difference in the T_g values for bulk PVC and USB-SPCL samples (> 147 ℃), indicating that PVC and USB-SPCLs were physically miscible.[42] The T_g values for bulk USB-SPCLs and PVC/USB-SPCL samples depended on the total molecular weights of USB-SPCLs regardless of the molecular architectures, and the T_g value of the PVC matrix was lowered to 71–74% of its neat value in K after blending with USB-SPCL molecules. These DSC results revealed that entangled linear

PVC chains were plasticized by USB-SPCL molecules, resulting in flexible PVC/USB-SPCL films, which is supported by the pseudo-bulk dynamic results obtained from the PCS technique.

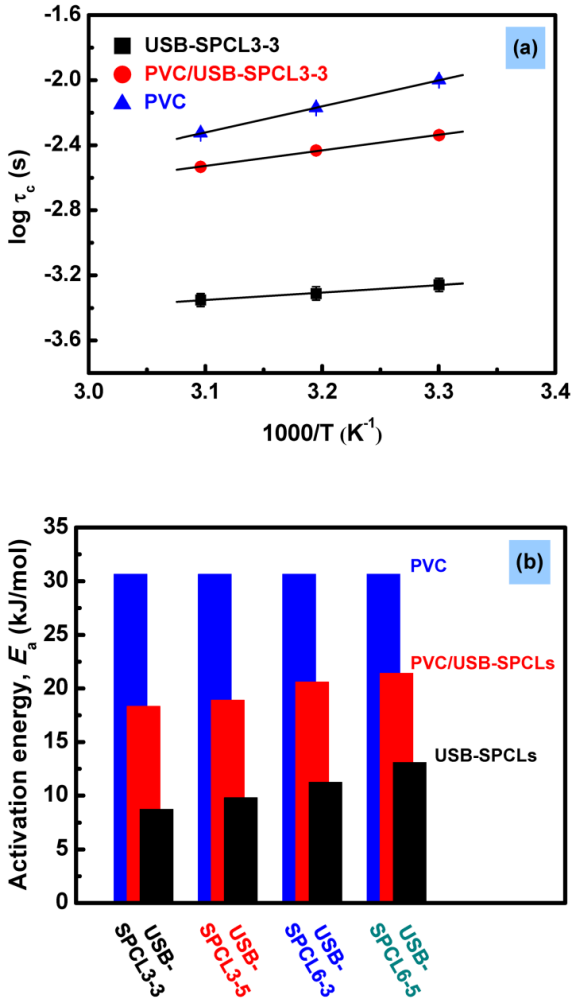

Figure V-6. (a) Arrhenius plots of $\log \tau_c$ for concentrated solutions of PVC, USB-SPCL3-3, and PVC/USB-SPCL3-3 in THF at scattering angle 40° as function of inverse temperature. Some error bars are smaller than symbols. (b) Estimated E_a values for concentrated solutions of PVC, USB-SPCLs, and PVC/USB-SPCLs in THF.

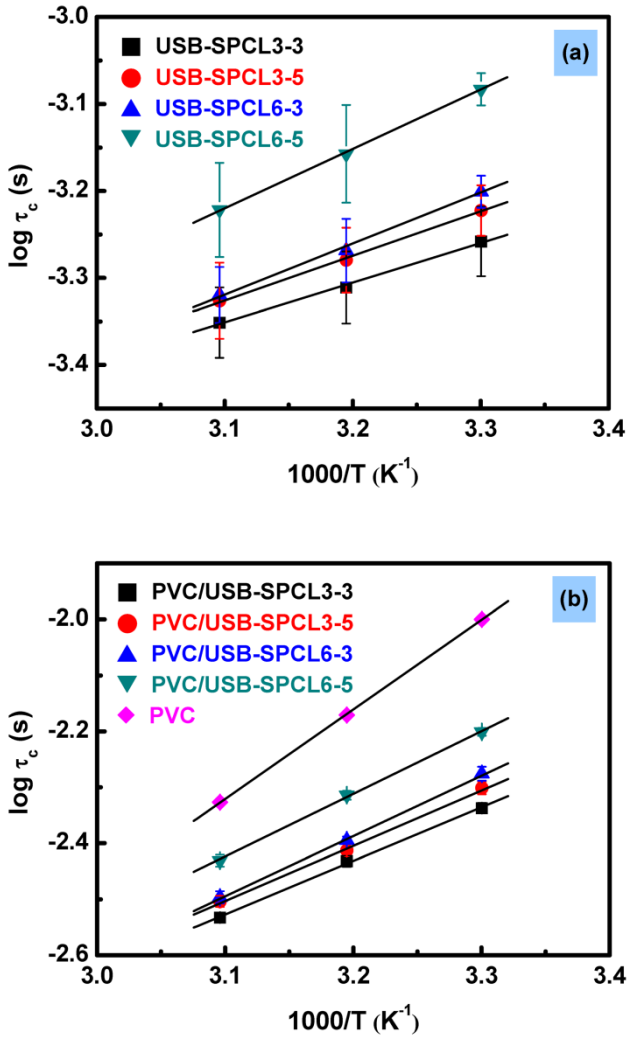

Figure V-7. Arrhenius plots of $\log \tau_c$ for concentrated solutions of (a) USB-SPCLs, (b) PVC/USB-SPCLs and PVC in THF at scattering angle 40° as function of inverse temperature. Some error bars are smaller than symbols.

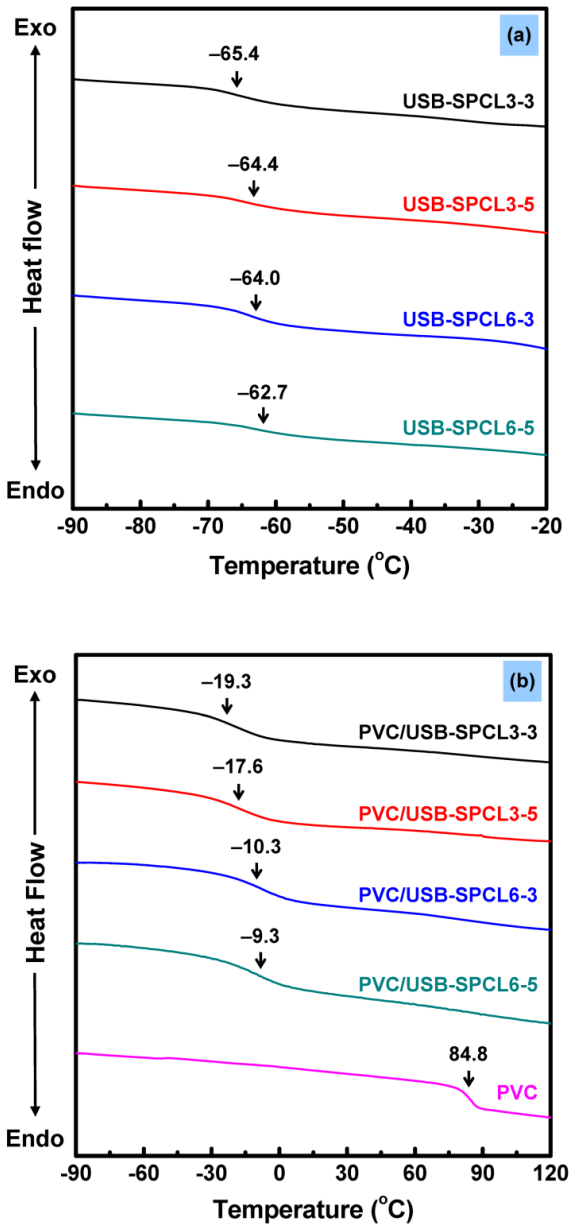

Figure V-8. DSC thermograms of bulk samples ((a) USB-SPCLs, (b) neat PVC and PVC/USB-SPCL films) recorded during a second heating step.

V-4. Conclusion

The pseudo-bulk dynamics of PVC, USB-SPCLs with different molecular architectures, and their blends at around room temperature in concentrated solutions were analyzed using the PCS technique. The intensity autocorrelation curves of PVC/USB-SPCLs exhibited single-exponential behaviors, indicating homogeneous dynamic behaviors because of their strong intermolecular interactions. The relaxation rate, correlation time, and apparent activation energy around room temperature showed that the cooperative diffusive chain mobility of USB-SPCLs is highly reduced by constraint of the entangled linear PVC matrix and, instead, PVC chain motion increases up to the same mobility level of the constrained USB-SPCLs in the PVC matrix. The molecular motions of the blends depended on the total-molecular-weight-dependent Rouse dynamic behaviors of USB-SPCLs, regardless of the molecular architectures. These pseudo-bulk dynamic results clearly showed the plasticization of the entangled linear PVC matrix by distinctive and rapid molecular mobility of USB-SPCLs. This study broadens the understanding of the molecular dynamic behaviors of unentangled star-shaped polymers with extremely small branches and further provides insights into the plasticizing effects of unentangled polymers with various molecular architectures on entangled linear polymer matrix.

References and Notes

1. Choi, W.; Chung, J. W.; Kwak, S.−Y. *Polymer* **2015**, *79*, 91−98.

2. Choi, W.; Chung, J. W.; Kwak, S.−Y. *ACS Appl. Mater. Interfaces* **2014**, *6*, 11118−11128

3. Guenza, M. *Phys. Rev. Lett.* **2001**, *88*, 025901-1–025901-4.

4. Guenza, M. *J. Chem. Phys.* **2003**, *119*, 7568–7578.

5. Ferry, J. D. *Viscoelastic Properties of Polymers*, 3rd ed.; Wiley: New York, 1980.

6. Chung, G.–C.; Kornfield, J. A.; Smith, S. D. *Macromolecules* **1994**, *27*, 5729–5741.

7. Štěpánek, P.; Tuzar, Z.; Kadlec, P.; Kříž, J. *Macromolecules* **2007**, *40*, 2165–2171.

8. Vyshivannaya, O. V.; Laptinskaya, T. V. *Polym. Sci. Ser. A* **2012**, *54*, 364–374.

9. Rizos, A. K. *Polymer* **1996**, *25*, 5743−5746.

10. Takenaka, M.; Miyazawa, M.; Nishitsuji, S.; Hashimoto, T. *Progr. Colloid. Polym. Sci.* **2005**, *130*, 97–104.

11. McBriety, V. J.; Packer, K. J. *Nuclear Magnetic Resonance in Solid Polymers*; Cambridge: Cambridge University Press, 1993.

12. Arbe, A.; Alegría, A.; Colmenero, J.; Hoffmann, S.; Willner, L.; Richter D. *Macromolecules* **1999**, *32*, 7572–7581.

13. Hair, D. W.; Hobbie, E. K.; Douglas, H.; Han, C. C. *Phys. Rev. Lett.* **1992**, *68*, 2476–2479.

14. Zhang, S. H.; Jin, X.; Painter, P. C.; Runt, J. *Macromolecules* **2003**, *36*, 7179–7188.

15. Chung, G.–C.; Kornfield, J. A.; Smith, S. D. *Macromolecules* **1994**, *27*, 964–973.

16. Munk, P. *Introduction to macromolecular science*; New York: Wiley, 1989.

17. Yang, H.; Zhu, P.; Wang, S.; Zeng, Y.; Guo, Q. *Eur. Polym. J.* **1998**, *34*, 1303−1308.

18. Dreval, V. E.; Malkin, A. Y. A.; Botvinnik, G. O. *J. Polym. Sci. Part B: Polym. Phys.* **1973**, *11*, 1055–1076.

19. Pezzin, G.; Gligo, N. *J. Appl. Polym. Sci.* **1966**, *10*, 1–19.

20. Brown, W. Ed. *Dynamic Light Scattering: the method and some applications*; Clarendon Press: Oxford, 1993.

21. Lin, Y.−H.; Lai, C. S. *Macromolecules* **1996**, *29*, 5200−5207.

22. Lai, C. S.; Juang, J.−H.; Lin, Y.−H. *J. Chem. Phys.* **1999**, *110*, 9310−9318.

23. Patel, A.; Mochrie, S.; Narayanan, S.; Sandy, A.; Hiroshi, W.; Balsara, N. P. *Macromolecules* **2010**, *43*, 1515–1523.

24. Ruegg, M. L.; Patel, A. J.; Narayanan, S.; Sandy, A. R.; Mochrie, S. G. J.; Watanabe, H.; Balsara, N. P. *Macromolecules* **2006**, *39*, 8822–8831.

25. Kwak, S.–Y.; Lee, H. Y. *Macromolecules* **2000**, *33*, 5536–5543.

26. de Oliveira, V. A. V.; de Morais, W. A.; Pereira, M. R.; Fonseca, J. L. C. *Eur. Polym. J.* **2012**, *48*, 1932–1939.

27. Kjøniksen, A.–L.; Nyström, B. *Macromolecules* **1996**, *29*, 7116–7123.

28. Choi, W.; Chung, J. W.; Kwak, S.−Y. *Polymer* **2016**, *103*, 19−26.

29. Choi, W.; Chung, J. W.; Kwak, S.−Y. *J. Polym. Sci. Part A: Polym. Chem.* **2015**, *53*, 1134−1142.

30. Adelman, R. L.; Klein, U. M. *J. Polym. Sci.* **1958**, *31*, 77−97.

31. Chiu, F.–C.; Min, K. *Polym. Int.* **2000**, *49*, 223–234.

32. Wang, D.; Wilkie, C. A. *J. Vinly. Addit. Technol.* **2002**, *8*, 238−245.

33. Varnell, D. F.; Moskala, E. J.; Painter, P. C.; Coleman, M. M. *Polym. Eng. Sci.* **1983**, *23*, 658−662.

34. Robeson, L. M. *J. Vinyl. Technol.* **1990**, *12*, 89−94.

35. Audic, J.−L.; Reyx, D.; Brosse, J.−C. *J. Appl. Polym. Sci.* **2003**, *89*, 1291−1299.

36. Fytas, G.; Floudas, G.; Ngai, K. L. *Macromolecules* **1990**, *23*, 1104−1109.

37. Štěpánek, P.; Brown, W. *Macromolecules* **1998**, *31*, 1889−1897.

38. Sun, C.; Ritchie, J. E. *J. Phys. Chem.* **2011**, *115*, 8381−8389.

39. Fox, T. G.; Flory, P. J. *J. Appl. Phys.* **1950**, *21*, 581−591.

40. Roovers, J. E. L.; Toporowski, P.M. *J. Appl. Polym. Sci.* **1974**, *18*, 1685−1691.

41. Shinyashiki, N. *Dynamics and Glass Transition of Aqueous Solutions of Molecular Liquid, Polymer, and Protein Studied by Broadband Dielectric Spectroscopy*; In: Kita, R.; Dobashi, T. Ed.; Nano/Micro Science and Technology in Biorheology; Springer Japan, 2015.

42. Haggard, K. W.; Paul, D. R. *Polymer* **2004**, *45*, 2313−2320.

CHAPTER VI

HETEROGENEOUS GLASS TRANSITION DYNAMICS OF INDIVIDUAL PVC COMPONENT PLASTICIZED BY ULTRA-SMALL-BRANCHED STAR POLY(ε-CAPROLACTONE)

VI-1. Introduction

The dynamics of polymers is one of the key factors which determine the mechanical and physical properties of bulk polymers, and thus many researchers have focused their attention on the polymer dynamic behaviors to achieve desired material performance (such as strength, modulus, dimensional stability, permeability to gases and water, and so on).[1–4] Various experimental techniques have been used to reveal how the polymer dynamic behaviors correlate with the mechanical and physical properties of polymer product. Serrano et al. observed the dynamics of polystyrene and polymethacrylic polymer films in the bulk and in the surface using time-resolved fluorescence decay measurement, and showed different microscopic properties of bulk and surface (that is, liquid-like domains were more frequent

on the surface than in bulk).[5] Kotsilkova et al. studied the reinforcing effect of epoxy-carbon nanocomposites through the overall dynamics of the epoxy polymer chains using dielectric relaxation spectroscopy, showing that decreased polymer mobility is an evidence for enhancing the elasticity of the nanocomposites.[6] Vilaplana et al. investigated the degradation mechanisms affecting the rubber phase in high-impact polystyrene through the mobility changes of cross-linked butadiene rubber during degradation processes, observed by nuclear magnetic resonance (NMR) relaxation.[7] Dobircau et al. showed the role of plasticizers on the molecular mobility of amorphous poly(lactide) during physical ageing using temperature modulated differential scanning calorimetry (DSC) analysis (related to the dynamic glass transition).[8] All these studies had in common that the dynamics of polymers was very strongly related to the free-volume changes of the polymer system, *i.e.*, the enlarged free volume led to increased polymer mobility and vice versa. However, they have mostly addressed the dynamic behaviors of the whole system (not individual polymer chains) as a result of the free-volume changes even though the free volume of the whole system mainly depended on the specific individual polymer component, and/or they have insufficiently addressed free-volume-dependent dynamic behaviors. Moreover, some of them occasionally showed the dynamic results that disagree with and even are contrary to the free volume theory.[9,10] Therefore, more intensive investigations into the correlation between the dynamic behaviors of

individual polymer chains and the controlled free-volume changes are positively necessary to deepen the understanding of the individual polymer component dynamics affecting the mechanical and physical properties of the bulk polymers.

The dynamic behaviors of individual polymer component with controlled free volume can be analyzed using many techniques, such as DSC analysis, dielectric relaxation spectroscopy (DRS), solid-state NMR spectroscopy, and fluorescence spectroscopy (FS).[11–14] DSC provides an attractive method for determining the glass transition dynamics of individual polymer component, but is much less effective at resolving separated glass transition behaviors within 50 ℃ of glass transition temperature, T_g, difference between two components.[11,15] DRS can show a wider utility in selectively probing the individual polymer component dynamics even in miscible blends, but is limited to detecting the chain motion only for the electric dipole of the chemical bonds in the backbone.[12,16] Solid-state NMR and FS analysis can probe the individual dynamic behaviors of very dilute polymer component in miscible blends because their observed dynamic behaviors are on a local scale and of a relatively low energy than those from other techniques.[13,14,17] While the glass transition dynamics, determined by NMR relaxation, requires extrapolation over 50 °C using Vogel−Fulcher−Tammann or Williams−Landel−Ferry equations, FS studies show highly sensitive dynamic

behaviors in the temperature range where the component transitions from its rubbery state to glassy state without data extrapolations.[15,18] In particular, FS enables to easily analyze the dynamics of the targeted region in various polymer systems using very low fluorescence-dye-doped or -labeled concentration which does not disturb at all or only slightly the original dynamics.[15,19] Many researchers actually have used FS to characterize several dynamic behaviors, *e.g.*, glass transition dynamics, temperature-dependent phase-separation dynamics, confinement dynamics, in homo-polymers, in miscible and immiscible blends, and under conditions of confinement.[15,19,20,21] Over the last decade, Torkelson at el. have intensively investigated the individual T_g values of several polymer blends and confined polymer chains using temperature-dependent FS techniques.[13–15,19,22–26] Such temperature-dependent FS techniques originated from the changes in total intensity, integrated intensity, and intensity ratio of fluorescence emission spectra with different temperature via non-radiative process related to thermal dynamic behaviors of polymer chains (e.g., intramolecular vibrations and rotations, etc.).[13,22,27] These thermal dynamic behaviors are closely associated with thermal free-volume fluctuations, but the previous studies still have poorly addressed concerning free-volume-dependent dynamic behaviors. Thus, we are supposed to specifically show the correlation between the dynamic behaviors of individual polymer chains and their free-volume changes using highly sensitive temperature-dependent FS techniques.

The plasticized poly(vinyl chloride) (PVC) system is very suitable for studying free-volume-dependent dynamic behaviors because of several obvious features of PVC, that is, PVC is a the most prolifically used linear, amorphous, and thermoplastic polymer and its free volume can be easily controlled by addition of plasticizers.[28–32] In fact, we developed ultra-small-branched star poly(ε-caprolatone)s (USB-SPCLs) as phthalate-free PVC plasticizers.[33,34] Then, the dynamic effects of extremely small branches in USB-SPCLs were successfully investigated on the plasticization of whole PVC/USB-SPCL blends, resulting in the entangled linear PVC matrix plasticized by distinctive and rapid molecular mobility of USB-SPCLs.[35,36] Now, in this study, free-volume-dependent dynamic behaviors of individual PVC component in miscible PVC/USB-SPCL blends were investigated using temperature-dependent FS techniques. The miscible PVC/USB-SPCL blend system exhibited heterogeneous dynamic behaviors with interestingly broad thermal glass transition of individual PVC component, differ from a typical glass transition dynamics of miscible polymer blend. This suggests that the motion of individual PVC component depended on both the enlarged free volume by fast-moved USB-SPCL molecules and the dynamic constraint by entangled PVC chains. These findings provide new insights into the plasticization of entangled linear polymer itself, plasticized by unentangled star-shaped polymer with extremely small branches, and further improve the

understanding of the correlation between the dynamic behaviors of individual polymer chains and the controlled free-volume changes.

VI-2. Experimental Section

VI-2-1. Materials

Suspension-grade PVC resin (P-1000) was kindly provided by the Hanwha Chemical Co., Ltd., Korea. 1-Ethylnylpyrene (96%) and ε-caprolactone (CL, 99%) were purchased from the Alfa Aesar Co., Ltd., USA. Sodium azide (NaN_3, 99.0%), *N*,*N*-dimethylformamid (DMF, 99.5%), tetrahydrofuran (THF, 99.0%), and methanol (MeOH, 99.5%) were purchased from the Daejung Chemicals & Metals Co., Ltd., Korea. Copper (I) bromide (Cu(I)Br), *N*,*N*,*N*′,*N*′,*N*″-pentamethyl diethylene triamine (PMDETA, 99%), dipentaerythritol (DPTOL, tech. grade), tin(II) 2-ethylhexanoate ($Sn(Oct)_2$, 95%) and acetic anhydride (Ac_2O, 99.5%) were purchased from Sigma-Aldrich Ltd., Korea. Songstab CZ-400 (Ca-Zn organic liquid complex) was supplied by the Songwon Co., Ltd., Korea. All chemicals were used without further purification.

VI-2-2. Preparation of L-PVC

PVC was labeled by pyrene using a click reaction between azide functionalized PVC and 1-ethylnylpyrene, using a previously described method.[37–40] Briefly, the azide functionalized PVC was obtained from the

azidation reaction of suspension-grade PVC (10 g, 160 mmol based on monomeric unit) with NaN_3 (10.4 g, 160 mmol) in DMF (400 mL). The mixture in a flask was heated at 60 ℃ under nitrogen for 5 min, and the reaction mixture was cooled to room temperature and then dissolved in THF and precipitated four times into cold MeOH and then dried in a vacuum oven at room temperature for 24 h (yield > 95%). This resulted in the partially azidated PVC (PVC-N_3), and the degree of azidation was determined by elemental analysis (38.71% C, 4.83% H, 0.23% N), indicating ca. 3.4 azide groups in one PVC molecule (displacement of Cl by N_3) because the degree of polymerization (DP) of P-1000 was 1,000 ± 100. The click reaction was carried out using PVC-N_3 (8 g) and 1-ethylnylpyrene (145 mg, 6.4 mmol) in the presence of Cu(I)Br (92 mg, 6.4 mmol), PMDETA (111 mg, 6.4 mmol), and DMF (160 mL). The mixture in a flask was stirred under nitrogen for 24 h at 40 ℃, and then the reaction mixture was diluted with DMF and passed through a column of neutral alumina to remove the copper catalysts and precipitated into cold MeOH. The adduct was purified three times by re-dissolving in THF and re-precipitating in MeOH. After drying in a vacuum oven at room temperature for 24 h, the L-PVC was finally obtained as a yellow solid with a yield over 96% (see Figure VI-1).

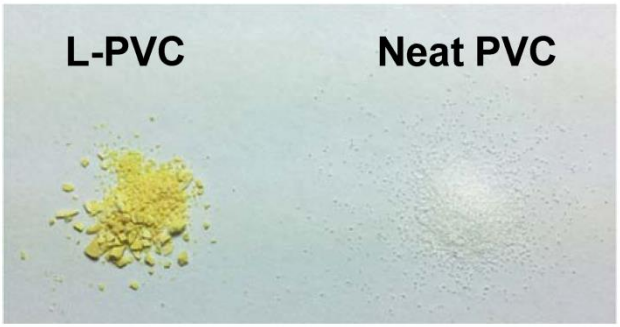

Figure VI-1. Images of L-PVC and neat PVC.

The successful preparation of L-PVC was verified by attenuated total reflection Fourier-transform infrared (ATR FT-IR) and ^{1}H nuclear magnetic resonance (NMR) spectroscopy (Figure VI-2). The azidation reaction of PVC with sodium azide resulted in the azide peak at 2101 cm^{-1} in the ATR FT-IR spectrum of PVC-N_3, which was not observed in the neat PVC spectrum. The ^{1}H NMR spectrum of PVC-N_3, however, was quite similar to that of PVC because the methylene protons adjacent to the azide group (peaks a′ and b′) had quite similar chemical shift to the methylene protons adjacent to the chloride (peaks a and b). After click reaction between PVC-N_3 and 1-ethylnylpyrene, the azide peak in the ATR FT-IR spectrum of PVC-N_3 was completely disappeared in the L-PVC spectrum, indicating that the azide groups in PVC fully converted into triazole groups without any residual azide group. Furthermore, the distinct aromatic C–H stretch at 850 cm^{-1} of pyrene was appeared in the ATR FT-IR spectrum of L-PVC, and, in the ^{1}H NMR spectrum of L-PVC, the aromatic protons of pyrenyl group was observed between 8.14 and 8.74 ppm without the proton on the triple bond (peak 1, 4.77 ppm) in 1-ethylnylpyrene. This indicated that pyrene covalently bonded to PVC and L-PVC was obtained without any unreacted 1-ethylnylpyrene. Finally, these results showed successful preparation of high-purity L-PVC.

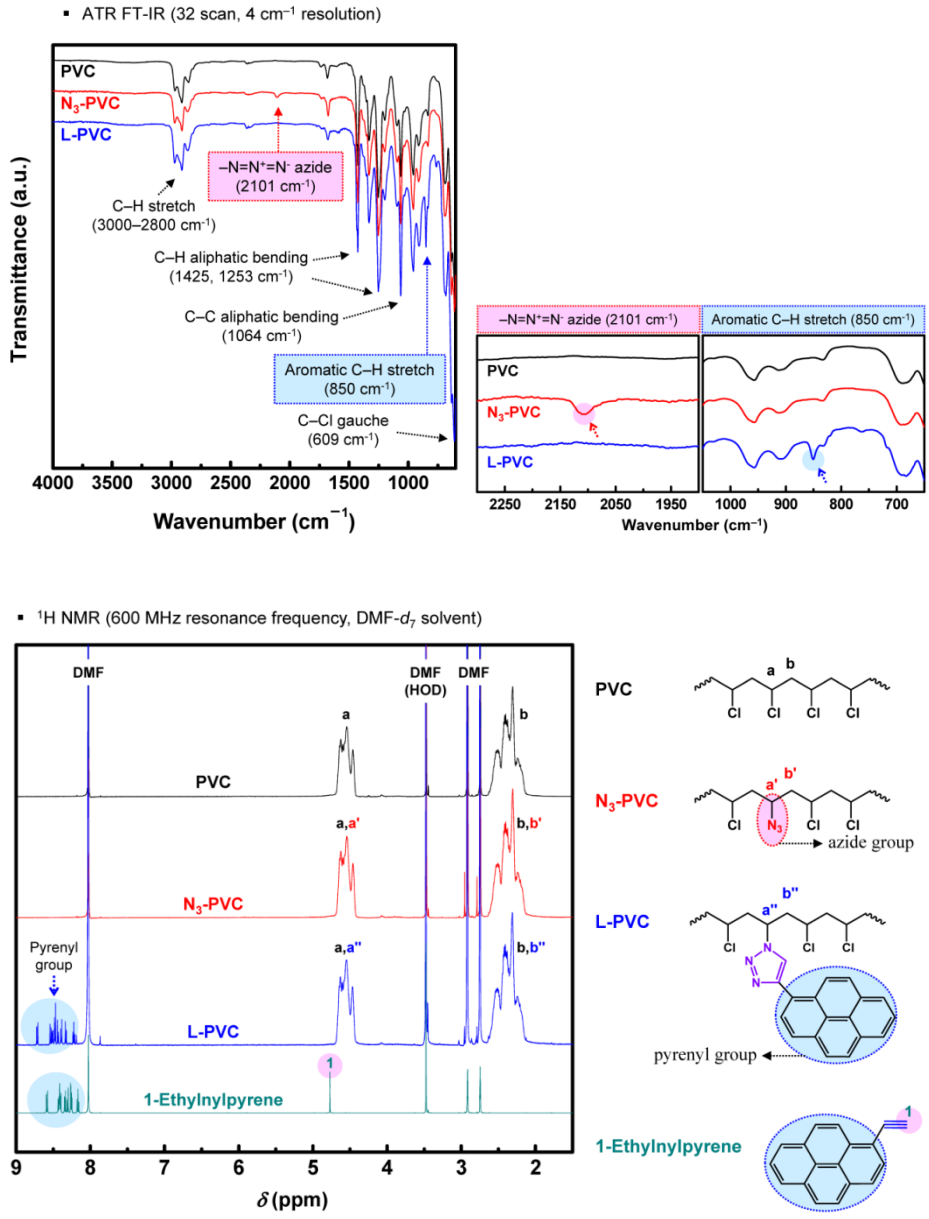

Figure VI-2. ATR FT-IR and ^{1}H NMR spectra of PVC, PVC-N_3, L-PVC, and 1-ethylnylpyrene.

VI-2-3. Preparation of USB-SPCL

USB-SPCL with a DPTOL core was synthesized following our previous publication.[33] The synthesis was performed by manipulating the monomer-to-core ratio, adjusting monomer-to-polymer conversion, end-capping the terminal hydroxyl groups, and vacuum purification, in a facile pseudo-one-pot bulk process without any organic solvent, in order to solve a chronic synthetic problem associated with cyclic PCLs. The number of branches, N_{number}, and the average length of the individual branches (the average DP per branch), N_{length}, in USB-SPCL were determined to be 6.06 and 5.20, respectively, using ^{1}H NMR spectroscopy. The number-average molecular weight, M_n, and the molecular weight distribution (MWD) were determined to be 3610 g mol^{-1} and 1.09, respectively, using matrix-assisted laser desorption/ionization time-of-flight mass spectrometry (MALDI-TOF-MS). More detailed information on the syntheses and general characterizations on USB-SPCL was well described in our previous publication.[33]

VI-2-4. Preparation of pyrene-labeled and -doped PVC/USB-SPCL films

All of the pyrene-labeled and -doped PVC/USB-SPCL film samples were prepared by solution blending, with THF as the solvent, using the method and formulation generally used for studying PVC films.[41] In the L-PVC/USB-

SPCL films, 100 parts per hundred (phr) of L-PVC and 3 phr of thermal stabilizer (CZ-400) were dissolved in THF with USB-SPCL of different mass ratios of 0, 10, 20, 30, and 40 phr. The mixture were vigorously stirred to ensure homogeneity and poured into glass petri dishes, and then the THF solvent was slowly evaporated in an oven at 40 ℃ for 24 h to eliminate all residual solvent. This gave yellow and semi-transparent L-PVC/USB-SPCL films with ca. 0.2 mm thickness (see Figure VI-3). The L-PVC/USB-SPCL films were named as L-PVC/USB-SPCL0, L-PVC/USB-SPCL10, L-PVC/USB-SPCL20, L-PVC/USB-SPCL30, and L-PVC/USB-SPCL40, where the number is the phr of USB-SPCL in the film. The detailed formulations of the L-PVC/USB-SPCL films used in this study were summarized in Table VI-1. As a counterpart to L-PVC/USB-SPCL, five different pyrene-doped PVC/USB-SPCL films (D-PVC/USB-SPCL0, D-PVC/USB-SPCL10, D-PVC/USB-SPCL20, D-PVC/USB-SPCL30, and D-PVC/USB-SPCL40) were also prepared with the same solution blending procedure using 100 phr of neat PVC (without pyrene label) and 1.24 phr of 1-ethylnylpyrene as an external pyrene chromophore dopant, instead of L-PVC, consistent with the amount of pyrene in the L-PVC/USB-SPCL films. The D-PVC/USB-SPCL films in Figure VI-3 showed transparent with a pale fluorescent color, in contrast with the L-PVC/USB-SPCL films. The pale fluorescent color faded with increasing the USB-SPCL amount in the D-PVC/USB-SPCL films, resulting from a decrease in the pyrene amount with decreasing neat PVC amount.

Figure VI-3. Images of L-PVC/USB-SPCL and D-PVC/USB-SPCL films.

Table VI-1. The formulations of L-PVC/USB-SPCL films.

Sample (10 g)	L-PVC	USB-SPCL	Thermal stabilizer
L-PVC/ USB-SPCL0	100 phr (97.09%, 9.71 g)	0 phr (0%, 0 g)	3 phr (2.91%, 0.29 g)
L-PVC/ USB-SPCL10	100 phr (88.50%, 8.85 g)	10 phr (8.85%, 0.88 g)	3 phr (2.65%, 0.27 g)
L-PVC/ USB-SPCL20	100 phr (81.30%, 8.13 g)	20 phr (16.26%, 1.63 g)	3 phr (2.44%, 0.24 g)
L-PVC/ USB-SPCL30	100 phr (75.19%, 7.52 g)	30 phr (22.56%, 2.26 g)	3 phr (2.26%, 0.23 g)
L-PVC/ USB-SPCL40	100 phr (69.93%, 6.99 g)	40 phr (27.97%, 2.80 g)	3 phr (2.10%, 0.21 g)

VI-2-5. DSC analysis

DSC measurements of L-PVC/USB-SPCL and D-PVC/USB-SPCL films were carried out using a TA Instruments DSC-Q1000 with a heating rate of 10 ℃ min^{-1} over the temperature range of −50 to 140 °C under a nitrogen atmosphere, where the film samples were heated to 140 ℃ and held for 20 min before measuring the DSC heating curves. The T_g value was determined based on the inflection point method and the onset and endpoint temperatures of the glass transition, $T_{g,o}$ and $T_{g,e}$, were determined based on the tangent method, using TA Universal Analysis software.

VI-2-6. FS analysis

Fluorescence emission spectra were measured using Photon Technology International QuantaMaster 40 UV−Vis spectrofluorometer with 2.0 nm bandpass emission slits. The excitation wavelength was set to 350 nm for the L-PVC/USB-SPCL films and 324 nm for the D-PVC/USB-SPCL films, and the emission intensity was monitored at 360−600 nm for the L-PVC/USB-SPCL films and 420−600 nm for the D-PVC/USB-SPCL films. After the film samples were annealed at 100 ℃ for 30 min, the fluorescence emission spectra were obtained upon heating by increasing the temperature from −11 to 100 °C at 3 °C intervals. Characterizing upon heating rather

than cooling eliminated the possibility of PVC thermal degradation before having the experimental temperature reach T_g. The film samples were held at each temperature for 5 min to ensure thermal equilibrium prior to data collection.

VI-3. Results and Discussion

Figure VI-4 shows that the DSC curves for all the samples had single glass transitions, resulting from high miscibility between PVC and USB-SPCL.[34] The glass transitions occurred at lower temperature with increasing the amount of USB-SPCL, which is an expected plasticization effect of providing free volume with very low T_g of USB-SPCL (−62.0 °C). In addition, each of the DSC curves for the L-PVC/USB-SPCL blends, including T_g, $T_{g,o}$ and $T_{g,e}$, were approximately the same as each of those for the D-PVC/USB-SPCL counterpart blends at a given composition. This reveals that both pyrene-labeled and -doped systems (L-PVC/USB-SPCL and D-PVC/USB-SPCL) resulted in the same dynamic behaviors regardless of whether PVC with or without pyrene label. Thus, it was possible to compare the dynamics of the individual PVC component in miscible PVC/USB-SPCL blends (L-PVC/USB-SPCLs) and that of the whole PVC/USB-SPCL blend system (D-PVC/USB-SPCLs) through FS analysis with pyrene.

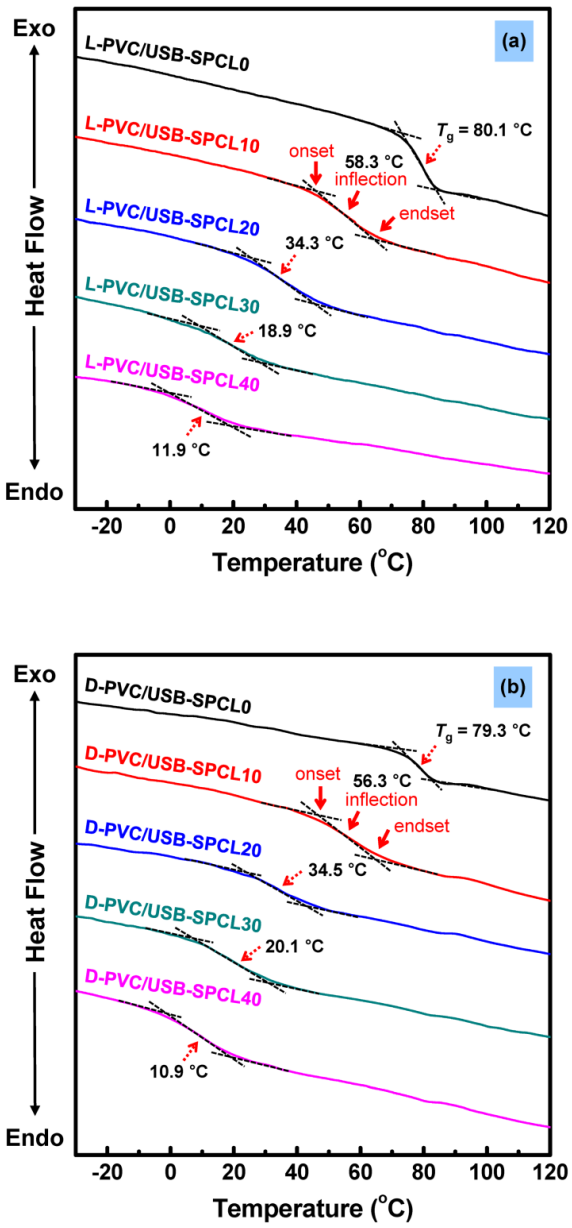

Figure VI-4. DSC thermograms of (a) L-PVC/USB-SPCL and (b) D-PVC/USB-SPCL blends recorded during a second heating step.

Figure VI-5(a) shows fluorescence emission spectra for the L-PVC/USB-SPCL blends with different amount of USB-SPCL. The broad fluorescence emissions of these blend samples were observed in the red-shifted wavelength range of 435–600 nm, which were differ from the typical fluorescence characteristics of a pyrene molecule or pyrenyl chromophore.[22] This is attributed to the dual fluorescence emission of triazolypyrene formed from the click reaction between azide in PVC and alkyne in 1-ethylnylpyrene, which were divided into a short wavelength emission band (locally emission (LE) band) and a the long wavelength emission band (intramolecular charge transfer (ICT) band).[42−43] In Figure VI-5(a), the short wavelength emission band (LE band) centered at 455 nm arose from the locally excited state, and the long wavelength emission band (ICT band) in 470−600 nm arose from the newly generated ICT state having higher dipole moment than the locally excited state. According to the Bag et al.'s reports, the ICT band did not originated from excimer emission, but the ICT of the L-PVC system in the excited state resulted from the PVC chain linked with triazole group which serves as an efficient electron donor and the pyrene group which acts as an electron acceptor.[42−43] Since the triazolypyrene probe consists of an efficient charge transfer property, its energy gap between ground and excited states decreases, and thus the ICT band was observed in the long wavelength emission compared to the LE band. Hence, the combined LE and ICT bands of L-PVC/USB-SPCL blends showed a broad dual fluorescence emission

band in the red-shifted wavelength range. In addition, as shown in Figure VI-5(a), the observed fluorescence intensities decreased as increasing the USB-SPCL amount in the L-PVC/USB-SPCL blends, resulting from a decrease in the pyrene amount in the L-PVC/USB-SPCL blends. The normalization of these fluorescence intensities was carried out using the higher intensity emission to compare the fluorescence emission spectra of the L-PVC/USB-SPCL blends with different amount of USB-SPCL in avoiding the effect of pyrene amount (Figure VI-5(b)). The normalized fluorescence intensities of the LE band decreased without any significant shift in the peak positions, and the maximum emission intensity in the ICT bands red-shifted from 505 to 519 nm, with increasing the USB-SPCL amount in the L-PVC/USB-SPCL blends. This reveals that the LE band energy gap of L-PVC/USB-SPCL blend is unaffected by the component ratio of L-PVC and USB-SPCL and that the ICT emission was favored by USB-SPCL molecules in L-PVC/USB-SPCL blend because a large number of ester polarity in USB-SPCL molecules stabilize the ICT state and decrease the ICT band energy gap.[42–43]

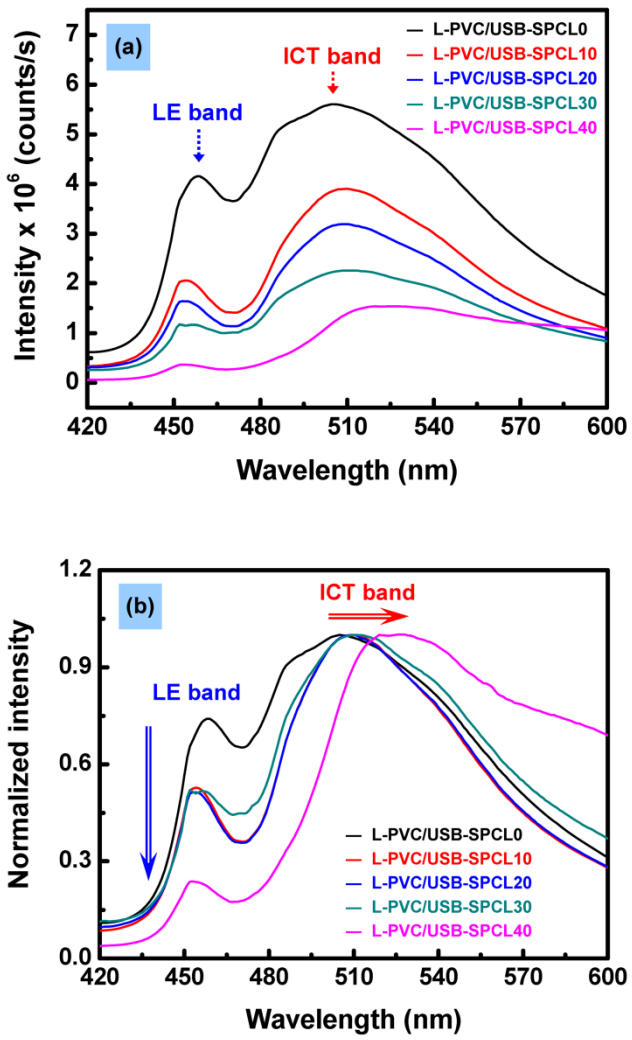

Figure VI-5. The fluorescence emission spectra and (b) the normalized fluorescence intensities for L-PVC/USB-SPCL blends with different amount of USB-SPCL.

The fluorescence emission spectra for the L-PVC (L-PVC/USB-SPCL0) and D-PVC (D-PVC/USB-SPCL0) blends are compared as representatives of two groups (pyrene-labeled and -doped systems) in Figure VI-6(a). The D-PVC/USB-SPCL blends, as contrasted with the L-PVC/USB-SPCL blends, had higher excitation energy (lower excitation wavelength) and lower fluorescence emission wavelength, which is typical fluorescence characteristics from the excited-state of a single pyrene molecule or pyrenyl chromophore.[22] This reveals that the fluorescence emission of D-PVC/USB-SPCL blends depended on the local environment experienced by single 1-ethylnylpyrene molecule without any charge transfer. The main fluorescence emission spectra for the D-PVC/USB-SPCL blends at 380−415 nm were shown in Figure VI-6(b) with different amount of USB-SPCL. The observed fluorescence intensities decreased with the same peak positions as increasing the USB-SPCL amount in the D-PVC/USB-SPCL blends because of the pyrene amount in the D-PVC/USB-SPCL blends. This indicates that any composition of PVC and USB-SPCL do not make a certain energy level or charge transfer in the fluorescence emission of D-PVC/USB-SPCL blends, in contrast to the dual fluorescence emission of L-PVC/USB-SPCL blends. Thus, the fluorescence emission spectra for the D-PVC/USB-SPCL samples provide the dynamic information with respect to the whole PVC and USB-SPCL blend system, whereas the L-PVC/USB-SPCL samples show the

fluorescence emission spectra for the individual PVC component in PVC/USB-SPCL blends.[13–14]

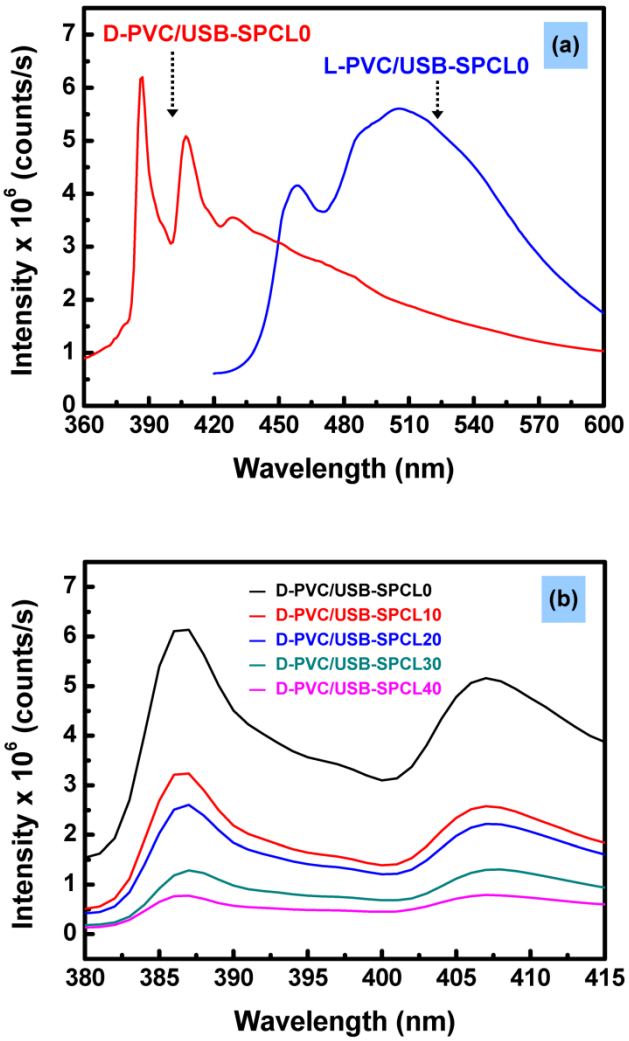

Figure VI-6. (a) The fluorescence emission spectra for L-PVC/USB-SPCL0 and D-PVC/USB-SPCL0 blends and (b) the main fluorescence emission spectra for D-PVC/USB-SPCL blends with different amount of USB-SPCL.

The temperature dependences of fluorescence emissions for all the samples were observed upon heating, in order to investigate the thermal dynamic behaviors associated with thermal free-volume fluctuations. Figure VI-7 shows the fluorescence emission spectra for the L-PVC (L-PVC/USB-SPCL0) and D-PVC (D-PVC/USB-SPCL0) blends with various temperatures from −11 to 100 °C at 3 °C intervals. The temperature-dependent fluorescence emission spectra for other samples (L-PVC/USB-SPCL and D-PVC/USB-SPCL blends) showed the same trends (data not shown). The fluorescence emission spectra at various temperatures for the L-PVC/USB-SPCL blends showed similar shapes with the same peak positions (Figure VI-7(a)). This reveals that the LE and ICT states of L-PVC/USB-SPCL blends remains unchanged and another charge transfer (except ICT) was not occurred in the measured temperature range. The fluorescence emission spectra for the D-PVC/USB-SPCL blends also showed similar shapes with the same peak positions at various temperatures (Figure VI-7(b)), indicating the temperature-dependent fluorescence emission with the same energy gap and without any charge transfer in the measured temperature range. Moreover, the entire fluorescence intensities for all the samples decreased with increasing temperature, and the stronger temperature dependence of the fluorescence emission was observed in the higher temperature range. This is associated with a decrease in quantum yield resulting from the activation of the pathways for non-radiative decay from the excited state with increasing temperature

because the local environment experienced by the pyrenyl dye in the samples becomes more mobile with higher free volume at higher temperature.[15,19,23,24,27] As a result, the temperature-dependent fluorescence emission spectra for the L-PVC/USB-SPCL and D-PVC/USB-SPCL blends depended on the thermal dynamic behaviors (*i.e*, thermal chain motions) of the individual PVC component in PVC/USB-SPCL blends and the whole PVC/USB-SPCL blend system, respectively.

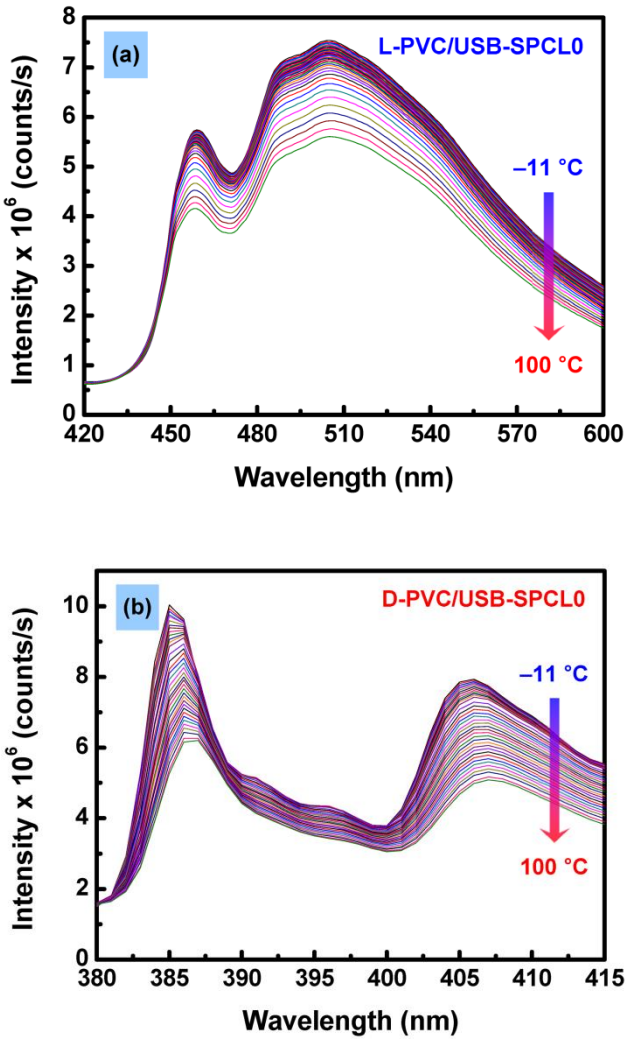

Figure VI-7. The fluorescence emission spectra for (a) L-PVC/USB-SPCL0 and (b) D-PVC/USB-SPCL blends with various temperatures from −11 to 100 ℃ at 3 ℃ intervals.

The thermal dynamic behaviors were quantitatively analyzed using integrated intensities of temperature-dependent fluorescence emission spectra for the L-PVC/USB-SPCL and D-PVC/USB-SPCL blends, determined in the measured temperature range at the wavelength of 420−600 nm and 380−415 nm, respectively. Figure VI-8 shows the normalized integrated intensity results of the L-PVC/USB-SPCL and D-PVC/USB-SPCL blends as a function of temperature and includes their glass transition behaviors ($T_{g,o}$, T_g, and $T_{g,e}$) obtained from DSC curves in Figure VI-4. The integrated intensity data for each of the D-PVC/USB-SPCL blends in Figure VI-8 were presented in two straight lines. The two lines were linear regressions fit to rubbery- and glassy-state data beginning with the highest and lowest temperature data points, respectively.[15,25] Additional data points were added until the fit line no longer passed through the next data point, where $R^2 > 0.990$ was used as the criterion for an acceptable linear regression fit. The intersection of two linear regressions obtained from rubbery- and glassy-state data was taken as the T_g of the D-PVC/USB-SPCL blends.[19,25] The T_g values decreased with increasing the amount of USB-SPCL, which showed excellent agreement with the T_g values obtained from DSC measurement. It was also observed that the integrated intensities of the D-PVC/USB-SPCL blends in the rubbery state had stronger temperature dependence than those in the glassy state, because the non-radiative decay pathways in a rigid environment of the glassy state were more suppressed.[15] These integrated intensity results for the D-

PVC/USB-SPCL blends can be well explained by the free-volume theory.[30,44,45] It is well known that the free volume of polymers expands with increasing temperature because of an increase in the polymer mobility. Such free-volume expansion generally originates from the nonharmonic oscillations of the atoms, frozen-in imperfections and holes of the submolecular and molecular size in the glassy state and originates from the bending and rotating of polymer molecules or segments in the rubbery state; hence, the thermal free-volume expansion coefficient of a polymer material is constant in the same state (rubbery or glassy state) and the value in the rubbery state is several times higher than that in the glassy state. Thus, the reduced integrated intensity curves for the D-PVC/USB-SPCL blends with increasing temperature were in good agreement with their thermal free-volume expansions, *i.e.*, two linear regression lines with different slopes that exhibited lower temperature dependence in the glassy state and stronger temperature dependence in the rubbery state. This indicates that the motion of the whole PVC/USB-SPCL blend system slowly (and constantly) increased below T_g and rapidly (and constantly) increased above T_g with increasing temperature, resulting in a sharp motional transition of the whole PVC/USB-SPCL blend system at T_g.

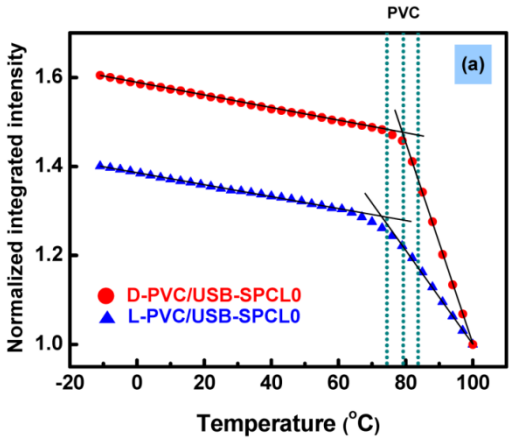
PVC
(a)
Normalized integrated intensity
1.6
1.4
1.2
1.0
D-PVC/USB-SPCL0
L-PVC/USB-SPCL0
-20
0
20
40
60
80
100
Temperature (°C)

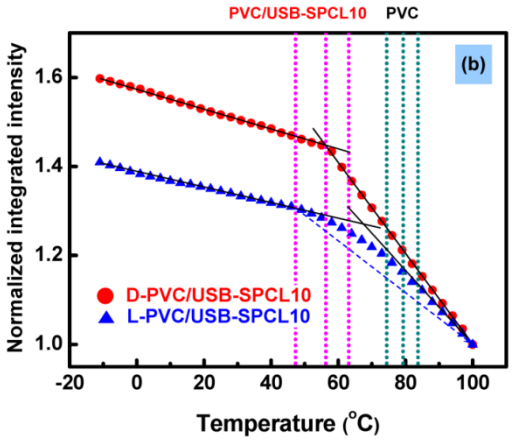
PVC/USB-SPCL10
PVC
(b)
Normalized integrated intensity
1.6
1.4
1.2
1.0
D-PVC/USB-SPCL10
L-PVC/USB-SPCL10
-20
0
20
40
60
80
100
Temperature (°C)

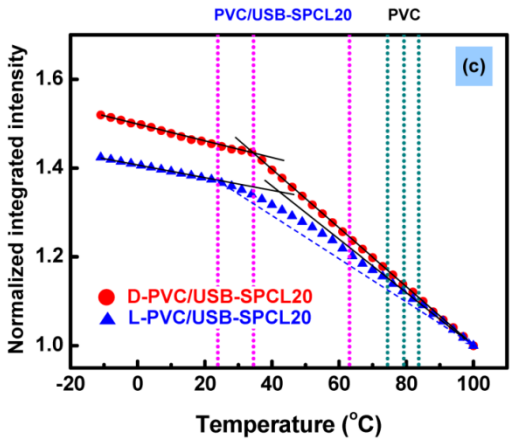
PVC/USB-SPCL20
PVC
(c)
Normalized integrated intensity
1.6
1.4
1.2
1.0
D-PVC/USB-SPCL20
L-PVC/USB-SPCL20
-20
0
20
40
60
80
100
Temperature (°C)

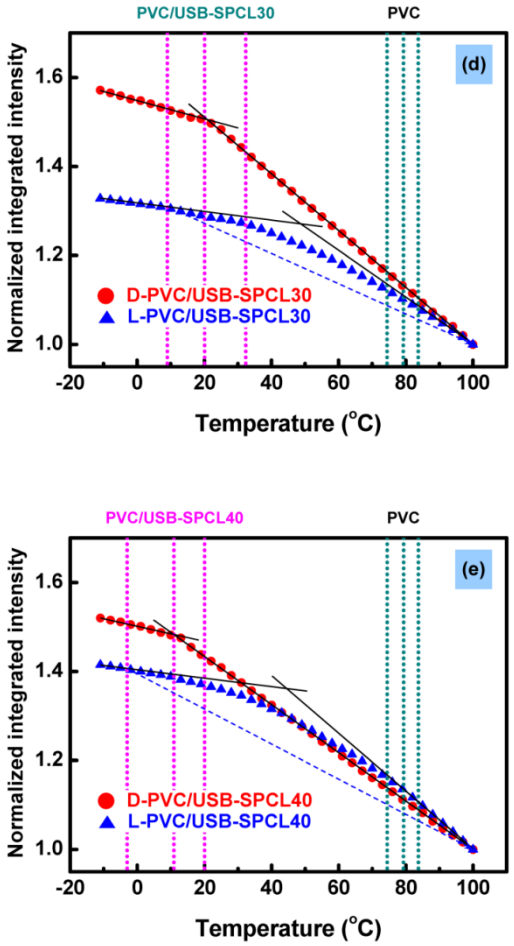

Figure VI-8. The normalized integrated intensities for L-PVC/USB-SPCL and D-PVC/USB-SPCL blends as a function of temperature including their glass transition behaviors ($T_{g,o}$, T_g, and $T_{g,e}$) obtained from DSC curves (shown by vertical dot lines). Solid lines are the best linear regression fits to the data, and dash lines are the expected integrated intensity curves.

The integrated intensities for all of the L-PVC/USB-SPCL blends, like the D-PVC/USB-SPCL blends, also decreased with increasing temperature, and the temperature dependence became stronger at higher temperature. However, unlike the D-PVC/USB-SPCL blends, all of the integrated intensity data points for the L-PVC/USB-SPCL blends (except for the L-PVC/USB-SPCL0 blend) were not fitted with two linear regression lines obtained from the same method as the above (see Figure VI-8). The data for the L-PVC/USB-SPCL blends linearly decreased with increasing temperature at lower temperature range in the glassy state, and then an unexpected gradual decrease was observed from near the glass transition of the whole blend system, in disagreement with thermal free-volume expansions. These unexpected data more slowly decreased compared to those for the D-PVC/USB-SPCL blends (the expected integrated intensity curves are dash line in Figure VI-8). Upon heating, the data linearly decreased again with stronger temperature dependence at higher temperature range in the rubbery state. The number of the data positioning out of the two linear regression lines increased with increasing the USB-SPCL amount in the L-PVC/USB-SPCL blends, indicating increase in the temperature range of unexpected data. Such temperature range of unexpected data is shown in Figure VI-9, which also includes the T_g values of the D-PVC/USB-SPCL blends obtained from FS measurement and the glass transition range together with the T_g values obtained from DSC measurement. The data for the L-PVC/USB-SPCL

blends appeared to get out of the two linear regression lines from the $T_{g,o}$ for the whole blend system to the $T_{g,e}$ for the neat PVC without USB-SPCL, whereas the T_g values of the D-PVC blends with different amount of USB-SPCL obtained from FS corresponded well with those values obtained from DSC. Although the data points for the L-PVC/USB-SPCL0 blend were satisfactorily fitted with two linear regression lines, the intersection of two linear regressions was found at near the $T_{g,o}$ for the neat PVC without USB-SPCL. These differences in the integrated intensity results between L-PVC/USB-SPCL and D-PVC/USB-SPCL blends were attributed to the fact that the fluorescence emission of the L-PVC/USB-SPCL blends depended on the dynamic behaviors of the individual PVC component in the blends, whereas the D-PVC/USB-SPCL blends showed the fluorescence emission determined by the dynamic behaviors of the whole PVC/USB-SPCL blend system. Thus, it is thought that the motion of the individual PVC component in the PVC/USB-SPCL blend constantly (and slowly) increased with increasing temperature before whole blend system started to bend and rotate. The motion then gradually quickened but more slowly increased than that of whole blend system. After the original PVC chain became completely rubbery (*i.e.*, after $T_{g,e}$ for the neat PVC), the motion constantly (and rapidly) increased again. These results clearly show a glass transition dynamic heterogeneity of PVC/USB-SPCL blends although PVC and USB-SPCL are thermodynamically miscible and are molecularly mixed, which is unfamiliar

because general glass transition dynamics of miscible polymer blend was sufficiently described by free-volume theory.[30,34] From these findings, we can presume that the glass transition dynamics of the entangled linear PVC matrix, plasticized by distinctive and rapid molecular mobility of USB-SPCLs, depended not only on the free volume of the whole blend system but also on the dynamic constraint of the PVC chain. In our presumption (see Figure VI-10), the heterogeneous glass transition dynamic behaviors of the PVC/USB-SPCL blend system are attributed to the chain entanglement and the molecular mobility of original PVC and USB-SPCL. The original PVC has higher molecular weight with linear and longer chain length, whereas USB-SPCL is unentangled star polymer with extremely small branches, resulting in ca. 12 times slower motion of entangled PVC molecules (see previous chapter, Table V-2).[35,36] In the glassy state of the PVC/USB-SPCL blend, the motion of the individual PVC component follows that of whole blend system (*i.e.*, the homogeneous dynamic behavior) because of the strong intermolecular interactions of PVC and USB-SPCL at lower temperature. The inside voids (*i.e.*, free volume) in the glassy state expand with increasing temperature, which is contributed from the equal molecular mobilities of both PVC and USB-SPCL. The USB-SPCL molecules significantly enlarge the inside voids from the glass transition of whole blend system because of very low T_g and rapid motion of unentangled USB-SPCL molecules. The PVC component starts to move faster with the dynamic constraint of the glassy

PVC chain in the enlarged inside voids. Upon heating, while the whole blend system becomes completely rubbery and the inside voids are more enlarged by USB-SPCL molecules, the PVC component still exists in the less rubbery state and slowly changes from glassy state to rubbery state with dynamic constraint. The dynamic constraint of the glassy PVC chain disappears after the PVC component becomes completely rubbery, and the completely rubbery PVC component follows the motion of the whole blend system in the rubbery state (*i.e.*, the homogeneous dynamic behavior again). As a result, the individual PVC component exhibits considerably broad thermal glass transition range from the glass transition of the whole blend system to the glass transition of original PVC. Such disagreement of thermal phase transition between the PVC component and the whole blend system results in the heterogeneous glass transition dynamic behaviors, depending on both the enlarged free volume by fast-moved USB-SPCL molecules and the dynamic constraint by entangled PVC chains.

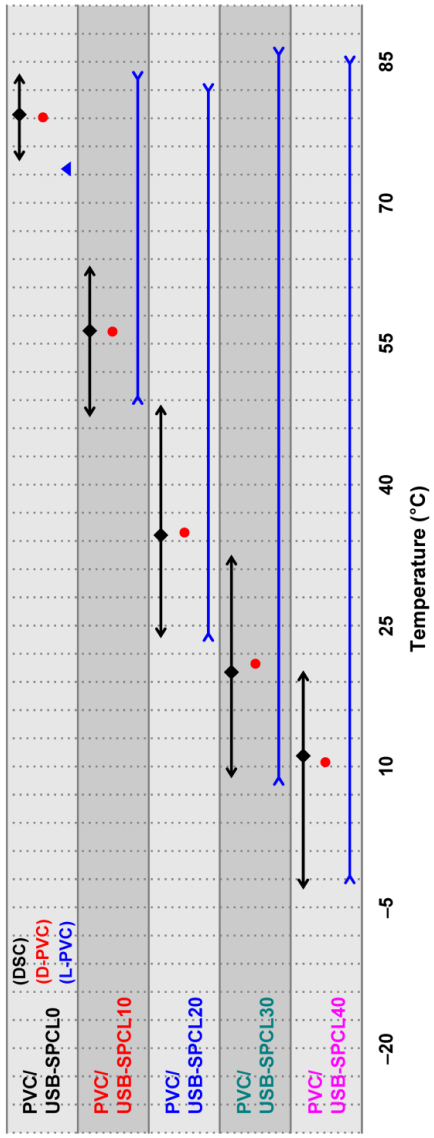

Figure VI-9. The temperature ranges of unexpected data for L-PVC/USB-SPCL blends includes the T_g values of the D-PVC/USB-SPCL blends obtained from FS measurement and the glass transition range together with the T_g values obtained from DSC measurement.

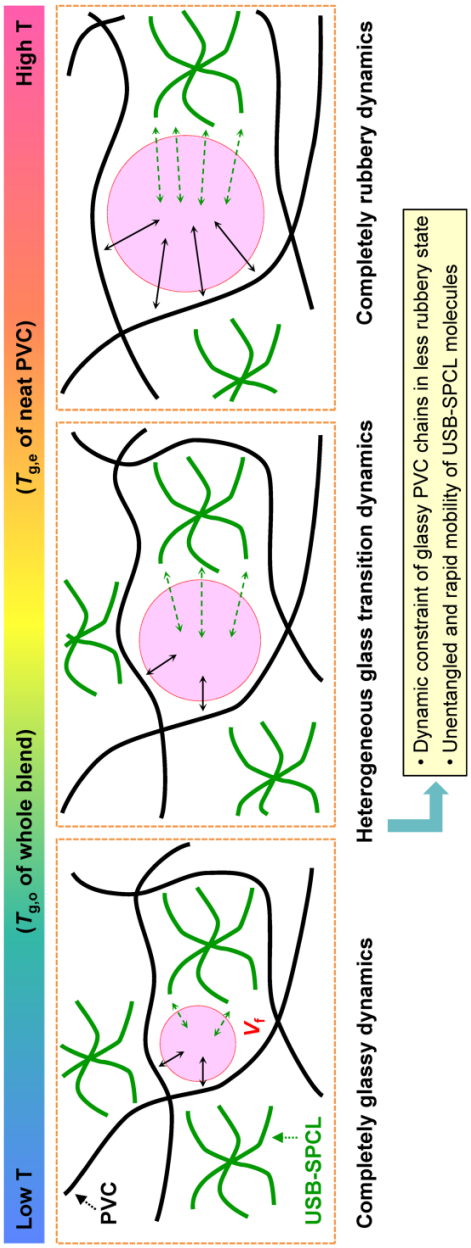

Figure VI-10. Presumed illustration of heterogeneous glass transition dynamics of individual PVC component in miscible PVC/USB-SPCL blend.

VI-4. Conclusion

The correlation between the dynamic behaviors of individual polymer chains and the controlled free-volume changes was investigated using plasticized PVC/USB-SPCL blends as a model system. The temperature-dependent fluorescence emissions for miscible PVC/USB-SPCL blends interestingly showed heterogeneous glass transition dynamics, *i.e.*, the individual PVC component in the PVC/USB-SPCL blends exhibited broad thermal glass transition range from the glass transition of the whole blend system to the glass transition of original PVC and the whole PVC/USB-SPCL blend system exhibited sharp glass transition with a single T_g. These results suggest that the motion of individual PVC component in PVC/USB-SPCL blends depended on both the enlarged free volume by fast-moved USB-SPCL molecules and the dynamic constraint by entangled PVC chains, whereas general glass transition dynamics was sufficiently described by free-volume of the whole blend system. We expect that this study may enhance the understanding of the dynamic behaviors and plasticization phenomena of the individual polymer matrix in a miscible polymer blend.

References and Notes

1. Zhang, Q.; Liu, W.; Dai, P. *Polymer* **1998**, *39*, 3787−3792.

2. Priya, L.; Jog, P. *J. Polym. Sci., Part B: Polym. Phys.* **2002**, *40*, 1682−1689.

3. Holt, A. P.; Griffin, P. J.; Bocharova, V.; Agapov, A. L.; Imel, A. E.; Dadmun, M. D.; Sangoro, J. R.; Sokolov, A. P. *Macromolecules* **2014**, *47*, 1837−1843.

4. Lee, J.; Grein−Iankovski, A.; Narayanan, S.; Leheny, R. L. *Macromolecules* **2017**, *50*, 406−415.

5. Serrano, B.; Baselga, J.; Piérola, I. F. *Polym. J.* **2002**, *34*, 905−910.

6. Kotsilkova, R.; Fragiadakis, D.; Pissis, P. *J. Polym. Sci., Part B: Polym. Phys.* **2005**, *43*, 522−533.

7. Vilaplana, F.; Karlsson, S.; Ribes-Greus, A.; Schade, C.; Nestle, N. *Polymer* **2011**, *52*, 1410−1416.

8. Dobircau, L.; Delpouve, N.; Herbinet, R.; Domenek, S.; Le Pluart, L.; Delbreilh, L; Ducruet, V.; Dargent, E. *Polym. Eng. Sci.* **2015**, *55*, 858−865.

9. Kim, E.; Kramer, E. J.; Osby, J. O. *Macromolecules* **1995**, *28*, 1979−1989.

10. Bendler, J. T.; Fontanella, J. J.; Shlesinger, M. F.; Wintersgill, M. C. *Electrochim. Acta* **2003**, *48*, 2267−2272.

11. Kalichevsky, M. T.; Jaroszkiewicz, E. M.; Ablett, S.; Blanshard, J. M. V.; Lillford P. J. *Carbohydr. Polym.* **1992**, *18*, 77−88.

12. Sengers, W. G. F.; van den Berg, O.; Wübbenhorst, M.; Gotsis, A. D.; Picken, S. J. *Polymer* **2005**, *46*, 6064−6074.

13. Ellison, C. J.; Kim, S. D.; Hall, D. B; Torkelson, J. M. *Eur. Phys. J. E: Soft Matter Biol. Phys.* **2002**, *8*, 155−166.

14. Ellison, C. J.; Torkelson, J. M. *J. Polym. Sci., Part B: Polym. Phys.* **2002**, *40*, 2745−2758.

15. Evans, C. M.; Torkelson, J. M. *Polymer* **2012**, *53*, 6118−6124.

16. Packter, A.; Nerurkar, M. S. *Kolloid Z. Z. Polym.* **1969**, *229*, 7−11.

17. Kulik, A. S.; Beckham, H. W.; Schmidt-Rohr, K.; Radloff, D.; Pawelzik, U.; Boeffel, C.; Spiess, H. W. *Macromolecules* **1994**, *27*, 4746–4754.

18. Lutz, T. R.; He, Y.; Ediger, M. D.; Cao, H.; Lin, G. Jones, A. A. *Macromolecules* **2003**, *36*, 1724–1730.

19. Evans, C. M.; Torkelson, J. M. *Polymer* **2012**, *53*, 6118−6124.

20. Búcsiová, L.; Hrdlovič, P.; Chmela, Š. *J. Photochem. Photobiol., A* **2001**, *143*, 59−68.

21. Martins, T. D.; Yamaki, S. B.; Prado, E. A.; Atvars, T. D. Z. *J. Photochem. Photobiol. A: Chem.* **2003**, *156*, 91–103.

22. Kim, S.; Roth, C. B.; Torkelson, J. M. *J. Polym. Sci., Part B: Polym. Phys.* **2008**, *46*, 2754−2764.

23. Mundra, M. K.; Ellison, C. J.; Rittigstein, P.; Torkelson, J. M. *Eur. Phys. J. Special Topics* **2007**, *141*, 143−151.

24. Evans, C. M.; Henderson, K. J.; Saathoff, J. D.; Shull, K. R.; Torkelson, J. M. *Macromolecules* **2013**, *46*, 4131−4140.

25. Evans, C. M.; Kim, S.; Roth, C. B.; Priestley, R. D.; Broadbelt, L. J.; Torkelson, J. M. *Polymer* **2015**, *80*, 180−187.

26. Jin, K.; Torkelson, J. M. *Polymer* **2017**, *118*, 85–96.

27. Valeur, B.; Berberan-Santos, M. N. *Molecular Fluorescence: Principles and Applications*, 2nd ed.; Wiley-VCH: Weinheim, Germany, 2012.

28. Chee, K. K. *Eur. Polym. J.* **1985**, *21*, 29−31.

29. Tande, B. M.; Wagner, N. J.; Kim, Y. H. *J. Polym. Sci., Part B: Polym. Phys.* **2007**, *45*, 1970−1975.

30. Sears, J. K.; Darby, J. R. *The Technology of Plasticizers*; John Wiley & Sons: New York, 1982.

31. Rahman, M.; Brazel, C. S. *Prog. Polym. Sci.* **2004**, *29*, 1223–1248.

32. Daniels, P. H. *J. Vinyl Addit. Technol.* **2009**, *15*, 219–223.

33. Choi, W.; Chung, J. W.; Kwak, S.−Y. *J. Polym. Sci., Part A: Polym. Chem.* **2015**, *53*, 1134−1142.

34. Choi, W.; Chung, J. W.; Kwak, S.−Y. *ACS Appl. Mater. Interfaces* **2014**, *6*, 11118−11128.

35. Choi, W.; Chung, J. W.; Kwak, S.−Y. *Polymer* **2015**, *79*, 91−98.

36. Choi, W.; Chung, J. W.; Kwak, S.−Y. *Polymer* **2016**, *103*, 19−26.

37. Moulay, S. *Prog. Polym. Sci.* **2010**, *35*, 303–331.

38. Pawlak, M.; Grygolowicz−Pawlak, E.; Bakker, E. *Anal. Chem.* **2010**, *82*, 6887−6894.

39. Earla, A.; Braslau, R. *Macromol. Rapid Commun.* **2014**, *35*, 666−671.

40. Cai, T.; Li, M.; Neoh, K.−G.; Kang, E.−T. J. Mater. Chem. B 2013, 1, 1304−1315.

41. Wang, D.; Wilkie, C. A. *J. Vinly Addit. Technol.* **2002**, *8*, 238−245.

42. Bag, S. S.; Kundu, R. J. Org. Chem. **2011**, *76*, 3348−3356.

43. Bag, S. S.; Kundu, R. *J. Fluoresc.* **2013**, *23*, 929−938.

44. Liu, D.; de Feyter, S.; Cotlet, M.; Stefan, A.; Wiesler, U.−M.; Herrmann, A.; Grebel−Koehler, D.; Qu, J.; Müllen, K.; de Schryber, F. C. *Macromolecules* **2003**, *36*, 5918−5925.

45. Kotch, T. G.; Lees, A. J.; Fuerniss, S. J.; Papathomas, K. I.; Snyder, R. W. *Inorg. Chem.* **1993**, *32*, 2570−2575.

KOREAN ABSTRACT

본 연구에서 우리는 무독성의 연질 폴리염화비닐(PVC)을 위한 친환경 대체가소제로서 초단가지 성형구조 폴리(입실론-카프로락톤)(USB-SPCL)을 개발하고 이들의 동역학적 특성과 가소화와의 상호작용에 대한 연구를 한다.

우선, 우리는 단량체와 중심물질의 몰 비율, 고분자 전환율, 말단 수산기 치환, 감압정제를 고려한 유사 단일반응기 공정을 이용하여 기존 개환중합의 고질적인 문제점을 해결하고 USB-SPCL을 성공적으로 대량합성한다. USB-SPCL의 가지길이는 단량체 5개 이하로 조절되고 수율은 93% 이상이다. 핵자기공명 분광분석(NMR)과 매트릭스 보조 레지저 탈착/이온화 질량 분석(MALDI-TOF-MS)를 통해 합성된 USB-SPCL이 목표로한 가지길이와 가지수를 가짐이 확인한다. USB-SPCL은 초단가지로 인해 낮고 넓은 범위의 녹는점과 결정화 특성을 보이지만, 흥미롭게도 가지길이와 가지수에 영향을 받지 않고 전체분자량에 의존하는 유리전이 거동을 보인다.

전형적인 성형구조 고분자에서 발견되지 않는 전체분자량에 의존하는 독특한 유리전이 거동을 명확하게 규명하기 위해, 동적

기계 분석(DMS)를 이용하여 초단가지가 USB-SPCL의 동역학적 거동에 미치는 영향을 연구한다. USB-SPCL의 점탄성 거동, 유동활성화에너지, 라우즈(Rouse) 완화시간 모두 전형적인 성형구조 고분자의 법칙을 따르지 않고, 사슬얽힘이 없는 선형 고분자의 라우즈(Rouse) 모델을 따른다. 이 결과들은 USB-SPCL의 초단가지가 동역학적 동등성을 지니며 전체 USB-SPCL 분자가 하나의 동역학적 단위로 움직이게 한다는 것을 제시한다.

이어서, 합성된 USB-SPCL을 연질 PVC 제조를 위한 무독성 가소제로서 활용 한다. USB-SPCL은 상온에서 사슬얽힘이 없는 액상으로 존재하며 급성독성이 없다. 기존에 사용중인 연질 PVC 제조법을 이용하여 USB-SPCL과 일반적으로 가장 널리 사용중인, 하지만 독성이 있는 것으로 알려진, 프탈레이트 가소제(이하, DEHP)로 가소화된 PVC시트를 각각 제조하고, 이들의 가공성, 연질성, 유출안정성을 비교분석한다. USB-SPCL은 DEHP와 비교하여 PVC와 높은 상용성, 유사한 가소화 성능을 지니며, 연질 PVC시트 가공 시 느린 흡수속도 및 빠른 퓨전속도를 갖는다. 특히, DEHP는 제조된 연질 PVC 외부로 상당부분이 유출될 때, USB-SPCL은 매우 뛰어난 유출안정성을 보인다.

아울러, 광자 상관 분광 분석(PCS)을 이용하여 USB-SPCL의 동역학 거동이 PVC의 가소화에 미치는 영향에 대해 연구한다. PVC와 USB-SPCL의 매우 큰 분자운동성 차이에도 불구하고, PCS로 분석한 PVC/USB-SPCL 혼합물(blend)의 동역학 거동은 PVC와 USB-SPCL의 매우 강한 분자간 상호작용과 매우 높은 상용성으로 인해 단일한 동역학적 거동(homogeneous dynamics)을 보인다. PVC/USB-SPCL 혼합물에서 PVC의 운동성은 USB-SPCL의 전체분자량에 의존하는 독특한 동역학적 거동을 따른다. 이는 PVC가 USB-SPCL의 운동성에 의해서 가소화된다는 것을 보여준다.

마지막으로, 형광 분광 분석(FS)을 이용하여 USB-SPCL로 가소화된 PVC 사슬자체의 운동성에 대해 조사하고 자유부피 변화에 따른 분자운동성의 상관관계를 연구한다. 전체 PVC/USB-SPCL 혼합물은 단일한 유리전이온도를 갖지만, 흥미롭게도 PVC 사슬자체는 매우 넓은 온도범위의 유리전이 거동을 보인다. 이는 PVC/USB-SPCL 혼합물이, 일반적은 상용성 고분자 혼합물의 유리전이 거동과 달리, 이종의 유리전이 거동(heterogeneous glass transition dynamics)을 갖는다는 것을 나타낸다. 이 결과들은 PVC 사슬자체의 운동성은 전체 PVC/USB-SPCL 혼합물의 자유부피뿐만 아니라 PVC

사슬자체의 얽힘으로 인한 동적 제약에 의해 결정된다는 것을 보여준다.

주요어: 초단가지, 폴리(입실론-카프로락톤), 성형구조 고분자, 가소제, 폴리염화비닐, 분자동역학, 동적 기계 분석, 광자 상관 분광 분석, 형광 분광 분석

학번: 2008-20691

LIST OF PAPERS, PATENTS AND SYMPOSIUMS

PAPERS

1. **Choi, W.**; Chung, J. W.; Kwak, S.–Y., "Unentangled Star-Shape Poly(ε-caprolactone)s as Phthalate-Free PVC Plasticizers Designed for Non-Toxicity and Improved Migration Resistance", *ACS Appl. Mater. Interfaces* **2014**, *6*, 11118–11128.

2. **Choi, W.**; Chung, J. W.; Kwak, S.–Y., "Synthesis of Ultra-Small Branched Star Poly(ε-caprolactone)s and Their High End Group Concentration Effects on Crystallization", *J. Polym. Sci., Part A: Polym. Chem*. **2015**, *53*, 1134–1142.

3. **Choi, W.**; Chung, J. W.; Kwak, S.–Y., "Total-Molecular-Weight-Dependent Rouse Dynamic of Ultra-Small Branched Star Poly(ε-caprolactone)s as a Single Coarse-Grain Unit", *Polymer* **2015**, *79*, 91–98.

4. **Choi, W.**; Chung, J. W.; Kwak, S.–Y., "Photon Correlation Dynamics of Unentangled Star-shaped Poly(ε-caprolactone)s with Extremely Small Branches and Its Interaction with Plasticization in Miscible Blend System", *Polymer* **2016**, *103*, 19–26.

PATENTS

1. 곽승엽, **최우혁**, 최경재, 윤경준, 최영균, "나노브러쉬형 친환경 대체가소제 화합물 및 단일반응기 공정을 이용한 이의 제조방법", 대한민국 특허등록 10-1354141 (2014. 1. 15)

   "Eco-friendly Alternative Plasticizer Based on Nanobrush Structure and Manufacture Method of Them Using One-pot Process", PCT출원 PCT/KR2012//001699 (2012. 3. 8)

2. 곽승엽, **최우혁**, 이규원, "고차가지구조의 폴리에테르 화합물 및 이를 포함하는 폴리염화비닐 조성물", 대한민국 특허등록 10-1390223 (2014.4. 23)

   "Hyperbranched Polyether Compounds and Poly(vinyl chloride) Composition Containing the Same", PCT출원 PCT/KR2012/010384 (2012. 12. 3)

3. 곽승엽, **최우혁**, 이규원, "고차가지구조의 폴리에테르 화합물 및 그의 제조방법", 대한민국 특허출원 10-2014-0022759 (2014. 4. 18)

4. 곽승엽, **최우혁**, 이규원, "고차가지구조 결사슬을 포함하는 폴리염화비닐 유도체", 대한민국 특허출원 10-2015-0132576 (2015. 9. 18)

SYMPOSIUMS

1. International Conference on Intelligent Textiles (2008), "Effect of Incorporating β-Cyclodextrin Derivative on Migration Behavior of Phthalate Plasticizer in Flexible PVC"

2. The 5th Asian Cyclodextrin Conference (2009), "Plasticizer Including β-Cyclodextrin Derivative to Effectively Reduce its Migration from Flexible Poly(vinyl chloride)"

3. 추계 고분자학회 (2009), "친 환경 대체가소제 제조를 위한 나노 브러쉬 구조 oligo(e-caprolactone) 중합 및 특성평가"

4. 춘계 고분자학회 (2010), "Manufacture and Characterization of Eco-friendly Poly(vinyl chloride) Plasticized with Nanobrush Structured Oligo(ε-caprolactone)"

5. 추계 재료학회 (2010), "Characteristics of Flexible Poly(vinyl chloride) Plasticized with Eco-friendly Nanobrush Structure Plasticizer"

6. Nanotech (2010), "Ag-TiO_2 Coated Polyurethane Composite Nanofiber Web for Application in the Protection against Chemical and Biological Warfare Agent"

7. Clean Technology (2010), “Nanobrush Structured Oligo(epsilon-caprolactone) as a Novel Plasticizer for the Manufacture of Eco-friendly Poly(vinyl chloride)”

8. **춘계 고분자학회** (2011), “Suppression of Plasticizer Migration Using the Three-armed Oligomeric Plasticizer with a High Plasticization Efficiency”

9. **춘계 고분자학회** (2012), “Large-Scale Synthesis of Nanobrush-Structured Oligomers and Their Applications as Green Plasticizers for Flexible Poly(vinyl chloride)”

10. **춘계 고분자학회** (2013), “Viscoelastic Properties of Star-shaped Oligo(*ε*-caprolactone)s in Melt State”

11. **추계 대한화학회** (2014), “Synthesis of Trimethylolpropane-cored Poly(*ε*-caprolactone) with Extremely Short Arms and Its Application to a Flexible PVC”

12. **춘계 대한화학회** (2015), “Synthesis of Star Polycaprolactone (SPCL) with Extremely Small Branchs and Their Rouse Dynamic Behavior”